EROSION ANALYSIS OF COARSE AND FINE GRAINED SEDIMENTS NATIVE TO THE STATE OF GEORGIA

A Thesis
Presented to
The Academic Faculty

by

Paul Richard Krehbiel Jr.

In Partial Fulfillment
Of the Requirements for the Degree
Master of Science in the
School of Civil and Environmental Engineering

Georgia Institute of Technology
December 2016

EROSION ANALYSIS OF COARSE AND FINE GRAINED SEDIMENTS NATIVE TO THE STATE OF GEORGIA

Approved by:

Dr. Terry W. Sturm, Advisor
School of Civil and Environmental Engineering
Georgia Institute of Technology

Dr. Laurie A. Garrow
School of Civil and Environmental Engineering
Georgia Institute of Technology

Dr. Hermann M. Fritz
School of Civil and Environmental Engineering
Georgia Institute of Technology

Date Approved: December 14, 2016

Acknowledgments

"If I have seen further, it is by standing on the shoulders of giants" – Isaac Newton. I would like to thank my advisor Dr. Terry Sturm for his constant encouragement, advice, support, and insight not only in the pursuit of this thesis, but also in my academic and professional career. I would also like to thank Dr. Hermann Fritz for his encouragement and assistance not only with this thesis, but also for originally instilling my interest in fluid mechanics as an undergraduate student. Dr. Laurie Garrow's feedback and assistance was excellent and appreciated immensely. A special thanks goes to Andy Udell, Blake Baklini, and Billy Plum for helping maintain the machinery and lab space that made the experiments conducted in this research possible. I am thankful for the donation by IMERYS for the sediment used in this research. I am very thankful for and appreciate the financial support by the Georgia Department of Transportation for this project. I wish to thank my friends, both in the lab at Georgia Tech and from my years as an undergraduate, who gave me help and advice throughout my scholarly career. Lastly, I would like to thank my parents Anne and Dick Krehbiel, and my sister Rohan Krehbiel whose financial and spiritual support gave me the opportunity to attend this fine institution.

Table of Contents

List of Symbols and Abbreviations

Acceleration due to Gravity	g
Adjusted R Squared Value	R^2_{adj}
Applied Bed Shear Stress	τ
Average Shear Stress	$\hat{\tau}$
Average Velocity	V
Bed Slope	S
Bulk Density	ρ_b
Clay Size Fraction	CSF
Coefficient of Curvature	C_c
Coefficient of Uniformity	C_u
Critical Shear Stress	τ_c
Density of Kaolin	ρ_{kaolin}
Density of Sand	ρ_{sand}
Density of Silt	ρ_{silt}
Density of Water	ρ_w
Dimensionless Grain Diameter	d_*
Displacement over Time	$\frac{\Delta D}{\Delta t}$
Dry Density	ρ_d
Dynamic Viscosity of Water	μ
Erosion Rate	E
Experimental Constant	M
Experimental Constant	n

Fine Sediment Content	$Fines$
Flow Rate	Q
Force by Buoyancy	F_B
Force by Weight	F_W
Froude Number	$\boldsymbol{F}$
Hydraulic Radius	R
Hydrodynamic Drag Force	F_D
Indirect Plasticity Index	PI^*
Kinematic Viscosity of Water	v
Mallows Value	C_p
Mass of Kaolinite	M_{kaolin}
Mass of Sand	M_{sand}
Mass of Silt	M_{silt}
Mean Square Error of Model	MSE_{total}
Median Particle Diameter	d_{50}
Number of Data Points	Z
Number of Variables	p
Particle Diameter	d
Particle Reynolds Number	$\mathbb{R}\boldsymbol{e}_{*\boldsymbol{c}}$
Particle Shape Factor	a_n
Particle Size for which 10% are Smaller by Weight	d_{10}
Particle Size for which 30% are Smaller by Weight	d_{30}
Particle Size for which 60% are Smaller by Weight	d_{60}
R Squared Value	R^2
Reynolds number	$\mathbb{R}\boldsymbol{e}$

Sediment Mass Dry	m_{dry}
Sediment Mass Wet	m_{wet}
Shields Parameter	τ^*_c
Specific Gravity	Gs
Specific Weight of Particle	γ_s
Specific Weight of Water	γ_w
Standard Error	SE
Submerged Specific Weight	$\gamma_s - \gamma_w$
Submerged Weight	W_s
Sum of the Squares of the Mallows C_p Errors	SSE_p
Sum of the Squares of the Errors	SSE
Suspended Sediment Concentration	SSC
Total Sediment Volume	V_t
Water Content	w
Water Depth	y

List of Tables

Page

List of Figures

Page

Summary

Sediment erosion in aquatic environments plays an important role in the design of bridges and other hydraulic structures with regard to scour, contaminant transport, and preservation of ecological systems. Erosion is the action of hydrodynamic forces overcoming the resistance by a sediment particle to being entrained and transported such that significant local erosion occurs. Sediments can be characterized as either non-cohesive or cohesive, as a classification determined by certain geotechnical properties. Non-cohesive sediments, consisting of sand and silt, primarily resist erosion due to the submerged weight of the particle and packing density of the sediment. Cohesive sediments, consisting of silt and clay, resist erosion via interparticle interactions, as determined by clay size fraction, water content or bulk density, and fines content, as well as other properties such as pH, organic matter, and mineralogy. Erosion of non-cohesive sediments that are primarily coarse-grained has been studied and documented by many researchers. While cohesive sediments have been investigated extensively, they are inherently more difficult to study because of the physicochemical properties that determine interparticle binding forces.

This study focuses on a few geotechnical parameters to predict the erodibility of sediment mixtures on the coarse-fine transition boundary and mimic sediments native to Georgia. Previous researchers have investigated the erosion properties of coarse-sediment field samples in Georgia (Navarro 2004 and Hobson 2008) and predominantly fine, laboratory-prepared samples (Wang 2013 and Harris 2015). In order to span this collection of data, a series of samples was prepared and tested in an erosion flume in the Georgia Tech Hydraulics Laboratory using the same methodology as previous investigators to measure critical shear stress. The silt to sand ratio was

held constant at 0.75, which is consistent with prior investigations of native Georgia sediments. Sand, silt, and Georgia Kaolinite were added to the samples, increasing the quantity of Kaolinite by weight in each subsequent sample from 10-30%. Sediment properties measured included water content, grain size distribution, clay size fraction, pH, temperature, and conductivity. Erosion rates for the mixtures were measured using a hydraulic flume. From these experiments, a critical shear stress for each mixture was determined based on water content. The critical shear stress data were analyzed as a function of measured geotechnical parameters using multiple regression analysis which provided a series of estimation equations. The relationships for critical shear stress derived in this research include a three-variable equation depending on water content, clay size fraction, and an interaction term; a fourth term that adds a fines content variable to the previous relationship; and a pair of equations that are implemented on separate coarse vs. fine data sets based on water content and particle size. While a weighted equation, which uses a combination of cohesive and non-cohesive equations, or two separate equations for coarse vs. fine sediment have merit, the optimal solution found in this research is the three-variable equation based on water content, clay size fraction, and an interaction term applied to all available data. However, more research should be conducted investigating the idea of two equations that are implemented on two separate datasets and on the criteria that best separate the data sets relative to cohesive vs. noncohesive erosion behavior. The results of this research can be used to find better predictions of sediment critical shear stress for Georgia sediments as a function of easily measured geotechnical parameters thereby providing better estimates of bridge scour and sediment stability for other structures in aquatic settings.

Chapter 1

Introduction

Infrastructure built in and over rivers and other large bodies of water are some of humanity's greatest achievements. These structures make it possible for reservoirs to hold water for large cities, channel storms away from populated areas, and allow for commerce to cross vast distances quickly. In the process of placing these structures into channels of flowing water as obstructions, the flow of water begins to change the natural properties of the river. These natural properties include the size distribution of the sediments in the bed, the sinuosity or curvature of the river, scour of the sediment bed, general roughness of the bed, and more. The erodible sediment bed and banks of the river adjust in response to changes in the flow field so as to achieve a new state of equilibrium. For example, the act of placing a structure in a river channel, even if just a set of bridge piers, can result in significant erosion of the river bed in the vicinity of the piers. Some unintended consequences such as bank erosion develop over a long period of time, and in the extremes, the destructive power of the river can manifest itself during large floods in the form of exposure and undermining of foundations, contributing to bridge collapses and failures. The degree of resistance to the destructive forces of flowing water is determined by the type of sediment in the river bed. Understanding how sediments erode is vital to constructing infrastructure without over-designing at great expense or under-designing at the risk of failure.

In open channel hydraulics, the process of sediment erosion is a topic that has been studied for quite some time; however, the intricacies of exactly how it works has been somewhat elusive to engineers and scientists. While the hydraulic conditions, notably the turbulent kinetic energy and/or the shear stress, are the main cause of the scour and erosion of a sediment, a

sediment's properties are what dictate the rates of erosion which can eventually lead to scour. Sediments are a collection of small particles that interact with each other to varying degrees. Fine-grained sediments may contain a significant fraction of clay minerals whose structure consists of small platelets that adhere to each other via electrochemical forces. Coarser particles on the other hand, are more governed by their individual resistance to flow through their submerged weight. As a result of these properties, research has been directed at trying to quantify erosion based on a sediment's geotechnical properties. If an erosion rate set by a specific shear stress can be quantified measuring a particular geotechnical property such as water content, bulk density, or percentage of clay, then field tests could make it easy to establish a proper depth for support structures to prevent washout and structural failure.

This research builds upon past studies and investigates whether conclusions about erosion rates can be applied to sediments that are not simply non-cohesive or cohesive, but a mixture of both based on types of sediments native to the State of Georgia. Navarro (2004) and Hobson (2008) began to look at erosion of sediments by taking Shelby tube samples from bridge pier locations directly affected by large scour storm events in Georgia. Using a recirculating flume, these Shelby tubes were extruded to specific heights above the flume bed to maintain the sample level with the surrounding bed as a function of time in order to measure erosion rates. Erosion rates were then compared to geotechnical properties for analysis. Most of their work was based on coarse material, but did have experiments that crossed into the area between fine and coarse sediments. Wang (2013) investigated fine sediment content by varying percentages of clay with ground silica and compared those levels with water content to critical shear stresses. Harris (2015) studied mixing clay and fine sand to try and bridge the previous three studies with an equation that is primarily based on cohesive sediment, but could be used for non-cohesive

sediment using combinations of independent variables consisting of fine sediment content (percent *Fines*), clay (clay size fraction, CSF), and water content, *w*. This paper aims to combine Georgia Kaolinite, ground silica, and fine sand based on naturally present proportions found by Navarro (2004) and Hobson (2008) during their research. By combining all three sediment constituents in a homogenized sample, interactions are measured in the lab resulting in the ability to draw comparisons between current and previous research.

All of the combined research from the past 12 years will be combined in an effort to predict the effectiveness of different equations when applied to sediments that are not only cohesive or granular, but also in the middle ground where both responses are possible. The five main equations are regression equations developed by Hobson (2008), Wang (2013), and Harris (2015), that provide a Shields parameter for the sediments in question.

The next chapter, Chapter 2 will provide a literature review of geotechnical characteristics, the causes of erosion, the methodology of erosion analysis, and the properties of the sediments involved. Chapter 3 will give an overview of the methodology of how the research was conducted. Chapter 4 will present the results of the experiments in detail. Lastly, Chapter 5 presents the discussion and analysis of the data. Chapter 6 will discuss the final conclusions and recommendations for future research.

Chapter 2

Literature Review

2.1 Sediment Properties

River sediments are commonly composed of differently sized particles that can be classified into sand, silt, and clay. These sizes are what have the most direct impact on how quickly a sediment may erode when subjected to hydrodynamic forces. The composition of these sediments has been subdivided into two classifications based on the way sediments are held together: coarse, non-cohesive vs. fine, cohesive sediments. According to the American Geophysical Union (AGU), fine sand is defined as a particle larger than 0.062 mm in diameter and is considered a coarse sediment. Similarly, silt particles have a size between 0.062 mm and 0.002 mm, and clays are any particles with sizes equal to or less than 0.002 mm, both of which are part of the fines category. Non-cohesive sediments have been studied by many previous researchers including Albert Shields in the 1930's. While his research was by no means exhaustive, it provided an important base that was built upon by others investigating coarse sediment erosion and the critical value of hydrodynamic shear stress at which erosion begins. Non-cohesive sediments are most reliant on their submerged weight in order to resist motion caused by fluid shear forces. Cohesive sediments are less reliant on the resisting gravity force and more on their physiochemical properties for resisting erosion. These properties include particle size, distribution of sizes, bulk density, salinity, pH, cations, and organic content (Grabowski et al. 2011). As a result of this far more diverse collection of relevant properties, pinning down a distinct method to determine erosion thresholds and rates has been far more complex than with non-cohesive sediments.

The importance of understanding erosion in bodies of water cannot be understated given the influence sediment plays on natural processes. Sediments are the primary habitat for benthic organisms which thrive in large quantities in the sediments, providing a region for nitrogen fixation processes, which makes river sediments an excellent natural fertilizer, among other benefits. Recently, humanity has altered the environment in such ways as to directly change the quantity and quality of sediment through land uses related to urbanization, applications of pesticides to crops, and hydrogeomorphological modifications such as dams and channelization. Given the changes at the physical and chemical levels which can change the biological environments, accurate methods of estimating erosion are necessary for proper design and planning. (Grabowski et al. 2011)

The complexity resulting from the wide ranging possibilities that can affect cohesive sediment has resulted in a series of individual studies holding onto specific properties that researchers believe are the most important in deciding erosion. Some research has looked into focusing on mud, or fines, content (silt and clay) as the primary factor in determining erosion. It has been shown that while mud has a role to play in cohesive sediment erosion, it has less to do with silt content and more to do with clay content thanks to its stronger interparticle cohesion versus that of silt (van Ledden et al. 2004). This can be based on the structural differences of silt and clay. Silt is a much like sand, with a larger mass than clay and less surface area, whereas clay has a smaller, flat plate structure with a high surface area to volume ratio that allows for electrochemical forces to have a greater role in its cohesion.

To properly understand how erosion can be measured, the properties of the sediments in a body of water must be understood. In the context of this study there were three components used: clay, silt, and fine sand. The clay implemented was Georgia sedimentary Kaolinite which

is a fine sediment with some particles in both the clay and silt ranges. Georgia Kaolinite has two categories that are based on the sediment age. The younger Kaolinite comes from the Palocene-Eocene which is "hard" and has 80% of its particles smaller than 0.002 mm by weight. The older "soft" Kaolinite dates from the Cretaceous period where 70% of the particles are larger than 0.002 mm (Pruett 2000). This study uses the older "soft" Kaolinite.

Within the classification of clays there are three groups based on their electrochemical activity and size: Kaolinite, Illite, and Smectites (Budhu 2011). All of these groups are fine clays, but their structures result in different types of clays. Kaolinite has silica and alumina sheets with a large surface area, 10-20 m^2 per gram. Illite is a pair of silica sheets which has an alumina sheet between them. Lastly, Montmorillonite clay, a smectite, is like Illite with silica layers and an alumina sheet between them. All of these clay exhibit the same interparticle forces due to van der Waals forces. However, Montmorillonite is the most susceptible to water intrusion which results in the clay expanding to a much greater degree than other clays, hence its nomenclature as an expansive clay. It has been found that Montmorillonite clay when mixed with sand has a lower erosion threshold compared to Kaolinite-sand mixtures and marine mud mixtures (Torfs 1996).

Clays are important to cohesive sediments as their surface areas are how individual particles can attract one another, rather than relying on submerged weight like that of non-cohesive mixtures. A non-cohesive particle like sand will have close to 0.01 m^2 per gram of surface area whereas montmorillonite can have 1000 m^2 per gram. As a result of this increased surface area and smaller size, electrochemical forces are stronger interparticle forces than they are for large particles.

Another important factor in determining interparticle forces is the spatial arrangement of the soil particles. There are three primary arrangements: Edge-to-Edge (E-E), Edge-to-Face (E-F), and Face-to-Face (F-F). Edge-to-Edge arrangements are not necessarily governed by any particularly dominant force. Edge-to-Face arrangements are primarily governed by Coulombian principles created by the counter charges existing at the intersection points. Face-to-Face arrangements are governed primarily by van der Waals forces overcoming the double layer repulsion force in mostly ionic mediums. Table 2.1 below shows the various configurations based on arrangements, the grouping of individual particles, and classification of groups (van Olphen, 1977).

Table 2.1: Particle Associations in Fine Grained Sediments

Clay Particles	Dispersed, Deflocculated		
	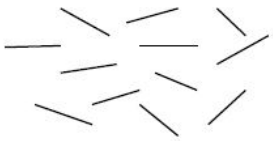		
Simple Particle Associations	F-F Aggregated, but Deflocculated	E-F Flocculated, but Dispersed	E-E Flocculated, but Dispersed
	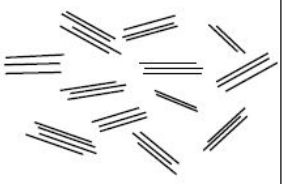	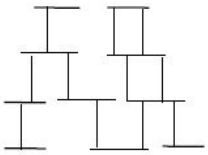	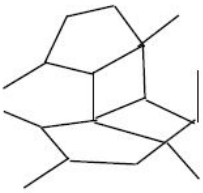
Complex Particle Associations	E-F Flocculated, F-F Aggregated	E-E Flocculated, F-F Aggregated	E-F, E-E Flocculated, F-F aggregated
	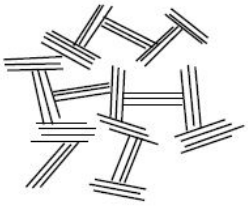	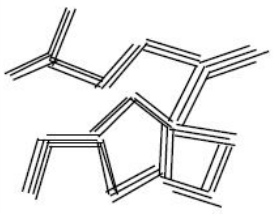	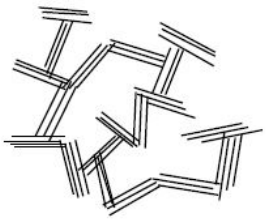

Source: van Olphen (1977) as reported in Wang (2013)

Silts are a bridging particle between clays and sands. Unlike the chemical weathering that clays undergo in order to attain their size and shape over time, silts are physically weathered and maintain an approximately spherical shape like that of the sands from which silts are derived. As a result of maintaining their spherical-like shape, silts are less influenced by electrochemical forces than clays. However, their size and surface area makes them slightly comparable to clays and they are considered to be part of the "fines" category of sediments.

Sand, as mentioned previously, is a non-cohesive substance given that its size is much larger than that of silt or clay (0.062 mm and greater). Gravity is a much stronger force than that of any the interparticle forces, so predominantly sandy materials result in non-cohesive sediment transport instead of the cohesive type.

2.2 Causes and Types of Erosion

The action of erosion occurs when the forces created by the fluid are greater than those that hold the sediment bed together. Erosion can be measured by considering the net loss of particles from flow over a given surface area in a specified time period. Erosion can come in four separate forms including entrainment, mass erosion, surface erosion, and floc erosion (Schofield and Wroth 1968, Winterwerp and Van Kesteren 2004). Entrainment is when fluid mud is ensconced by turbulent flow into the fluid. Mass erosion can be identified by the lumps of material that are eroded from an undrained material at high stresses. Surface erosion happens in a drained process where the mean erosion threshold is smaller than the mean bed shear stress. Lastly, floc erosion is the removal of flocs, or small groups of sediment, from the surface due to localized high shear stresses caused by fluxes in the fluid flow (Jacobs et al. 2011). Winterwerp et. al (2012) was able to characterize the critical shear stress (τ_c) ranges for these modes of

erosion as compared to the average bed shear stress ($\bar{\tau}$). When $0.5\ \tau_c < \bar{\tau}$, stable bed; $0.5\ \tau_c < \bar{\tau} < \tau_c$, floc erosion; $\tau_c < \bar{\tau} < 1.7\ \tau_c$, floc and surface erosion; and $\bar{\tau} > 1.7\ \tau_c$ surface erosion.

Other types of erosion categorization include Type I and Type II erosion, which are time-decreasing and time-independent erosion, respectively. Type I is time-decreasing erosion because it assumes that the bed is stratified and therefore different layers of the sediment will erode at different rates with respect to depth of the sediment (Jacobs et al. 2011). Type I can be further subdivided into Type IA, the erosion of superficial "fluff", and Type IB, the continued erosion of material underneath Type IA but before Type II. Type II erosion is described as time independent because the erosion rate is constant over time due to homogeneous conditions throughout the sediment bed.

Erosion below the critical threshold, $\bar{\tau} < \tau_c$, can occur due to local variations in flow and sediment makeup, but in the context of this research it can be neglected. This is because all erosion below the critical threshold is assumed to be floc erosion as noted by Jacobs et al. (2011). By considering floc erosion (Type IA) to be negligible, the critical threshold is the lowest point at which erosion will happen.

2.3 Erosion Measurement and Equations

2.3.1 Erosion Devices

Erosion devices have been crafted over many years by different researchers in response to the need for accurately measuring erosion parameters with the result that several different experimental setups have been devised. These setups are designed to hold certain parameters constant while allowing others to vary and be measured by the researcher. The first important decision in designing these flumes is whether the researcher wishes to perform tests in the field

or in the laboratory. Based on this preference, the researcher can then choose from three general categories of devices: laboratory flumes, benthic in situ flumes, and submerged jets. Laboratory flumes can provide a controlled environment in which any number of parameters can be controlled. The flumes can be straight or rotation annular flumes and while they are normally recirculating, it is possible for straight flow-through flumes to be implemented as well. Benthic in situ flumes are placed in the natural environment to measure sediment erosion in rivers, lakes, estuaries, bays, and other bodies of water. The flumes can be either straight flow-through or recirculating, but in both cases the suspended sediment concentration (SSC) is measured in order to determine the rate of erosion under varying hydrodynamic conditions. Lastly, there is the submerged jet method. These portable units use a jet of pressurized water to erode sediment in a test chamber or at a channel bank. The test chamber is measured for its ability to allow light to pass through it which can give measurements for erosion and settling rates (Wang 2013). The various uses of these devices in studies can be seen in Table 2.2.

Lab flumes are the most common devices where applied shear stresses are fixed using hydrodynamic principles and critical shear stress is measured using a series of methods. Roberts (2003) defined erosion as the point when 10^{-3} to 10^{-4} cm/s of erosion occurred, but also included direct measurement of sediment via sediment traps downstream of the sample. Righetti and Lucarelli (2007) instead would use a progressive scan DV camera to record the amounts of sediment in a particular control volume downstream of the sample. Similarly, Ternat et al. (2008) used optical backscatter sensors to measure the quantity of sediment in the flow field to provide an erosion flux measurement.

Benthic in situ flumes rely on the relationship between turbidity and the amount of sediment eroded by measuring the suspended sediment concentration (SSC). These flumes are

placed over a sediment in an aquatic area while flow is passed over the sediment mechanically. Amos et al. (1992b) implemented a trio of optical sensors to detect suspended particles while an electromagnetic senor would measure the flowrate. The Seaflume by Gust and Morris (1989) used optical attenuation meters at the inlet and outlet of the flume for instant SSC measurements.

Submerged impinging jets deliver rapid, short pulses of by a water jet placed perpendicularly to the sediment surface would disturb the sediment where changes in light through the test chamber were measured to indicate the sediment lost through erosion. Most of these are primarily an in situ device, but lab based experiments have been conducted by Mazurek et al. (2001) and others. Tolhurst et al. (1999) showed this was applicable for sediments between 0.002 mm and 1.5 mm. Particles smaller than 0.002 mm could not have their critical shear stress measured accurately. Williamson and Ockenden (1996) reversed the setup of the jet and instead of directing a jet towards the surface, they drew water away from the surface to entrap particles in the flow and measured the turbidity of this water. Flow rate was increased until a noticeable increase in turbidity was measured, from which erosion could be measured.

A number of researchers including Black and Paterson (1997), Cornelisse et al. (1997), and Tolhurst et al. (2000) have completed studies comparing the different methods. While they have shown that the different methods of measuring results in similar trends, the differences in flows, operation times, and shear stress calibration make it difficult for cross comparison of results.

Table 2.2: Examples of Erosion Devices and Their Implementation (Source: Wang 2013)

Type			Sample Source	Author(s)
Applied in	Flume shape	Device name		
Laboratory	Straight, recirculating flume		Kaolinite; river samples	Dennett (1995)
		Sedflume	Undisturbed samples from riverbeds	McNeil et al. (1996)
			Reconstructed samples for riverbeds	Jepsen et al. (1997)
			Quartz particles	Roberts et al. (1998)
			Undisturbed and reconstructed samples from field; pure clay (Kaolinite, Bentonite); Quartz particles	Lick and McNeil (2001)
		ASSET	Quartz particles	Robert et al. 2003
		--	Georgia Kaolinite	Ravisangar et al. (2001, 2005)
		--	Sand and clay mixture	Barry et al. (2006)
		--	Undisturbed samples from riverbed and coastal area	Ganaoui et al. (2007)
		--	Undisturbed samples from lakes	Rightti and Lucarelli (2007)
		--	Undisturbed samples from riverbeds	Ternat et al. (2008)
	Straight, recirculating duct	EFA	Silt and clay mixture; Kaolinite	Briaud et al. (1999, 2001, 2004)
	Rotating annular flume	--	Boston Blue Clay	Zriek et al. (1998)
		--	Sand and clay mixture	Jiang et al. (2004)
Field	Submerged impinging jet	--	Mixture of clay (40%), silt (53%), and fine sand (7%)	Mazurek et al. (2001)
		--	Sand and clay mixture	Ansari et al. (2003)

(Table 2.1 continued)

	Benthic recirculating annular flume	Sea Carousel	Bay of Fundy, Canada	Amos et al. (1992a, b)
		VIMS Sea Carousel	Chesapeake Bay and Middle Atlantic Bight	Maa et al. (1993)
			Baltimore Harbor	Sandford and Maa (2001)
		--	Humber estuary, U.K.	Widdows et al. (1998)
	Benthic recirculating race-track shaped flume	MORF	South Wales, U.K.	Black and Cramp (1995)
	Benthic vertical recirculating flume	ISEF	Dutch Wadden Sea coast	Houwing and van Rijn (1998); Houwing (1999)
	Benthic flow-through flume	Sea Flume	Buzzards Bay, Mass	Young (1977)
			Puget Sound Basin	Gust and Morris (1989)
		--	Boston harbor	Ravens and Gschwend (1999)
		NIWA I, II	Several rivers, wetlands, and lakes	Aberle et al. (2003, 2004, 2006) Debnath et al. (2007)
	Submerged impinging jet	CSM	Severn estuary, U.K.	Paterson (1989)
		modified CSM	Asylt mudflat, Germany	Tolhurst et al. (1999)
			Tollesbury, Essex, U.K.	Watts et al. (2003)
		--	Urbanizing basin near Toronto, Canada	Shugar et al. (2007)
	Circular inverted bell-shaped funnel	ISIS	Severn estuary, U.K.	Williamson and Ockenden (1996)

2.3.2 Erosion Relationships

2.3.2.1 Non-cohesive Sediments

The forces that resist the movement of non-cohesive sediments originate from the weight and buoyancy of a particle as given by

$$F_W = \gamma_s a_1 d^3 \quad \text{(Eqn. 2.1)}$$

$$F_B = \gamma_w a_1 d^3 \quad \text{(Eqn. 2.2)}$$

in which F_W and F_B represent the forces due to weight and buoyancy, respectively; γ_s is the specific weight of the particle; γ_w is the specific weight of water, a_1 is a particle shape factor; and d is the particle diameter. Submerged weight, W_s, is represented as the difference between these two forces shown as

$$W_s = F_W - F_B = (\gamma_s - \gamma_w) a_1 d^3 \quad \text{(Eqn. 2.3)}$$

The submerged weight resists the hydrodynamic drag force F_D on the particle and can be written in terms of a shear stress by

$$F_D = \tau a_2 d^2 \quad \text{(Eqn. 2.4)}$$

where F_D is the drag force; a_2 is another particle shape factor; and τ is the applied bed shear stress. The mean value of the boundary shear stress for steady uniform flow is given by

$$\tau = \gamma RS \quad \text{(Eqn. 2.5)}$$

in which R is the hydraulic radius and S being the bed slope. At incipient motion of a sediment particle on the river bed, the bed shear stress assumes its critical value τ_c. In dimensionless form,

the ratio of the critical drag force to the submerged weight of the particle becomes the Shields parameter given by (absent the shape factors):

$$\tau_{*c} = \frac{\tau_c}{(\gamma_s - \gamma_w)d} \quad \text{(Eqn. 2.6)}$$

As described by Sturm (2010), dimensional analysis of the problem of initiation of motion for coarse sediment proceeds from

$$\tau_c = f_1(\gamma_s - \gamma_w, d, \rho_w, \mu) \quad \text{(Eqn. 2.7)}$$

in which $(\gamma_s - \gamma_w)$ is the submerged specific weight and μ is the dynamic viscosity of water. The result is

$$\tau_{*c} = \frac{\tau_c}{(\gamma_s - \gamma_w)d} = f_2\left(\mathbb{R}\boldsymbol{e}_{*\boldsymbol{c}} = \frac{d\sqrt{\frac{\tau_c}{\rho_w}}}{\nu}\right) \quad \text{(Eqn. 2.8)}$$

in which τ_{*c} and $\mathbb{R}\boldsymbol{e}_{*\boldsymbol{c}}$ are the Shields parameter and Particle Reynolds number, respectively, and ν is the kinematic viscosity of water. These parameters, developed by Albert Shields (1936) and applied to flume experiments using a variety of sediments of varying specific gravity and size, resulted in presentation of the results in terms of the Shields parameter, which can be interpreted as the ratio of shear stress to the submerged weight of a particle (per unit area) at critical conditions, and the particle Reynolds number which is the ratio of the grain diameter to the viscous sublayer thickness. While useful, the fact that critical shear stress is implemented in both numbers prevents a direct calculation of critical shear stress. This problem was overcome with further dimensional analysis resulting in an additional dimensionless number (Julien 1995)

$$\tau_{*c} = f_3\left(d_* = \left(\frac{\left(\frac{\gamma_s}{\gamma}-1\right)gd^3}{\nu^2}\right)^{\frac{1}{3}}\right) \qquad \text{(Eqn. 2.9)}$$

where d_* is a dimensionless grain diameter. The inclusion by Julien to plot the Shields parameter versus the dimensionless grain diameter allows for the ability to calculate the critical shear stress required for the initiation of motion directly from the grain size. This graph can be seen in Figure 2.1 below.

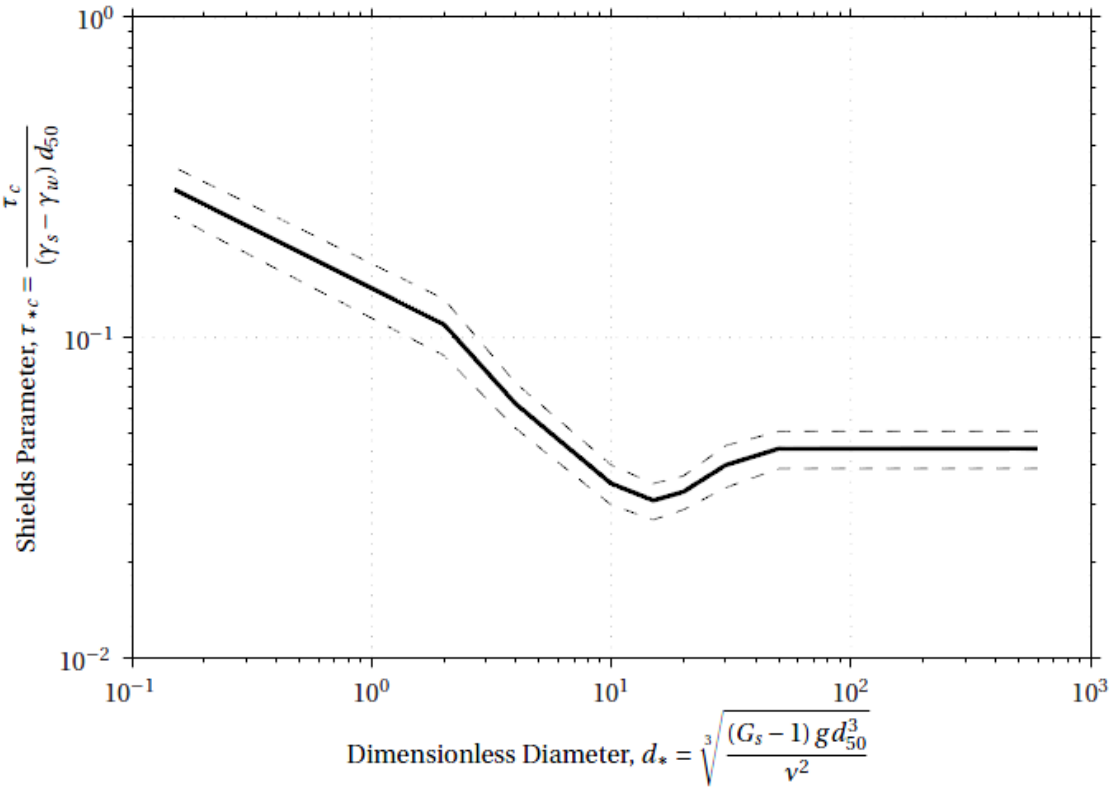

Figure 2.1: Shields Diagram $\tau_{*c}\ vs.\ d_*$ (Sturm 2001)

2.3.2.2 Cohesive Sediments

Cohesive sediments, as previously mentioned, have critical shear stresses that depend on many more variables compared to those in non-cohesive sediments. This can be accounted for

by considering the interparticle forces that are at work between cohesive particles. The two predominant interparticle forces are van der Waals forces and the diffuse double layer (Budhu 2011). The van der Waals force between two similar particles in a suspension can be calculated given the size of the particles, the distance separating them, and the shape of the particles. When considering the van der Waals force the shape of the interacting particles is an important factor. A pair of plate like particles will interact in a stronger fashion than a pair of spheres thanks to the exposed surface area and the distance that separates the two particles. After particle shape the chemical makeup of the particles can make a difference in the van der Waals force exerted by the particles (Santamarina et al. 2001). Lastly, size plays a key role in determining the dominant forces at work between particles as show below in Figure 2.2.

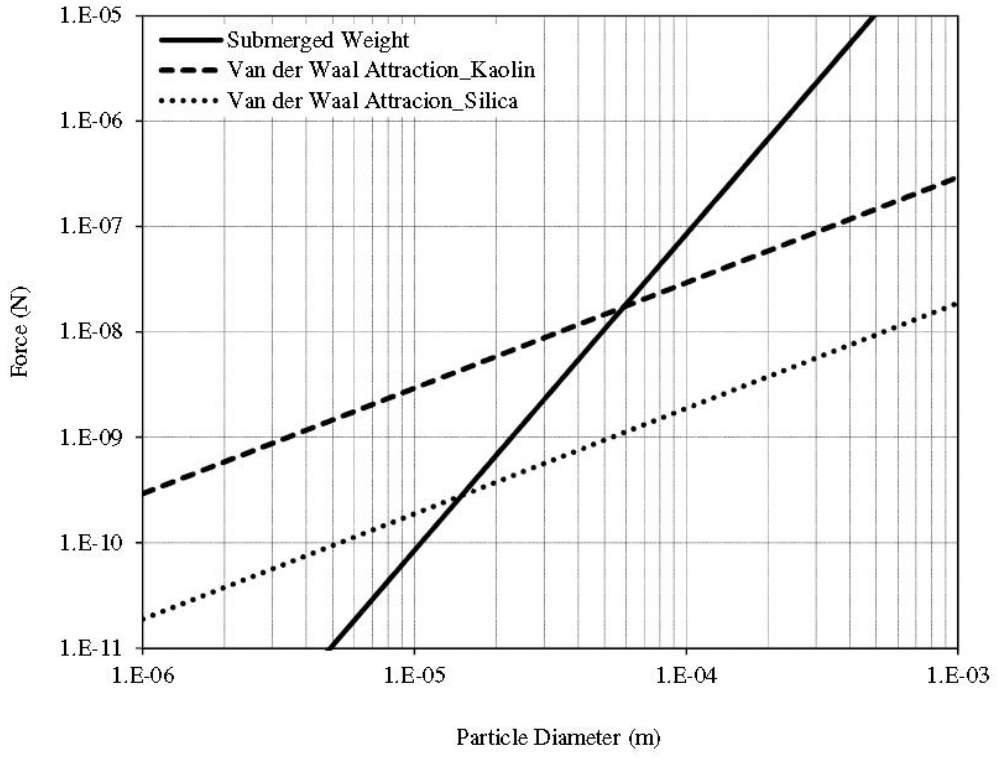

Figure 2.2: Force vs. Particle Size using Submerged Weight and van der Waals Equations

Source: Santamarina et al. (2001) as reported by Wang (2013)

The figure shows the van der Waals force acting on platy particles made of Kaolin and Silica and the force of submerged weight on a spherical particle. When the particle diameter is less than 60 μm and 15 μm, for Kaolin and silica respectively, the gravitational force is overwhelmed by the van der Waals forces. Given that the coarse-fine transition boundary is at 62 μm this limit where a van der Waals force and a submerged weight could have equal exertion on a particle and should be treated as such. Conversely, when two clay particles approach each other, their double layers form a repulsive force, and the water molecules and hydrated ions between them are displaced. The double layer repulsion force per unit area is based on interparticle distance and double layer thickness. While different calculation for the double layer repulsion force can be found, Santamarina et al. (2001) concludes that "two particles move closer to each other when ions are replaced with higher valence ions, when the ionic concentration of the pore fluid increases, or when the temperature decreases."

Because of the difficulty in quantifying interparticle forces in a sediment with variable mineralogy and particle structure, experimentalists have resorted to measuring the parameters in empirical erosion equations. A sampling of the equations that have been proposed can be seen in Table 2.3 complete with a short description. Many of the erosion equations have incorporated applied bed shear stress, critical shear stress, and sediment bed density with the goal of predicting an erosion rate. A common and frequently implemented equation relates erosion rate (E) to applied bed shear stress (τ). This equation as expressed below:

$$E = M(\tau - \tau_c)^n \qquad \text{(Eqn. 2.10)}$$

is known as the shear stress-flux equation and is the equation that will be used in this study. In Equation 2.10, E is the erosion rate (kg/m^2/s); τ is the bed shear stress (Pa); τ_c is the critical bed shear stress (Pa); and M and n are experimental constants. Not including τ , all of the variables

in the equation are directly related to the sediment's ability to resist erosion given a specific applied bed shear stress (Grabowski et al. 2011, Winterwerp and van Kesteren 2004, Mehta et al. 1989a).

In past research regarding cohesive sediments, n was assumed to have a value of 1.0. Many researchers simply assumed that the response to soil erosion was a linear response, yet it can be shown that a linear response is not always the case. When studying non-cohesive erosion, a number of researchers found exponential values greater than 1 to describe their erosion curves including Meyer-Peter Müller n=1.5 (1948), Van Rijn n= 2.1 (1984a), Engelund-Hansen n=2.5 (1967), Einstein-Brown n=3 (1950). When studying erosion rates of cohesive sediments with mud fractions varying between 22-87%, Walder (2015) found that the exponent $n \approx 1.75$. Given previous researchers having found that for non-cohesive substances $1<n<3$ and that cohesive sediments were assumed to be 1 based on Type II erosion; this study will consider the transition range between cohesive and non-cohesive sediments based on the concept of Type I erosion.

Table 2.3: Mathematical Expressions for Cohesive Sediment Erosion

Investigator(s)	Expression	Note
Ariathurani (1974)	$E = M(\tau - \tau_c)$	E: erosion rate ($kg/m^2/s$) τ: bed shear stress (N/m^2) τ_c: critical shear stress, value of τ as E≈0 (N/m^2) M, n: experimental constant
Lick (1982) and others	$E = M(\tau - \tau_c)^n$	
Kandiah (1974)	$E = M\left(\frac{\tau}{\tau_c} - 1\right)$	
Mehta (1991)	$E = M\left(\frac{\tau - \tau_c}{\tau_c}\right)$	
Gularte et al. (1980) and others	$E = \varepsilon_f \exp\left[\alpha(\tau - \tau_c)^\beta\right]$	E: erosion rate ($kg/m^2/s$) τ: bed shear stress (N/m^2) τ_c: critical shear stress, value of τ as E≈0 (N/m^2) ε_f: the flow erosion rate when τ-τ_c = 0, no mean flow velocity dependent surface erosion by definition; empirically determined. α, β: experimental constants
Roberts et al. (1998)	$e = A\tau^n \rho_b^m$ $Define$: $\tau_c = \left(\frac{e}{A}\right)^{\frac{1}{n}} \rho_b^{-\frac{m}{n}}$ @ $e = 10^{-4}$ (cm/s)	e: volumetric erosion rate (cm/s) τ: bed shear stress (N/m^2) ρ_b: bulk density (g/cm^3) A, n, m, c, k: experimental constants
	$e = c\tau^n \exp(-k\rho_b)$	
Bruid et al. (1999)	$e = \left(\frac{5.54\tau - 2.77}{\tau + 0.875}\right) + 0.178\tau - 0.809$ $\tau_{max} = 0.094\rho_w V^2 \left(\frac{1}{log\mathbb{R}e} - \frac{1}{10}\right)$ $e = e_i \; @ \; \tau = \tau_{max}$ $z_{max} = 0.18\mathbb{R}e^{0.635}$ $z = \frac{t}{\left(\frac{1}{e_i} + \frac{t}{z_{max}}\right)}$	e: scour rate (mm/hr) τ: bed shear stress (N/m^2) ρ_w: density of water (kg/m^3) V: mean flow velocity $\mathbb{R}e = \frac{VD}{v}$; D: pier diameter, v: kinematic viscosity of water e_i: erosion rate at τ_{max} (mm/hr) z: scour depth (mm) after a period of scour development time, t (hr)

Krone (1999)	$E = a_0 + a_1\rho_b$ where $a_i = b_{2i}\tau^2$ $\rightarrow E = b_{20}\tau^2 + b_{21}\tau^2\rho_b$	E: mass erosion rate ($kg/m^2/s$ or $g/cm^2/s$) τ: bed shear stress (N/m^2) or ($dynes/cm^2$) ρ_b: bulk density (kg/m^3) or (g/cm^3)
	$E = K_2(\rho_{max} - \rho_b)\tau^2$, $\rho_b < \rho_{max}$ Dimensional considerations: $E = \left(\frac{k}{\mu g}\right)\left(\frac{\rho_{max} - \rho_b}{\rho_s - \rho_w}\right)\tau^2$	ρ_{max}: the maximum bulk density that can be reached before the sediment structure becomes denser; can define from the plot of E vs. ρ_b ρ_s: density of particle (kg/m^3) or (g/cm^3) ρ_w: density of water (kg/m^3) or (g/cm^3) μ: viscosity of water (N*s/m^2) g: acceleration of gravity (m/s^2)
Sanford and Maa (2001)	$E = \rho_b\beta(\tau - \tau_{c0})\exp[-\gamma\beta(t - t_0)]$	E: erosion rate ($kg/m^2/s$) τ: bed shear stress (N/m^2) τ_c: critical shear stress (N/m^2) $\gamma = \frac{d\tau_c}{dt}$ t_0: time at which a new stress level is applied τ_{c0}: the value of τ_c evaluated at $t = t_0$

Source: Wang (2013) Table 2.3

2.4 Selection of Experimental Scope

Because determining the value of critical shear stress is important not only in calculating erosion rates but also in classifying and predicting bridge scour, this study focuses on obtaining experimental values of τ_c using Equation 2.10 and determining the soil properties on which it depends.

Torfs et al. (1996) found that there is a strong relationship between increasing mud content and a resultant increase in τ_c, where mud is a combination of silt and clay with water. Particularly if a predominantly sandy mixture has mud added to it, the increase in τ_c could be by a factor of 10, whereas if sand is added to a predominantly mud mixture the τ_c may only increase by a factor of 2. Torfs et al. suggests that if mud is greater than 15% by weight, the sediment will have a cohesive response rather than a granular response.

Van Ledden et al (2004). also investigated the erosion characteristics of sand-mud sediments. In this study the researchers looked at the network structure of the sediments and further analyzed the mud content of sample. Network structure, as based on particle density, was considered in this analysis to see if it had an effect on the sediments. A concept of using network structure and cohesion was developed to provide a basis to analyze previous experiments based on sediment properties, especially that of a sand-silt-clay triangle. Reanalyzing previous studies, it was shown that mud content was not as reliable as clay content for denoting a sediment as cohesive or not. When applied to a transition triangle, a definition of critical shear stress can be formed based on soil texture. Using this information six distinct textural types classified by the dominant network structure and cohesion properties can be defined: sand with no cohesion, sand with cohesion, a combination of sand-silt-mud with no cohesion, clay with cohesion, silt with no cohesion, and silt with cohesion. Additionally, implementing network structure, the differences in critical shear stress of clay types can be resolved, further refining the various levels of critical shear stress within the soil textural types.

Winterwerp et al. (2012) investigated purely cohesive soil types in order to gain a better conceptual framework involving floc erosion, surface erosion, and mass erosion. The conceptual

framework uses a combination of hydrodynamic and soil mechanics to address a better way of describing the three modes of erosion as described previously.

The soil mechanics of the framework showed that there are three size scales within which the soil can be analyzed for cohesive properties or properties that impart a cohesive-like strength. At the smallest scale, where individual particles are present, there are two types of cohesion; apparent cohesion and true cohesion. In apparent cohesion the strength of the soil is derived from a deformation rate and the permeability of the soil. True cohesion mainly relies on the electrochemical bonds of the soil which are much weaker (0.1-1 Pa) than those of the apparent cohesion (1-100 Pa).

Stepping up by another scale, particles are now influenced by group properties. At this level the packing structure of the particles plays a significant role especially when considering water content. When pressure is applied to the soil water is pushed out of the voids, but depending on the drained or undrained nature of the soil, the properties can be different. The properties at this level can be quantified using the undrained triaxial test.

The third scale is a macro scale where the soil is observed with the eye to see what level of a solid it is. This leads to the tests of water content using plastic limit, liquid limit, the plasticity index (*PI*), and activity. The plastic and liquid limits are the various levels of undrained shear strength while the *PI* is the difference between the two limits, and activity is determined by plotting the *PI* versus the percent clay. A soil with a plasticity index greater than 7 is considered to be when cohesive behavior begins (Winterwerp et al. 2012).

In general, the concept of using geotechnical properties such as water content, packing density, particle size, mud content, fines content, and clay content finds adequate basis for use in this research.

2.4 Prior Research at Georgia Tech

Navarro (2004) and Hobson (2008) took samples from bridge foundations around the state of Georgia with the intention of relating erosion to geotechnical parameters. The parameters *Fines* and d_* are good selections for this model considering that the variables have an inverse relationship and widely vary (0-75% *Fines* and d_* between 0.19 and 30.48) with each other in this data set. On the other hand, *w* is relatively constant (15-39%). The equation that they developed

$$\tau_{*c} = 0.644x10^{2.68Fines}d_*^{-0.409} \qquad \text{(Eqn. 2.11)}$$

works well for non-cohesive sediments with $d_{50} > 100$ μm. However, since the equation does not include water content or clay content, it is limited in its predictive capabilities especially where *Fines* is a large value and d_* is not small.

Wang (2013) took a different approach and investigated the fine sediments more in depth. In her experimentation she prepared a series of lab generated samples that were entirely fine (*Fines* =100%). The underlying objective was to see how cohesive sediments that contained Georgia Kaolinite and silica powder would alter the sediment erodibility. The data collected had a very wide range of water content (35-183%) and a decent range of *CSF* (3%-30%) that is similar to that found in the data from Navarro and Hobson. This analysis took into account not only the d_{50}, but also water content (*w*) and clay size fraction (*CSF*) as seen here:

$$\tau_{*c} = 8.46 - 27.76w + 73.69CSF + 83.22(w * CSF) \qquad \text{(Eqn. 2.12)}$$

However, this formula is limited to relatively fine sediments, $d_{50} < 100$ μm. The most interesting development from this equation is the use of an interaction term (*w x CSF*). This interaction term provides a number of benefits including a ratio between *w* and *CSF* for the modeling of

cohesive behavior and a size distribution modifier for statistics. Much in the same way that *Fines* and d_* had an inverse relationship in Equation 2.11 this equation also exhibits a linear relationship between *w* and *CSF*.

The investigation conducted by Harris (2015) studied sediments that were a composition of sand and clay to bridge the divide between non-cohesive and cohesive sediments. His data exhibited a similar series of proportions like that of Wang, but instead of having 100% *Fines* for all data points, there was some variation between 43% and 100%. An initial assessment found that a formula much like the one formulated by Wang fit the data best; the key difference was that Harris (2015) added a *Fines* term. The presence of the *Fines* term in this equation as well as that of Navarro and Hobson reinforced the importance of using it as a parameter. As a result, a weighted formula was generated to combine Equations 2.11 and 2.12. The resulting formula is

$$\tau_{*c} = (Fines^{0.235}) * \left(3.54 - 22.2w + 93.7CSF + 63.0(w * CSF)\right) + (1 - Fines^{0.235}) * (0.668 * 10^{2.51Fines} * d_*^{-0.423}) \quad \text{(Eqn. 2.13)}$$

His formula worked well in predicting the Shields parameter for both combined data sets of Navarro, Hobson, and Wang, but was not perfect in describing his own data set. This was still accepted as the preferred equation as it could still predict the non-cohesive and cohesive sediments accurately.

This study will aim to test this formula by implementing the use of sediments that span the transition zone between non-cohesive and cohesive. The combination of sand, silt, and clay in ratios that are naturally present should provide a proper data set in order to test Equations 2.11-2.13 properly or possibly define a new relationship that can more accurately predict critical shear stress.

2.5 Summary of Literature Review

The information in this chapter represents a brief, but comprehensive overview of the attempts by the scientific community to describe sediment transport related to geotechnical parameters in the sediments. Initially, research was conducted on non-cohesive, or coarse, sediments based on the physical properties of sediments such as grain size, density, and properties of the fluid to which the sediment is subjected. This provided excellent data from which investigators began to investigate cohesive, or fine, sediments. These cohesive sediments had different properties that changed the way erosion had to be considered. The cohesive particles have additional factors such as electrochemical interactions and structural interactions that make erosion and critical shear stress more difficult to predict. These factors can be determined roughly using water content and sediment content measurements. Cohesive sediments have been known to exhibit four types of erosion, but only two of them, surface and floc erosion, are in the scope of this study. The two modes listed are quite different and as a result have different thresholds of erosion. Four previous studies at Georgia Tech have explored this area in depth (Navarro 2004, Hobson 2008, Wang 2013, Harris 2015). Navarro and Hobson provided field data for comparison with controlled samples. Wang and Harris provided laboratory based processes and results that allowed for more controlled results and developed equations that proved effective for their data. Harris proposed an equation that can predict the Shields parameter for non-cohesive and cohesive sediments which will be tested in this study. The next chapter will go into detail about the processes and methods that were implemented in this study for analysis of sediment properties, erosion rates, and critical shear stresses.

Chapter 3

Experimental Methodology

This chapter will describe the processes and reasoning behind the setup, execution, and conclusion of testing required for this erosion research. The methods for measuring sediment properties of water content, temperature, pH, conductivity, bulk density, and size distribution are summarized, and the scope of erosion testing is discussed within. Also, the preparation of samples, the use of the tilting flume, and any other relevant equipment during the tests are described in detail. In order to ensure that the results of this research are repeatable, the steps involved have been recorded to allow for future testing and to isolate any experimental errors present in the analysis.

3.1 Sediment Classification, Selection, and Preparation

Preparation of the samples required three types of sediments in varying quantities: Georgia Kaolinite (Kaolin), ground silica, and fine industrial sand. These three sediments represent clay, silt, and sand sediment types present in sediments native to Georgia. The Georgia Kaolinite was purchased from IMERYS in Roswell, Georgia. The Kaolin is mined in Dry Branch, Georgia and is graded as Hydrite Flat DS. The Kaolin is processed wet and is graded using the Sedigraph technique. The material is roughly 95% Kaolin with small amounts of mica that varies from batch to batch based on the natural source of the material. During production, no additives are used. The ground silica (SIL-COSIL 106) was supplied by the US Silica Company in Ottawa, Illinois. The fine industrial sand comes from the Standard Sand and Silica Company and was purchased from Surface Prep Supply in Haines City, Florida. The sand is graded between #70 and #200 sieves, has a median particle diameter of 0.147 mm and a specific

gravity of 2.65. Tables 3.1, 3.2, and 3.3 outline the properties for each of the above sediments, respectively.

Table 3.1: Clay Characteristics

Property	Units	Value
Median particle size (d_{50}) hydrometer	μm (*micron*)	2.7
Median particle size (d_{50}) Sedigraph (a)	μm (*micron*)	4.0
Brightness (a)	(GE% of MgO)	81.5
pH	(20% Solids)	4.83
Residue on 325 mesh screen (a)	(wt. %)	0.25
Oil Absorption	(%)	34
Surface area	(B.E.T. Nitrogen - m2/g)	7
Specific Gravity (b)	--	2.58

(a) Reported by Harris (2015)
(b) Reported by Wang (2013)

Table 3.2: Silica Characteristics

Property	Units	Value
Median particle size (d_{50})	μm (*micron*)	32
Hardness (Mohs)	--	7
Mineral	--	Quartz
pH	--	7
Specific gravity	--	2.65

(Source: Wang 2013 Table 3.2)

Table 3.3: Fine Sand Characteristics

Property	Units	Value
Median Particle size (d_{50})	μm (*micron*)	147
Mineral	--	Quartz
Specific Gravity	--	2.65

The selection process of the mixture ratios was based on the idea of mimicking natural sediment ratios. Hobson and Navarro had taken samples from sediments at the bases of bridge piles in Georgia abnormally affected by Tropical Storm Alberto 1994. This analysis included

plotting and categorizing the sediment samples based on sand, silt, and clay content and the physiographic region within which each one was taken from. By plotting this information on a soil textural diagram, x and y axes representing sand and silt, respectively, with clay as a series of plotted dotted lines, the individual points can tell if the geophysical regions dictate variability between sediment types. This variability can then show hotspots of sediment types that can be investigated in order to cover the most sample types with the smallest possible scope, thereby reducing the size of the research to a manageable quantity. Based on the soil textural diagram shown in Figure 3.1 below, a few hotspots are seen towards the sandy regions and high clay regions. Both of these regions have been investigated before as they represent the non-cohesive and cohesive erosion responses mentioned previously.

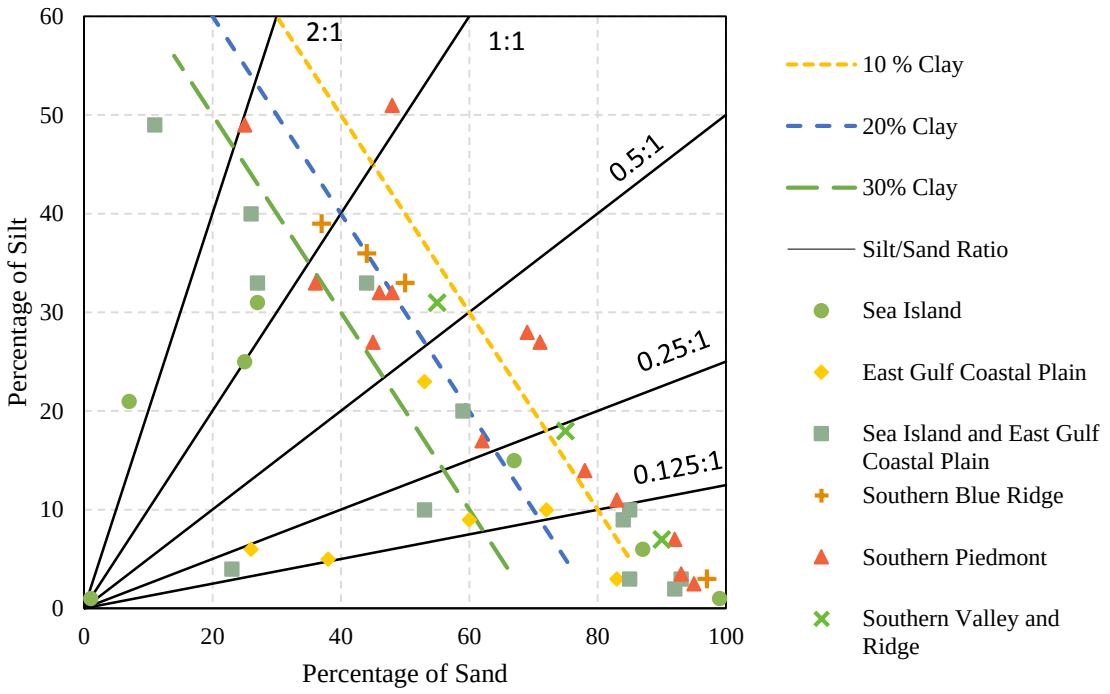

Figure 3.1: Soil Textural Diagram of Sediment Samples from Georgia Bridge Foundations

It should be noted though that there is a densely packed region in the area between 10% and 30% clay and between the 1:1 and 0.5:1 silt to sand ratios. Beneath 30% clay, sediments exhibit a more cohesive response and beyond 10% they are primarily granular. As a result, this region became the scope of interest for this research investigation. Samples were prepared the same way using a constant ratio of 0.75:1 silt to sand ratio and varied with clay content being 10%, 20%, or 30%.

Upon completion of the sediment selection, mixtures were then prepared for testing using a repeatable method. With a constant silt to sand ratio by weight and variances in the sediments only with respect to the percentages of clay, three mixtures were prepared for each series of critical bed shear stress tests. Each test was performed under fully saturated conditions, so for 600 g of sediment, 800 g of water was added and then uniformly mixed using an electric blender (Wang 2013). Immediately after the mixing, an Oakton Waterproof PC 300 was used to measure the pH, temperature, and conductivity of the mixtures. The probes are inserted into the slurry at the same depth to ensure repeatability. The mixture was then poured into a Shelby tube with a movable bottom that could be moved upward by a piston for the extrusion of the sample during testing. Five tubes with an inner diameter of 72.8 mm, external diameter of 76.2 mm, and an average height of 290 mm were used to hold the samples. The samples were allowed to settle to full sedimentation over 24 hours which was determined to be an adequate time for this research (Wang 2013). At the end of 24 hours, the sample was then placed onto a piston beneath the flume and advanced into the flume to remove excess water before testing. In Table 3.4 the various samples with dry weights and percentages of mass for each sediment component are listed.

Table 3.4: Mix Types and Proportions of Sediment Components

Sediment Mix Type	Fine Sand		Ground Silica		Georgia Kaolin		Total Mass (g)
	Dry Weight (g)	Proportion of Mix (%)	Dry Weight (g)	Proportion of Mix (%)	Dry Weight (g)	Proportion of Mix (%)	
10% Kao	308.4	51.4%	231.6	38.6%	60.0	10.0%	600.0
20% Kao	274.2	45.7%	205.8	34.3%	120.0	20.0%	600.0
30% Kao	240.0	40.0%	180.0	30.0%	180.0	30.0%	600.0

3.2 Sediment Characteristics

Each sediment sample type was subjected to a series of tests in order to determine properties that could be important in determining erosion rates. The samples were subjected to tests for grain size distribution, water content, dry and bulk densities, temperature, pH, and conductivity of the sediment.

Grain size distribution was determined using both sieve analysis and hydrometer tests. The fine sand and ground silica were subjected to sieve tests individually using the standards set by ASTM C136-01 (ASTM International 2001). Sieves with open area sizes of 0.250 mm (#40), 0.210 mm (#70), 0.150 mm (#100), 0.106 mm (#140), 0.075 mm (#200) were utilized for the sand and silica. Given the much smaller size of the silt and clay particles, a hydrometer test was conducted following the standards in ASTM D7928-16 (ASTM International 2016). The results of these tests can be seen in Figure 3.2 below.

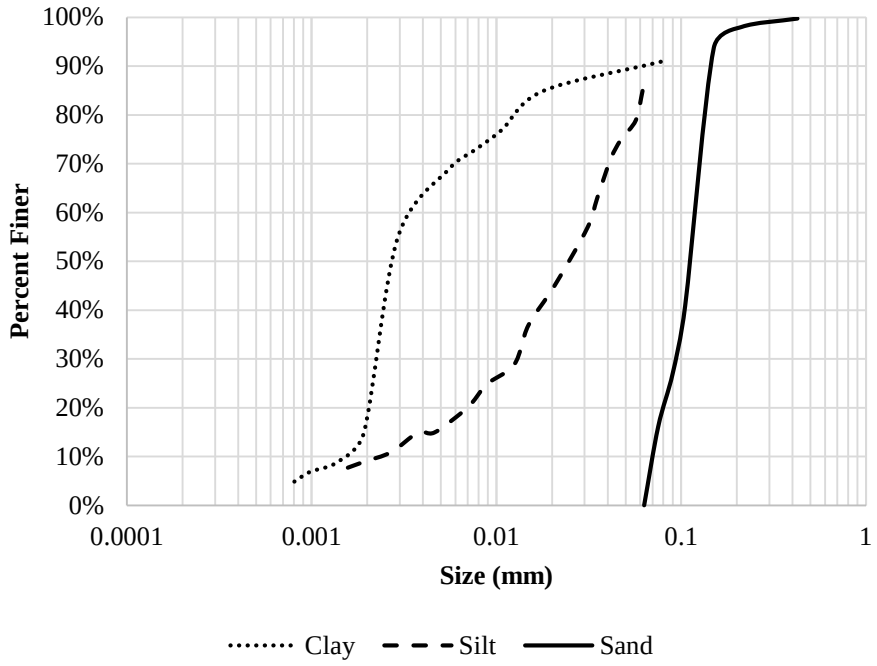

Figure 3.2: Grain Size Distribution of Sediment Components

Water content is also used in order to find the bulk (ρ_b) and dry (ρ_d) densities of the sediment sample. The equations below show the calculations for bulk and dry density using the mass of wet sediment or dry sediment, respectively over the total sediment volume.

$$\rho_b = \frac{m_{wet}}{V_t} \quad \text{(Eqn. 3.1)}$$

$$\rho_d = \frac{m_s}{V_t} \quad \text{(Eqn. 3.2)}$$

As in previous studies, this study assumes that all specimens tested were 100% saturated and so the total volume (V_t) is comprised of water and sediment only with negligible air present. This means that V_t depends on water content and can be summarized as shown below.

$$w = \frac{m_{wet} - m_{dry}}{m_{dry}} \quad \text{(Eqn. 3.3)}$$

$$V_t(w) = V_w + V_s = \frac{m_w}{\rho_w} + \frac{m_s}{\rho_s} = \frac{w*m_s}{\rho_w} + \left[\frac{m_{Sand}}{\rho_{Sand}} + \frac{m_{Silt}}{\rho_{Silt}} + \frac{m_{Kaolin}}{\rho_{Kaolin}}\right] \quad \text{(Eqn. 3.4)}$$

Where V_w = the volume of water; V_s = the volume of solids; ρ_{Sand} = the dry density of sand (2.65 g/cm^3); ρ_{Silt} = the dry density of silt (2.65 g/cm^3); ρ_{Kaolin} = the dry density of Georgia kaolin (2.58 g/cm^3).

The masses of each sediment property are related to each other but require some additional derivation in order to simplify to a single unknown. Silt and sand have a fixed ratio of 0.75 as discussed previously, so this is used to find the fraction of sand in the overall equation and then is used in the initial equation to find the fraction of silt. Below is the next step of the volume derivation accounting for these additional factors.

$$0.75 = \frac{Silt}{Sand} \quad \text{(Eqn. 3.5)}$$

$$m_{Sand} = m_s(Sand) \quad \text{(Eqn. 3.6)}$$

$$m_{Silt} = m_s(Silt) = m_s(0.75 * Sand) \quad \text{(Eqn. 3.7)}$$

$$m_{Kaolin} = m_s(Kaolin) \quad \text{(Eqn. 3.8)}$$

$$V_t(w) = \frac{w*m_s}{\rho_w} + \left[\frac{m_{Sand}}{\rho_{Sand}} + \frac{m_{Silt}}{\rho_{Silt}} + \frac{m_{Kaolin}}{\rho_{Kaolin}}\right] = \frac{w*m_s}{\rho_w} + \left[\frac{m_{Sand}}{\rho_{Sand}} + \frac{m_s(0.75*Sand)}{\rho_{Silt}} + \frac{m_{Kaolin}}{\rho_{Kaolin}}\right] \quad \text{(Eqn. 3.9)}$$

Where *Sand*, *Silt*, *and Kaolin* are the portion of sand, silt, and kaolin by dry weight in decimal fraction, respectively.

3.3 Hydraulic Flume Testing Procedure

The erosion testing performed for this paper was conducted in the Dalton Hydraulics Laboratory in the School of Civil and Environmental Engineering at the Georgia Institute of Technology. All samples were placed in a tilting, rectangular, recirculating flume of dimensions

6.1 m long and 0.38 m wide. The flume is supplied by a 1.9 m^3 tank that is connected to a variable speed 6-in. slurry pump and can pump water and solids to the headbox of the flume. The flume bed is lined with a fixed gravel that has a d_{50} = 3.3 mm to ensure a fully rough turbulent flow leading to the sample insertion point in the bed of the flume (Hobson 2008). The specimen that settled in the Shelby tube on the previous day was then placed onto a hydraulic jack that pushed a piston to extrude the sample into the flume. Comprehensive images of the experimental layout can be seen in Figures 3.3 and 3.4 below.

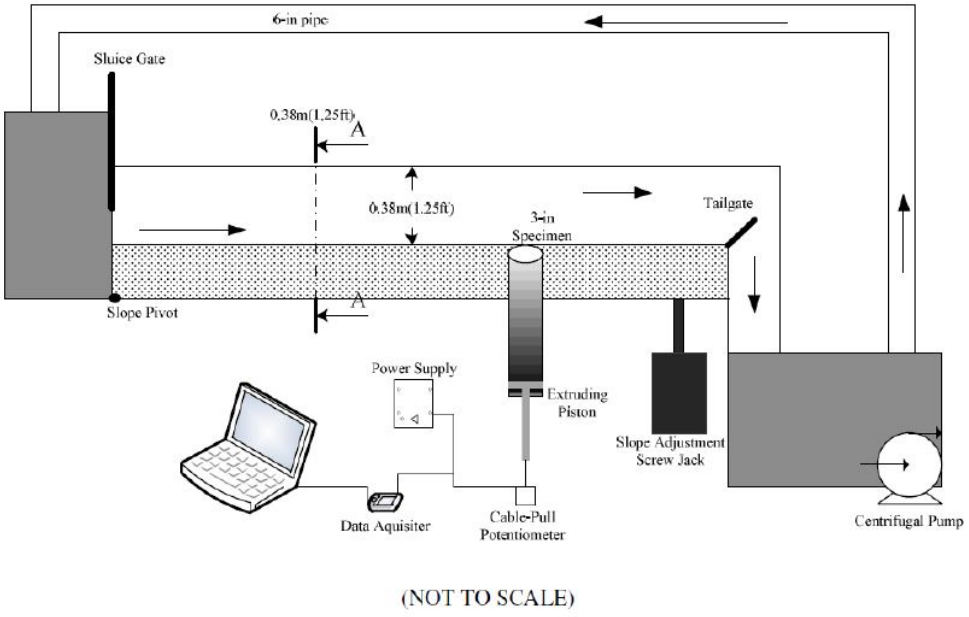

Figure 3.3: Flume Apparatus and Collection System (Wang (2013) Figure 3.7)

Figure 3.4: Experimental Sediment Erosion Flume in Operation

For each erosion test the flume had to have certain parameters set so that the required bed shear stress (τ) would be attained. The bed shear stress was established as a function of bed slope (S), flow rate (Q), and flow depth (y). The bed slope was set by using an electric screw jack set near the end of the flume with the far end of the flume near the head tank set on a simple pivot. The screw jack revolution counter was used to determine the slope of the flume, and this counter was calibrated using a rod and level surveying system. The flow rate was measured using a manometer which is connected to a bend meter that was gravimetrically calibrated. The calibrations for these two systems are seen below in Figures 3.5 and 3.6, respectively. The calibration of the slope counter was performed during this experiment due to a mechanical failure of the screw jack that needed to be replaced before experiment could be conducted.

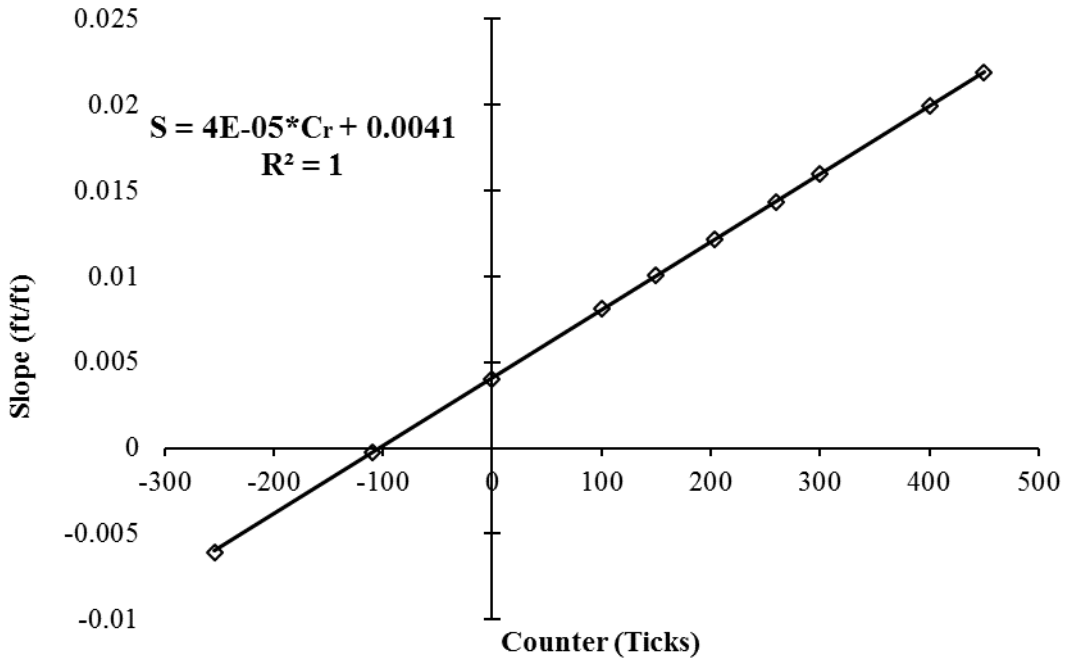

Figure 3.5: Calibration of Flume Slope Counter and Slope. 0 Ticks is 00000 on the Counter. Positive Values Increase the Counter and Negative Values Count Downward from 99999.

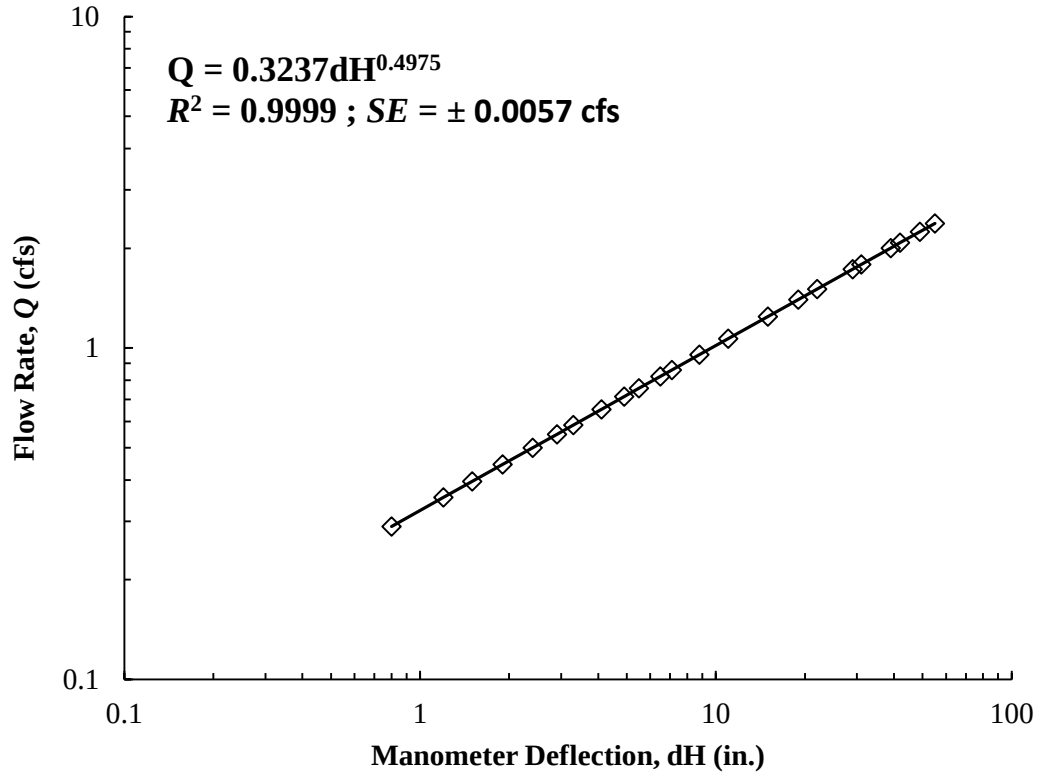

Figure 3.6: Calibration of Manometer and Flowrate (Source: Navarro 2004)

Uniform flow depth was set by raising or lowering the tailgate at the end of the flume using a threaded rod and handle. This is possible since all flows that were tested were subcritical flows. The normal depth was measured from the asymptotic approach depth of mild slope water surface profiles for gradually-varied flows. Given a uniform flow condition and the normal flow depth, the bed shear stress can be determined using the open channel uniform flow equation (Sturm 2001):

$$\tau = \gamma_w y S \qquad \text{(Eqn. 3.10)}$$

where γ_w is the specific weight of water; y is the normal depth; and S is the bed slope. This equation was validated by using a Laser Doppler Velocity meter (LDV) to measure the centerline velocity profiles from which the bed shear stress was determined using the Clauser method. It was found that the wall effects could be safely neglected in the calculation of the bed shear stress. The resulting test information was established by previous investigators in this flume (Ravisanger et al. 2001; Navarro 2004; Hobson 2008). The complete list of hydrodynamic conditions present during testing is shown in Table 3.5 below.

Table 3.5: Hydrodynamic Conditions

Flow Rate $Q\left(\frac{m^3}{s}\right)$	Slope $(x10^{-3})$	Water Depth y (cm)	Average Velocity V (m/s)	Bed Shear Stress τ (Pa)	Froude Number $Fr = \frac{V}{\sqrt{gy}}$	Reynolds Number $Re = \frac{4RV}{v}$
0.0156	2.00	8.66	0.474	1.71	0.514	$2.83*10^5$
0.0227	1.99	10.95	0.543	2.15	0.523	$3.51*10^5$
0.0283	1.99	12.65	0.588	2.48	0.528	$3.89*10^5$
0.0227	3.00	9.60	0.619	2.83	0.638	$3.93*10^5$
0.0283	3.00	11.00	0.677	3.24	0.651	$4.39*10^5$
0.0283	4.00	10.05	0.741	3.94	0.746	$4.73*10^5$

After all the hydrodynamic conditions were set for the current test, flow was halted, with the pump running in order to maintain proper system head. The sample area was drained to allow for insertion of the Shelby tube with the sediment sample. The sample was extruded from the tube sufficiently to remove excess water at the top of the sample that remained after 24 hours of settling. Once the top of the sediment column was extruded just above the flume bottom, a sample was taken with a spatula to measure the water content at that level within the sediment. The sediment column was then covered with a metal plate to protect it until testing time when test conditions were reached again. To record the thickness of specimen extrusion, a cable-pull potentiometer was connected to the bottom of the hydraulic jack. A computer data acquisition system controlled by a Matlab program read a voltmeter and recorded the voltage change as the specimen was extruded with respect to time. The potentiometer calibration can be seen in Figure 3.7 below.

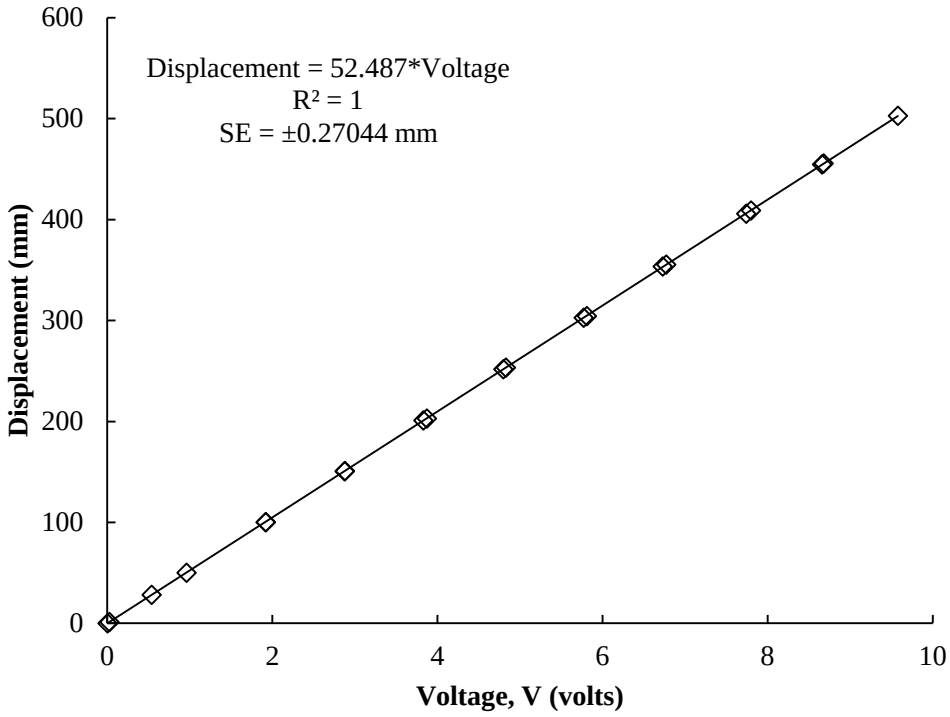

Figure 3.7: Calibration of the Potentiometer (Source: Harris 2015)

During the erosion test the operator visually maintained a consistent sample height by extruding the sample as time progressed. When the sample eroded to a level just beneath the surrounding bed level as guided by a fixed laser pointer, the operator raised the sample using the hydraulic jack to a level just above the top of the sediment in the flume bed. This process continued until the end of the test which varied from 60 to 420 seconds as determined by the amount of time it took to erode a specimen roughly 1/3 of the full height. As the test proceeded, due to the recirculating nature of the flume, the water gradually became cloudy and reached a point where visual contact with the specimen in the flume was either impaired or completely blocked. At this point, flume operation was stopped in order to drain it, refill the reservoir, and reset the hydrodynamic conditions.

Before and after each erosion test of a portion of the sediment column, a small sample was extruded and collected with a spatula for use in the determination of the water content. Error was reduced by using an average of the two water content measurements for each erosion test. Erosion rate (E) was calculated from the measured depth eroded and time recorded during the erosion of each layer in the experiment as:

$$E = 0.001 \frac{\Delta D}{\Delta t} \rho_d \qquad \text{(Eqn. 3.11)}$$

in which E is the erosion rate per unit area in kg/m^2/s; $\frac{\Delta D}{\Delta t}$ is the slope of the best-fit line of measured displacement (mm) vs. time (sec) from the recorded data; and ρ_d is the measured dry density of the eroded layer in kg/m^3. An example of the erosion rate data from the 20% Kaolinite (by weight) test conducted with τ = 2.84 Pa is shown in Figure 3.8.

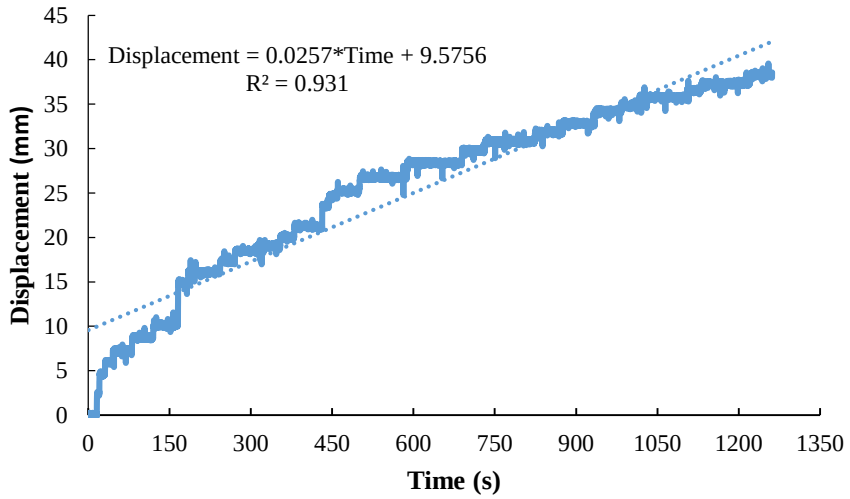

Figure 3.8: Erosion of 20% Kaolinite Sample where τ=2.84 Pa

After all experiments had been completed, the results were organized based on percent clay content (by size fraction with $d \leq 0.002$ mm) and water content. The data were separated into three kaolin mixture content groups and then subdivided water content based groups. These water content groups contain erosion data with at least four of the five tested bed shear stresses. This allows for comparison of the erosion data to the geotechnical data by water content rather than by depth.

Each water content group was plotted on its own graph of erosion rate versus applied bed shear stress. Microsoft Excel 2010 software was then used to implement a Generalized Reduced Gradient (GRG) nonlinear solving method to obtain parameters of a best fit of Equation 2.9, $E = M(\tau - \tau_c)^n$. The solver had a constraint precision of 0.01. The fixed bed shear stresses associated with each of the measured erosion rates provided the input data, and values of *M*, *n*, and τ_c were optimized until a best-fit curve that minimized the summed square of errors (*SSE*) between measured and predicted erosion rates was determined. The value of *SSE* is given by

$$SSE = \sum\left(E_i - \widehat{E}_i\right)^2 \quad \text{(Eqn. 3.12)}$$

and E_i is the measured valued and $\hat{E}_i$ is the predicted value. The parameters *M* and *n* vary by water content and sediment mixture type. Critical shear stress (τ_c) is the *x*-intercept for the best-fit curve since it defines the point at which no erosion is occurring or the point of incipient motion. This process has been implemented by several other researchers who have validated its goodness of fit (e.g. Ravisanger 2001; Ravisanger et al. 2001, 2005; Navarro 2004, Hobson 2008, Wang 2013, Harris 2015).

3.4 Summary of Experimental Procedures

The contents of this chapter have described the processes and procedures that were implemented to measure the erosion of various sediments that are comprised of sand, silt, and clay. The succeeding chapter will describe in depth the results of these experiments to relate the properties of sediments to the critical shear stress. This work follows in the thread of that completed by Navarro (2004), Hobson (2008), Wang (2013), and Harris (2015) by investigating the relationship of sediment particle sizes to erosion rates in the transition zone between non-cohesive and cohesive sediments. Navarro and Hobson investigated field samples of mostly coarse Georgia sediments. Navarro and Hobson also provided information that can help tie together the results from all four previous studies and the current study. The field data that were collected by Navarro and Hobson allowed for a soil textural diagram to be created. This provided a basis from which specific sediments could be generated in the lab that would mimic the sediment ratios of those in nature. Wang and Harris followed suit by investigating the relationship of silt-Kaolinite and sand-Kaolinite mixtures, respectively, that were prepared in the lab. This current study aims to bridge the gap between the analysis of field samples native to

Georgia and the laboratory mixed samples. The next two chapters will describe the relationship between the field and lab samples.

Chapter 4

Experimental Results

This chapter summarizes the data that have been collected for this thesis implementing the methods outlined in Chapter 3. Section 4.1 covers the geotechnical properties of the sediments that were analyzed in the course of these experiments. This includes the sample distribution of sediment particle size, water content, percentage of fines, clay size fraction, pH value, temperature, and conductivity of the sediment mixtures. Section 4.2 describes the results of the erosion tests.

4.1 Sediment Properties

The main objective of this thesis is to correlate critical shear stresses with the properties of a given sediment. In this section, the properties of the tested sediments will be outlined with regards to particle size distribution, water content distribution, pH, temperature, and conductivity. Particle size distribution samples were prepared exactly like those for erosion analysis in accordance with the procedures in Chapter 3. Size distribution was performed on pure samples of kaolin, silt, fine sand, and mixed composition samples with 0.75 silt to sand ratio and varying kaolin contents of 10%, 20%, and 30% by weight. In the case of the erosion tests, samples were taken before and after each erosion test for determination of the average water content during an erosion test. Values of pH, temperature, and conductivity were measured for a series of replicated samples having proportionally similar mixtures by weight.

4.1.1 Size Distribution

Size distribution tests were performed on the pure components of the sediments, kaolin, silt, fine sand, as well as the composition mixtures. For the composition mixtures each one was

prepared like those that were prepared for the erosion tests. After 24 hours, the sample was extruded into groups of 25 mm long sections and analysis was performed using the wet sieve technique and ASTM 7928-16. Figure 4.1 shows the composite samples below.

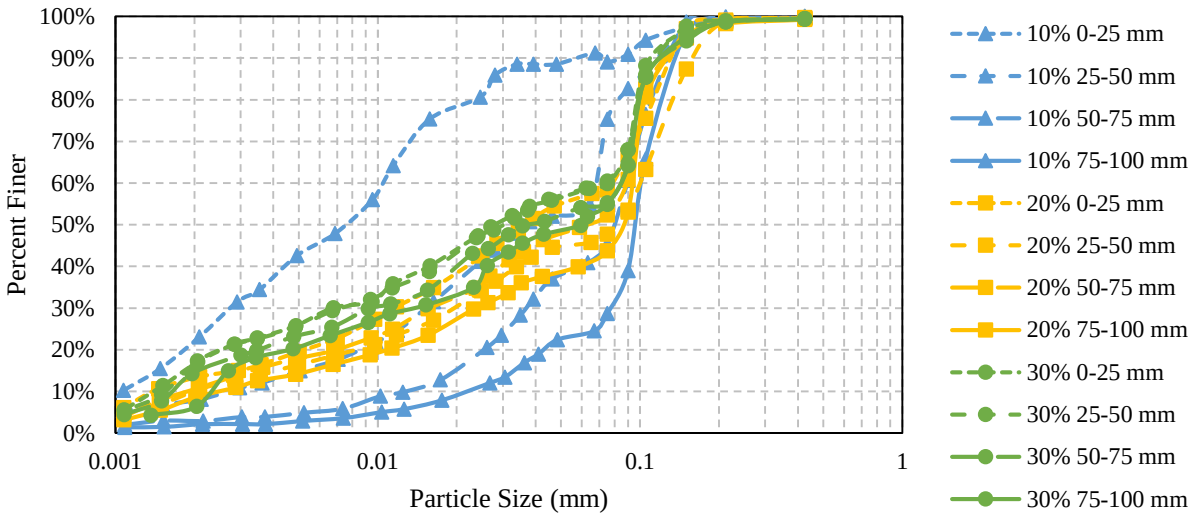

Figure 4.1: Size distribution of composite samples based on depth

Using this figure, particle sizes can be determined for the various sediment mixtures based on depth in the sediment sample. These measures of size (d_{xx}) are the particle sizes for which xx percentages of the total sample are smaller by weight. This means that the values of d_{60}, d_{50}, d_{30}, and d_{10} are the diameters of particles which are 60%, 50%, 30%, and 10% are smaller by weight, respectively. In Figure 4.1, it can be seen that as the clay content increased, the segregation of the sediments during settling decreased as shown by the size distribution curves for each sediment layer collapsing to nearly the same curve for higher Kaolinite content. This is especially noticeable between the 10% and 20% mixtures. Also, the average particle size (d_{50}) decreased with increasing Kaolinite content as expected.

In addition to the size distribution diameters, the coefficient of uniformity (C_u) and coefficient of coefficient of curvature (C_c) were calculated from.

$$C_u = \frac{d_{60}}{d_{10}} \quad \text{(Eqn. 4.1)}$$

$$C_c = \frac{{d_{30}}^2}{d_{10}d_{60}} \quad \text{(Eqn. 4.2)}$$

These values are useful for classifying sediments, primarily those that are considered to be coarse with a d_{50} value equal to or greater than 0.075 mm. Based on the information in Table 4.1 the samples from the 75-100 mm layer in both the 10% and 20% mixtures are coarse. An additional pair of values in Table 4.1 include the Clay Size Fraction (*CSF%*), which is the percentage of particles that are finer than 0.002 mm by weight, and the Percent Fines (*Fines*) which is defined as the percentage of particles smaller than 0.062 mm.

Table 4.1: Sediment Particle Properties and Distribution

Mixture	Depth (mm)	d_{60} (mm)	d_{50} (mm)	d_{30} (mm)	d_{10} (mm)	C_u	C_c	*CSF*	*Fines*
100% Sand	N/A	0.120	0.110	0.093	0.070	1.71	1.03	0%	0%
100% Silt	N/A	0.031	0.025	0.013	0.002	15.50	2.73	10%	84%
100% Kaolinite	N/A	0.0033	0.0028	0.0024	0.0015	2.20	1.16	15%	90%
10% Kaolinite	0-25	0.011	0.0078	0.0027	0.0011	10.00	0.60	22%	90%
	25-50	0.067	0.037	0.015	0.0027	24.81	1.24	8%	54%
	50-75	0.089	0.070	0.036	0.013	6.85	1.12	2.85%	40%
	75-100	0.100	0.095	0.078	0.023	4.35	2.65	2%	23.50%
20% Kaolinite	0-25	0.080	0.037	0.012	0.0014	57.14	1.29	13%	57%
	25-50	0.100	0.071	0.020	0.002	50.00	2.00	10%	45%
	50-75	0.089	0.062	0.016	0.0018	49.44	1.60	10.50%	50%
	75-100	0.092	0.075	0.024	0.0016	57.50	3.91	8.60%	41%
30% Kaolinite	0-25	0.075	0.030	0.006	0.0014	53.57	0.34	17%	58%
	25-50	0.070	0.028	0.0070	0.0016	43.75	0.44	17%	58.50%
	50-75	0.082	0.039	0.0094	0.0016	51.25	0.67	14.50%	54.50%
	75-100	0.082	0.043	0.011	0.0017	48.24	0.87	14.90%	53%

4.1.2 Water Content

Water content measurements were taken via sampling before and after every erosion test which allowed for an average water content to be calculated for erosion calculations. Each Shelby tube containing a specific sediment mixture had three to four erosion tests performed on it at the same shear stress resulting in four to five water content samples. These tests were repeated on identical Shelby tube samples for all five bed shear stresses. The thickness of the eroded layer varied for each test, resulting in different depths for a given water content. Water contents versus depth for all three mixtures can be seen in Figure 4.2 (a) through (c) below.

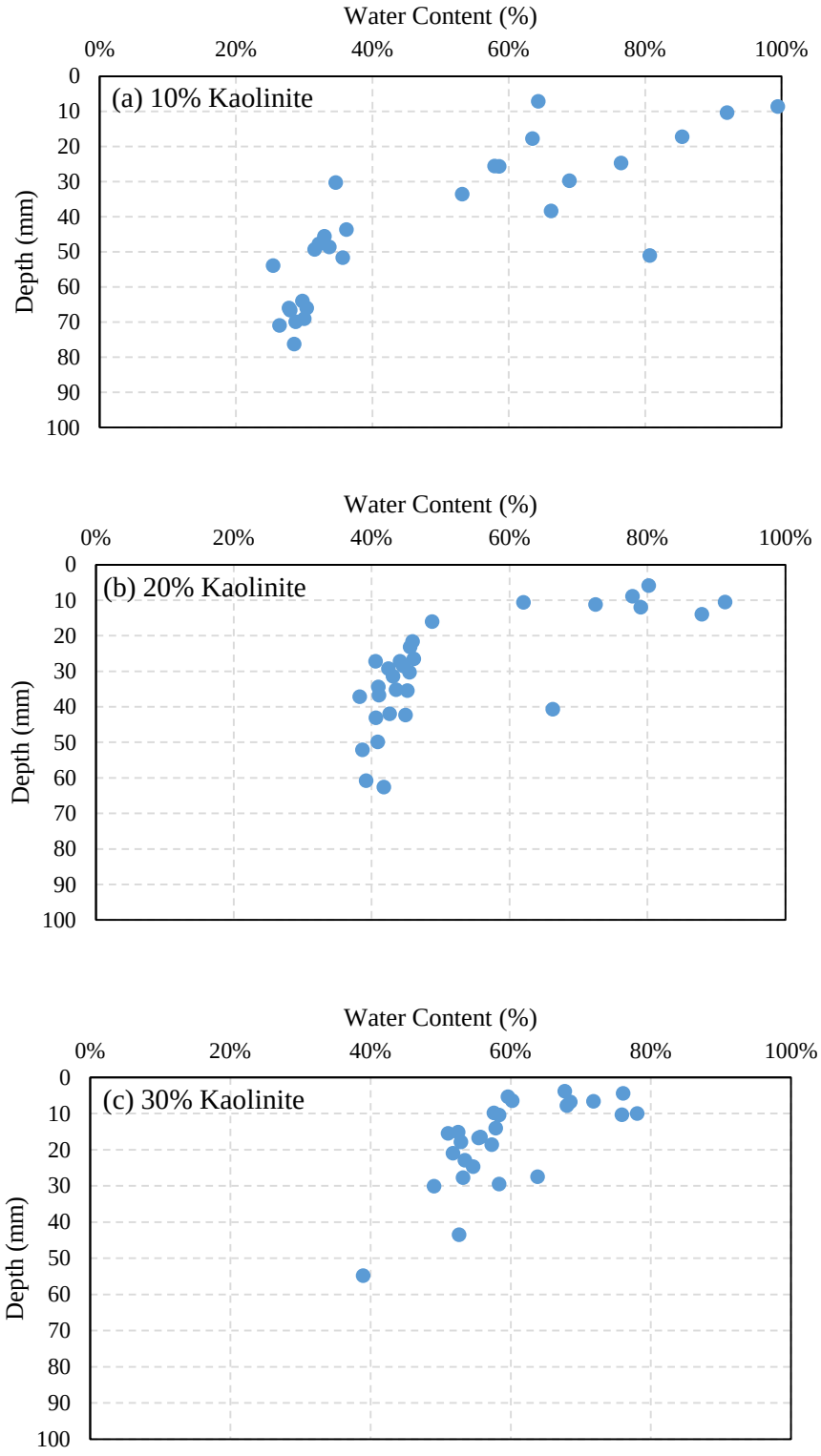

Figure 4.2: Water Content Versus Depth for Erosion Layers Collected During Tests of (a) 10% Kaolinite, (b) 20% Kaolinite, (c) 30% Kaolinite

4.1.3 Sediment Properties Grouping

The sediment properties as previously mentioned were calculated in groups of 25 mm per Shelby tube mixture, so there are four groups per Shelby tube with varying sediment properties. However, the grouping of samples from the erosion tests was different. Because water content affects the erosion rate and the critical shear stress, all the tests for a particular mixture type were broken into distinct groups based on the average water content of the eroded sample. For a Kaolinite mixture, the erosion layers and associated properties from each layer were placed highest to lowest by water content. Each Kaolinite mixture group would have subgroups separated by similar water content values which resulted in three subgroups of similar water content values, Group 1 (G1), Group 2 (G2), and Group 3 (G3). These refer to the groups of decreasing water content with increasing depth in all mixtures. These water content groups also have rates of erosion that were established by the flume tests set for specific applied shear stress amounts. The relationships between depth and both d_{50} and water content can be seen below in Figure 4.3 (a) through (c).

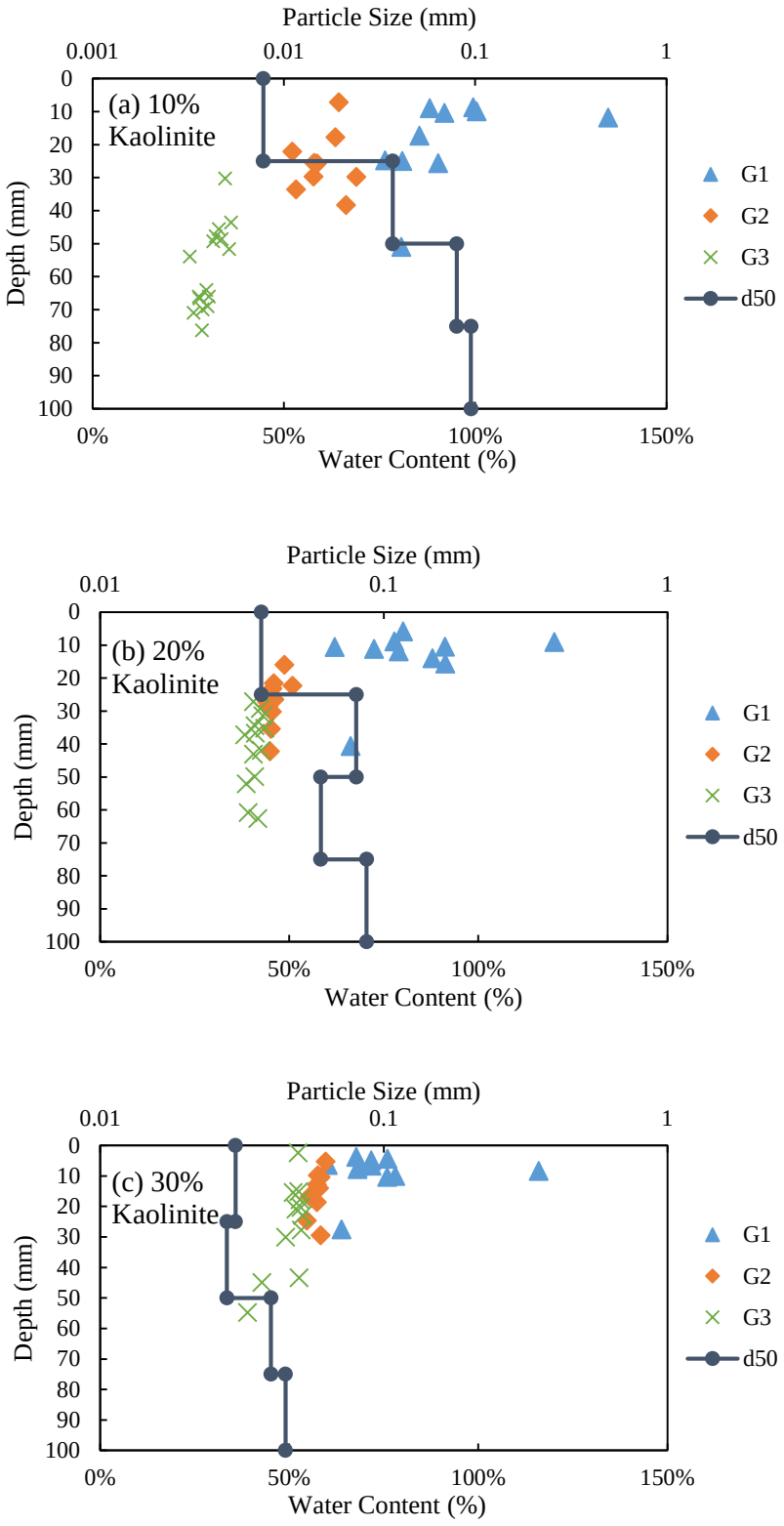

Figure 4.3: Water Content Versus Depth for Erosion Layers and Sediment Size Versus Depth for Sediment Layers Collected During Tests of (a) 10% Kaolinite, (b) 20% Kaolinite, (c) 30% Kaolinite

Once the grouping of water content was decided upon depending on the stratification with water content and thus bulk density, relating sediment size properties from the size distribution tests to the water content and thus erosion groups became the next step. Size distribution tests were conducted on fixed sediment layer thicknesses. This led to two problems related to associating a water content group with sediment properties. Firstly, there is not a simple linear trend of depth vs. sediment size with respect to all mixtures and secondly, the water content groups overlap in the different sediment size regions. Both of these observations can be seen in Figure 4.3. The solution was to relate the depth of the water content group samples to the fixed depth ranges of the sediment size samples using a weighted average based on the relative number of water content group members inside each sediment size region. For example, if 75% of the samples in water content Group 1 resided in the 0-25 mm region by depth and 25% fell into the 25-50 mm layer, then the sediment properties were weighted accordingly. If the 0-25 mm sediment range had a d_{50} of 0.0078 mm and the 25-50 mm layer had a d_{50} of 0.037 mm, then Group 1 had a $d_{50} = (0.75 * 0.0078) + (0.25 * 0.037) = 0.0151\ mm$. This process was repeated for all water content groups in all three mixture types for all sediment properties which are given in Table 4.2 below.

.

Table 4.2: Sediment Properties and Distribution by Water Content Group

Kaolinite Percentage	Group	Water Content (%)	d_{60} (mm)	d_{50} (mm)	d_{30} (mm)	d_{10} (mm)	*Cu*	*Cc*	*CSF*	*Fines*
10%	G1	92.86%	0.0283	0.0188	0.0080	0.0025	11.43	0.91	17.7%	78.9%
	G2	60.29%	0.0483	0.0273	0.0109	0.0022	22.31	1.13	12.7%	66.0%
	G3	30.74%	0.0814	0.0592	0.0308	0.0098	8.34	1.19	4.73%	44.2%
20%	G1	82.82%	0.0820	0.0404	0.0128	0.0015	56.16	1.37	12.7%	55.8%
	G2	46.15%	0.0920	0.0574	0.0168	0.0018	52.27	1.74	11.2%	49.8%
	G3	41.04%	0.0975	0.0689	0.0191	0.0020	49.88	1.91	10.1%	46.2%
30%	G1	74.35%	0.0745	0.0298	0.0061	0.0014	52.56	0.35	17.0%	58.1%
	G2	57.23%	0.0745	0.0298	0.0061	0.0014	52.46	0.35	17.0%	58.1%
	G3	50.33%	0.0739	0.0301	0.0066	0.0015	49.83	0.40	16.8%	57.9%

4.1.4 pH, Temperature, and Conductivity

A series of replicable sediment mixtures were generated to create a profile of the pH, temperature, and conductivity of the sediment mixtures specified in these experiments. The mixtures were replicated on a percentage by weight basis and measurements were made immediately after mixing and before settling could occur. The 25 measurements were made with an Oakton Waterproof PC 300 using the same method at consistent depths. The average values and their standard deviations are reported in Table 4.3 below.

Table 4.3: Sediment Properties and Distribution by Water Content Group

	pH	Conductivity (μs)	Temperature (C)
Mixture	Average ± Std. Dev	Average ± Std. Dev	Average ± Std. Dev
Pure Water	6.97 ± 0.08	104.04 ± 1.66	21.40 ± 0.06
10% Kaolinite	5.17 ± 0.12	112.36 ± 3.39	21.80 ± 0.17
20% Kaolinite	4.83 ± 0.03	110.16 ± 3.94	21.92 ± 0.24
30% Kaolinite	4.74 ± 0.01	99.79 ± 2.21	21.82 ± 0.29
100% Kaolinite	3.99 ± 0.09	78.34 ± 7.86	21.82 ± 0.18

The mixtures showed a downward trend with increasing percentage of Kaolinite in terms of pH. Pure water being very close to a pH of 7 while the 100% Kaolinite was close to a pH of 4. Similarly starting with 10% Kaolinite and increasing to 100% Kaolinite it can be seen that the conductivity deceased with increasing Kaolinite content. The temperature, however, was a consistent value ranging between 21 and 22 ^{o}C.

4.2 Erosion Test Results

Erosion rate was quantified by measuring the change in depth, or displacement of sediment by the piston, per unit time, $\left(\frac{\Delta D}{\Delta t}\right)$, and the dry density (ρ_d) (see Eqn. 3.11). As previously described, the erosion groups were separated into three water content groups given the theoretical importance of water content to erosion rates and critical shear stress. Each erosion group is comprised of a series of erosion tests for which there is a series of fixed bed shear stresses and corresponding rates of erosion. After grouping by water content, average values of water contents and erosion rates were taken for each specified shear stress value. Each water content group was then placed into a solver analysis system to minimize the Standard Error of Estimate (*SE*) in erosion rate *E* relative to the deviation between measured and predicted erosion rates. Parameters of *M*, *n*, and τ_c in Equation 2.9 were optimized.

In the process of using the solver it was observed that there were possible local maxima and minima that may give the solver a solution, but these solutions were not necessarily the global solutions. As a result, another step was taken in order to ensure that the solution was not only correct, but also repeatable. A range of *n* values from one to three as a practical matter, in 0.1 increments were selected and manually substituted into the solver with only the values for *M* and τ_c being allowed to vary in order to find the minimum *SE*. This procedure was conducted for

all three mixture types and all three water content groups in each mixture. The resulting graph as shown in Figure 4.4 shows how the *SE* can have local maxima and minima that would effectively isolate a local solver solution without providing the global solution.

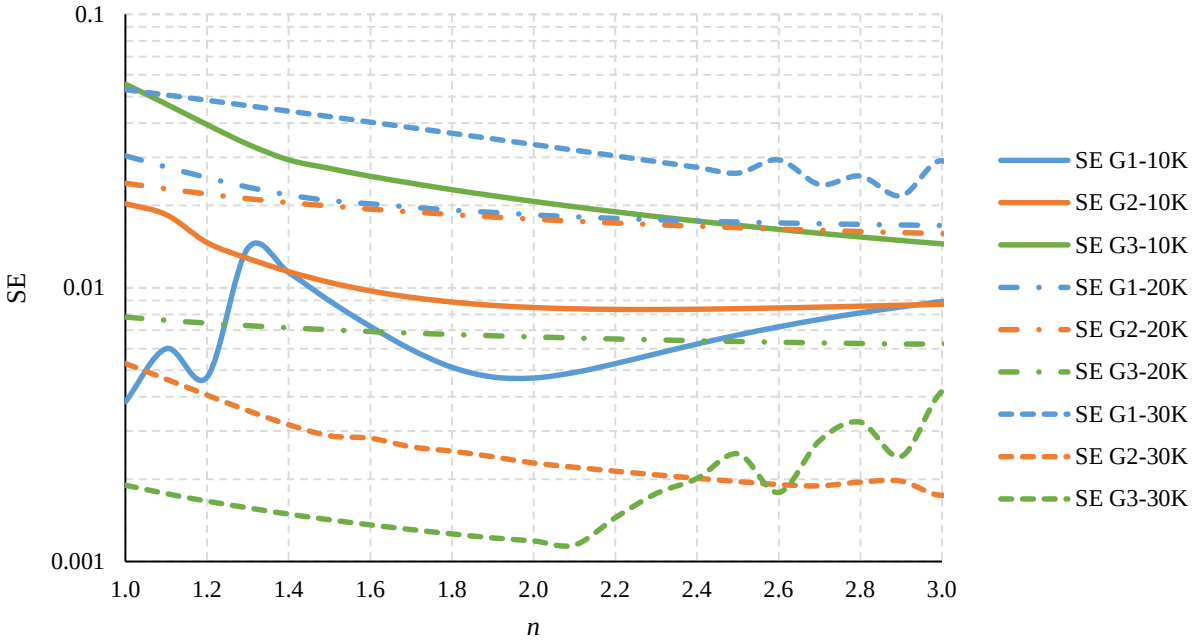

Figure 4.4: The Variation of *SE* with Respect to a Fixed *n* Value for All Water Content Groups and Mixtures

The range of *n* values considered is between one and three because previous researchers have found that this is the range of the exponent on shear stress in experimental and field relationships for coarse and fine sediment transport. It was decided that there are effectively three types of curves present in Figure 4.4 based on local and global trends. The first type is also the simplest in which the global *SE* minimum is within an acceptable range of *n* and can be seen clearly, e.g. Group 3 for 30% Kaolinite. The next type is where the *SE* value either plateaus over a wide range of *n*, e.g. Groups 1, 2, and 3 for 20% Kaolinite and Group 2 for 10% Kaolinite, or is

continuously sloping in one direction without any local minimum in *SE* as in Group 3 for 10% Kaolinite. The last type contains properties of the previous groups, but also has variations along the trend lines where certain regions of *n* values have many local maxima and minima indicating instability in the solution. These are encompassed by Groups 1, 2, and 3 for 30% Kaolinite and Group 1 for 10% Kaolinite which all have sections of variable SE for minor changes in *n*.

Selecting a proper *n* value in order to determine the parameters *M, n,* and especially τ_c, is easiest for the curves of Type one. These types can be found visually thanks to the singular minimum in the curve outside regions of oscillation. Type two curves were analyzed such that for the minimum value of *SE* within the plateau zone, a conservative value of *n* was selected subject to the condition that *SE* was less than or equal to 1.05 SE_{min} as *n* increased toward SE_{min}. This approach was taken to avoid overfitting with larger values of *n* than necessary while recognizing the inherent uncertainty in the measured erosion rate. The solution procedure for the last type of curve was to choose $n = 3$ which is its maximum value based on previous experimental and field data even though *SE* continued to decrease slowly for $n > 3$.

Upon selection of the appropriate variables *M, n,* and τ_c, the measured and estimated rates of erosion rate versus bed shear stress can be plotted according to the specific sediment mixture and water content group. The resulting graphs can be seen in Figure 4.5 with each graph representing a mixture and each curve a representation of the best-fit erosion rate estimation for that water content group. The data points and their best-fit curves demonstrate an increasing erosion rate with increasing applied shear stress at an increasing rate. Values of *n* for the curves in Figure 4.5 vary from 1.9 to 3.0 as shown in Table 4.4. In the case of the 10% Kaolinite mixture the highest water content group represents the highest curve; however, the lowest water content group corresponds with the next highest curve, and the water content group in the middle

is the lowest curve. The 20% and 30% Kaolinite mixtures have a more expected grouping of curve responses with the highest curve represented by the highest water content group and the lowest curve by the lowest water content group because lower water content corresponds with higher bulk density which provides greater resistance to erosion. The erosion rates for a given percent Kaolinite are also affected by grain size in the cases of stratification due to differential settling. This is especially true for the 10% Kaolinite erosion rate curves. In this case, the highest water content group corresponds to the more easily eroded fluff layer near the surface with a high *CSF* while the lowest water content group is mostly sand without much influence of the *CSF*. The middle water content group erosion rates are likely subject to the simultaneous influences of sediment size, *CSF*, and water content, or bulk density.

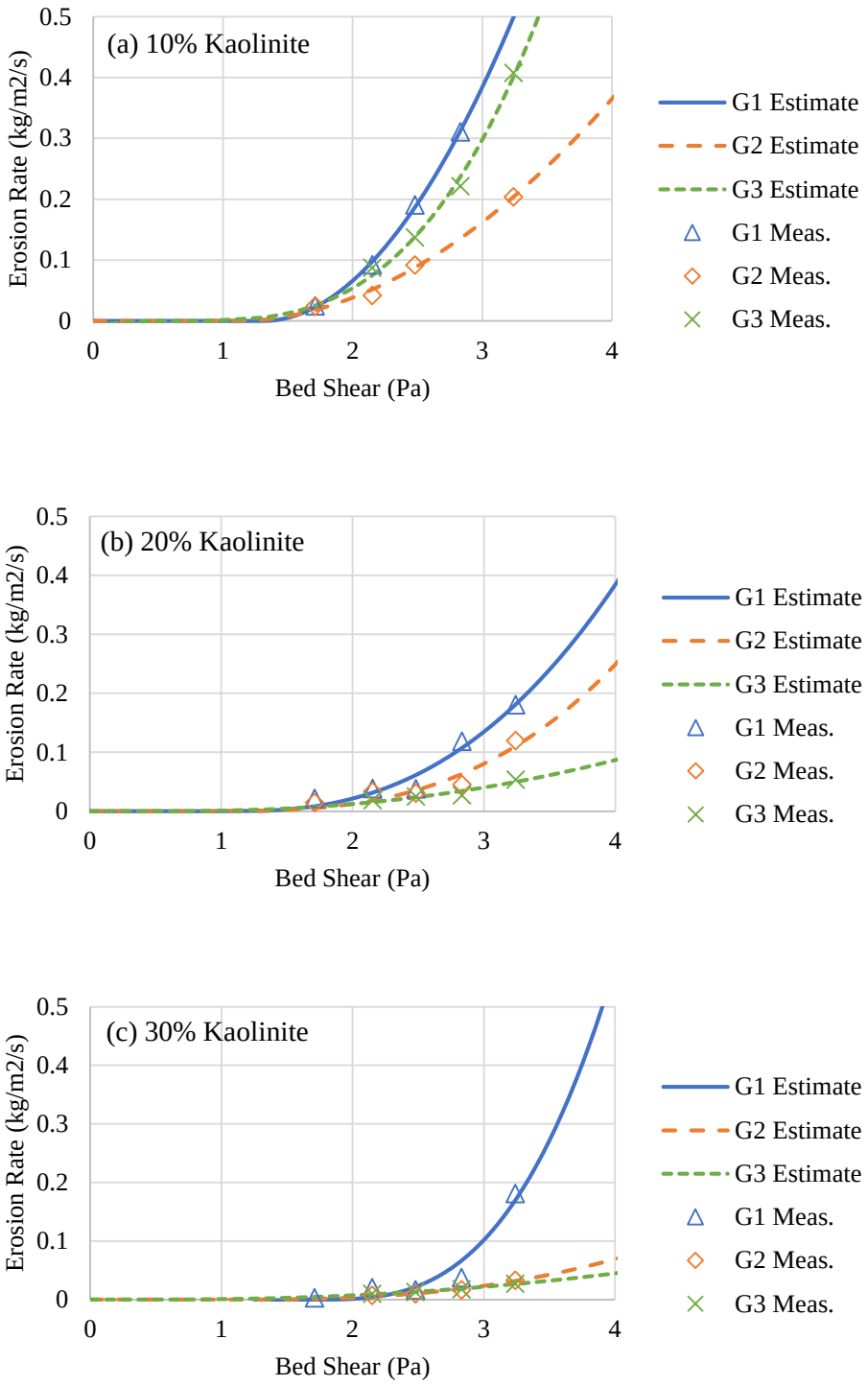

Figure 4.5: Erosion rate versus bed shear stress with best-fit curves of estimation for each water content group of (a) 10% Kaolinite, (b) 20% Kaolinite, and (c) 30% Kaolinite

The values of *M*, *n*, and τ_c are reported for each water content group in Table 4.4 below. As average depth increases, the water content decreases and bulk density increases. As the percentage of Kaolinite in the mixture increases, the degree of stratification in Clay Size Fraction (*CSF*) and d_{50} with depth decreases. For the 10% and 20% Kaolinite mixtures, the decrease in *CSF* with an increase in depth corresponds to a higher percentage of fine sand and lower values of critical shear stress which is consistent with the finding in the literature that. as sand content increases, erosion threshold decreases (Gerbersdorf et al. 2005, 2007). The reason for the decrease in critical shear stress with depth for the 30% Kaolinite mixture in the absence of stratification is not clear.

Table 4.4: Properties and Values of Water Content Groups for Best Fit Curves

Kaolinite Mix	Water Content Group	Water Content (%)	d_{50} (mm)	Average Depth (mm)	τ_c (Pa)	*M* Value	*n* Value	*CSF*	*Fines*
10%	G1	89.0%	0.0188	19.32	1.312	0.1376	1.96	17.7%	78.9%
	G2	62.1%	0.0273	25.52	1.122	0.0489	1.90	12.7%	66.0%
	G3	30.4%	0.0592	57.46	0.701	0.0245	3.00	4.7%	44.2%
20%	G1	76.3%	0.0404	13.83	1.080	0.0264	2.50	12.7%	55.8%
	G2	45.3%	0.0574	27.34	0.899	0.0094	2.90	11.2%	49.8%
	G3	41.1%	0.0689	41.69	0.601	0.0059	2.20	10.1%	46.2%
30%	G1	70.5%	0.0298	8.80	1.710	0.0561	2.50	17.0%	58.1%
	G2	57.2%	0.0298	15.84	1.152	0.0051	2.50	17.0%	58.1%
	G3	48.8%	0.0301	26.34	0.552	0.0033	2.10	16.8%	57.9%

4.3 Summary of Experimental Results

This chapter describes the results of all the experiments performed as per the methods outlined in the previous chapter. The results show various trends occurring with the variation of Kaolinite ratios by weight in the overall sediment mixture. In general, water content decreased

with the increase in depth of the sediment sample, and so did *CSF* and *Fines* for the 10% and 20% Kaolinite mixtures. The measured pH and conductivity decreased as the percent Kaolinite increased in a sample from 0-100%. Critical shear stress decreased with depth for all three Kaolinite mixtures which might be due to stratification and increasing values of d_{50} and percent sand with depth for the 10% and 20% mixtures, but the reason for decrease in τ_c with depth for the 30% mixture requires further investigation.

Chapter 5

Data Analysis and Discussion

This chapter reanalyzes the information from previous sediment erosion research under the lens of new data collected in the current study. Four previous researchers at Georgia Tech used the erosion flume in the Hydraulics Laboratory to conduct erosion tests of coarse field sediment samples and fine laboratory mixed sediment samples. Navarro (2004) and Hobson (2008) tested Shelby tube core samples from bridge sites distributed throughout Georgia. In these field samples the sediment d_{50} data are largely in the coarse size range (> 0.062 mm). The laboratory samples were tested in research by Wang (2013) and Harris (2015). While the mixed Kaolinite and silt samples of Wang had a much finer composition with d_{50} < 0.04 mm, Harris mixed Kaolinite and fine sand resulting in some samples extending across the fine-coarse sediment delineation, but many of his samples were still classified as fine. Despite the various grain-size mixtures present in the sediments, a common factor was the Kaolinite present in almost every sample. As mentioned in Chapter 2, the influence of clay particles to decrease the erodibility of a sediment is important. This influence is found in clay's ability to retain more water due to increased surface area and a capacity to overpower gravitational forces of small particles with strong interparticle forces. As a result, this study investigated a relationship derived from linear regression that can be applied to sediment samples that could effectively estimate the erodibility of a sample based on several variables including factors such as particle size, water content, and particularly *CSF*.

The initial inquiry for an equation to predict critical shear stress began by compiling previous research that had been conducted in the Georgia Tech Hydraulics Lab erosion flume.

Previous researchers included a variety of data points ranging from field samples to lab-prepared samples favoring finer or coarser sediment composition. The current study was focused primarily on finer sediments based on d_{50} of the mixtures of Kaolinite, silt, and fine sand. The *Fines* percentage was 44% to 79%, and the clay size fraction (*CSF*) of the samples was relatively constant with a range between 5% and 18%. A comparison of the sediments tested in previous studies and the current study can be seen in Table 5.1 below.

Table 5.1: Range of Sediment Properties Sorted by Study

Study	d_{50} (mm)	Water Content (%)	CSF (%)	Fines (%)
Navarro (2004) Hobson (2008)	0.0074-1.19	15%-39%	0%-35%	0%-75%
Wang (2013)	0.0026-0.04	35%-183%	3%-30%	100%
Harris (2015)	0.0033-0.090	38%-131%	10%-25%	43%-100%
Current Study	0.019-0.095	30%-90%	5%-18%	44%-79%

In addition to using data sets developed in previous Georgia Tech studies, the data from the current study was added to previously collected data to show if existing equations could be refined or improved with a new independent variable. Previous studies indicated a series of regression equations for critical shear stress that built upon each other. Navarro (2004) and Hobson (2008) found their data for τ_c was best described in terms of d_* and *Fines* as independent variables. Wang (2013) observed that an equation relating *w*, *CSF*, and an interaction term (*w x CSF*) could effectively describe fine sediments. Recently, Harris (2015) established that an equation similar to Wang's performed best, but also proposed a weighted formula incorporating both formulas from Navarro and Hobson, and Wang.

The addition of data points that contain less *CSF* and that better mimic the field samples of Navarro and Hobson's work would help fill an existing gap between the field and lab data. The field data have much higher coarse sediment content as compared to the previous lab samples and as a result, stand out from the other data points. Filling this gap can help bring the engineering community a step closer to finding an equation that can describe the erodibility of a sediment through analysis of geotechnical properties.

To ease discussion in the subsequent section, the work of Navarro (2004) and Hobson (2008) shall simply be referred to as "Navarro and Hobson" or "field data", Wang (2013) will be "Wang", and Harris (2015) "Harris". All of the work from before this study shall be "previous work" or "previous research" and information gleaned from this work shall be referred to as "current study".

5.1 Findings of Previous Research

This section will present the conclusions found by the previous researchers in their work along with data from the current study. One of the most important observations regarding the previous research is that there is a distinction between τ_c values of fine and coarse sediment with the dividing line being a particle size of 0.062 mm that separates silt and sand as defined by the American Geophysical Union (AGU). The work by Navarro and Hobson found all of their samples to be coarse, moderately low in clay content, but having a large range in *Fines*. By contrast, Wang's data was entirely of a fine composition, and as such all of her sediment was classified as cohesive. Harris' work sought to bridge this gap by mixing lab samples with coarser material instead of the purely fine material that Wang had worked with. This effort provided results that spanned into the coarse region, but there were not many data points in that range as much of it was in the fine range. The current study also provides data on the coarse-fine

sediment border. All of these data sets for measured τ_c in terms of the range of d_{50} values covered can be seen graphically in Figure 5.1.

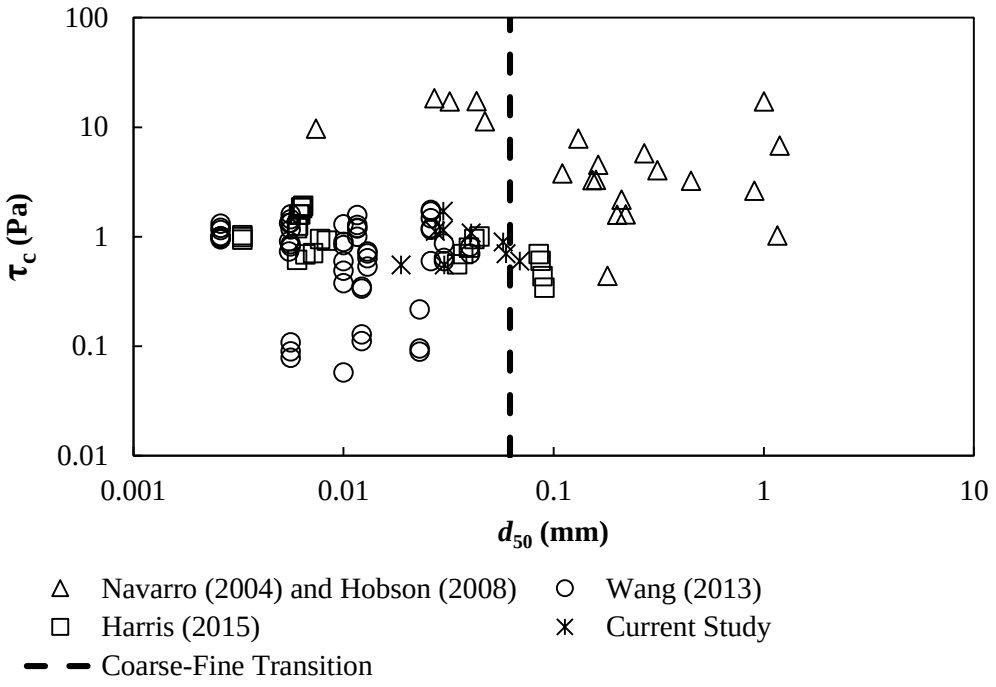

Figure 5.1: Particle Size Measured Against the Group Critical Shear Stress

In Figure 5.2 the same data sets are plotted in terms of water content versus critical shear stress. The lab data have consistent τ_c values in the range of 0.1 to 1.0 Pa over a broad range of water content values from about 40% to 180%. Some of the field data overlap with the lab data for water content < 40% but a distinct portion of the field data have much higher values of τ_c for w < 40%.

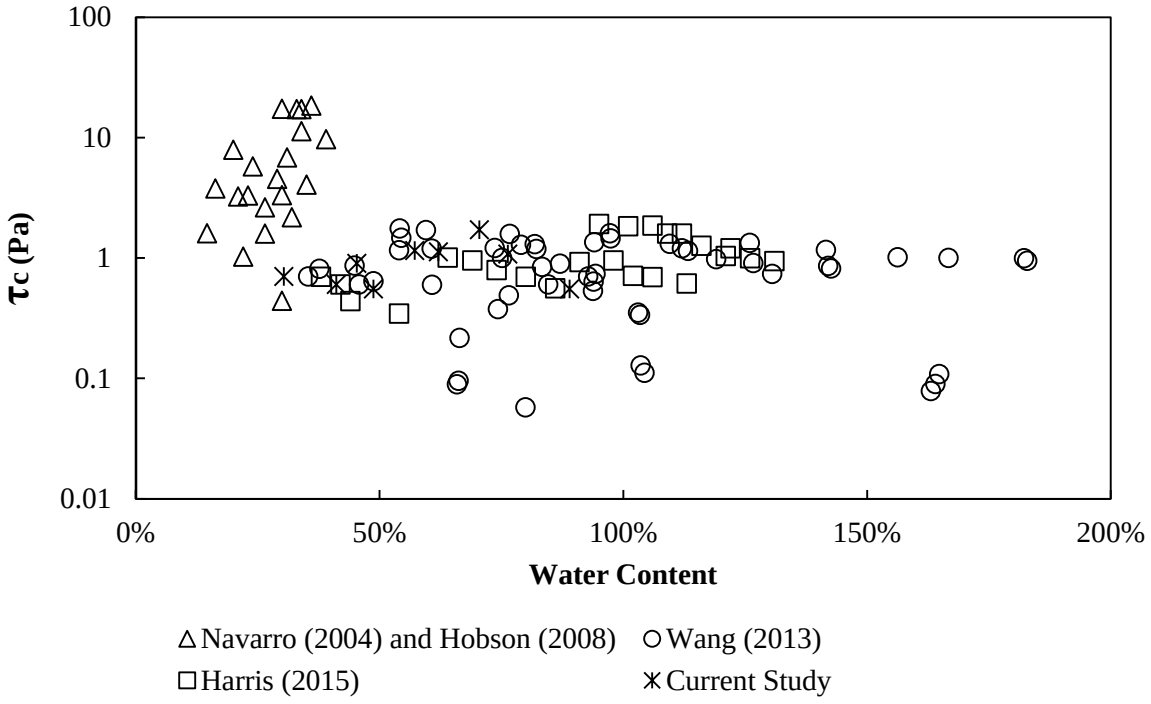

Figure 5.2: Particle Size Measured Against the Group Water Content

As in previous research, this study focused on the Shields parameter (τ_{*c}) as the key dependent variable to associate with geotechnical parameters for the provision of the best estimate of τ_c. The Shields parameter was originally derived by Albert Shields as a dimensionless variable to describe the incipient motion of a particle based on a ratio of the critical hydrodynamic force acting on a sediment particle to its submerged weight (Shields 1936). The parameter has been used previously to great success as an important variable since it can be applied to cohesive and coarse sediments, its dimensionless nature, and the incorporation of d_{50}. In the past it has been related to water content, clay size fraction, percent fines, and dimensionless particle size (Navarro 2004, Hobson 2008, Wang 2013, Harris 2015).

Navarro and Hobson used the Shields comparison to relate their work with that of Albert Shields, whose data was collected on a variety of sizes and types of sediments. Their work was best summarized by Equation 5.1 below:

$$\tau_{*c} = 0.644x10^{2.68Fines}d_*^{-0.409} \qquad \text{(Eqn. 5.1)}$$

which is shown by the dashed lines of varying *Fines* content (as a decimal fraction) in Figure 5.3. For a given *Fines* content, the slope of Equation 5.1 matches closely that of the Shields equation in the silt size range. The work completed by Navarro and Hobson is shown in Figure 5.3 by black diamonds, the current study is shown by the open symbols, and the work completed by Harris is all other symbols.

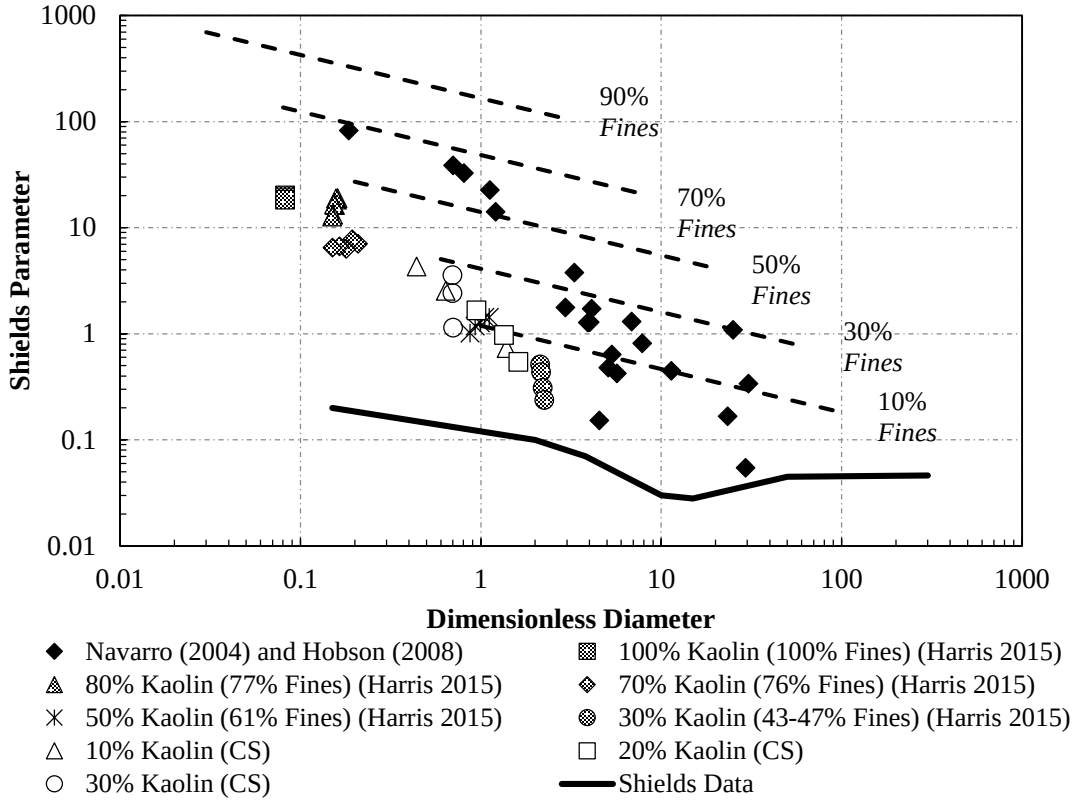

Figure 5.3: Shields Parameter data from Navarro and Hobson, Harris, and the Current Study

Source: Adapted from Harris (2015) Figure 5.2

The diagram shows a problem that Harris first experienced, and with the addition of the current study, is reinforced. The field data and the lab data do not overlap in this presentation.

The Navarro and Hobson equation relies on the variability of *Fines* in order to explain part of the variation in the Shields parameter, which is taken as the dependent dimensionless variable for τ_c in both the data from Harris and the current study. However, the data collected by Wang is 100% *Fines* and is not well predicted by Navarro and Hobson, Equation 5.1 (R^2 = 0.77, *SE* = 435.49). Subsequently, Wang developed an entirely new equation in order to provide a Shields parameter for finer sediments which places more emphasis on the water content (*w* as a decimal fraction) and clay size fraction (*CSF* as a decimal fraction) as seen in Equation. 5.2 below.

$$\tau_{*c} = 8.46 - 27.76w + 73.69CSF + 83.22(w * CSF) \qquad \text{(Eqn. 5.2)}$$

The water content variable in this equation accounts for the influence of porosity in sediments and is a direct function of bulk density for saturated sediments. Fine sediments have more water in their interstitial spaces due to the adsorbent nature of clay particles, which is confirmed by the data in Table 5.1. Furthermore, as water content increases, bulk density decreases. The influences of *w* and *CSF* on erodibility of a sediment are opposite. The critical shear stress of a sediment decreases with increasing water content, but if the clay size fraction increases so does the critical shear stress. This relationship is reflected in the equation above (Eqn. 5.2) where the coefficient on water content parameter is negative and on the clay size fraction parameter is positive. The relative contribution of *w*, *CSF*, and their interaction term on τ_{*c} provides an equation that is quite effective, especially with higher water content and clay size fraction. In Figure 5.4 below, the Shields parameter data from Wang, Harris, and the current

study have all been plotted against water content and the dashed lines show the application of Equation. 5.2.

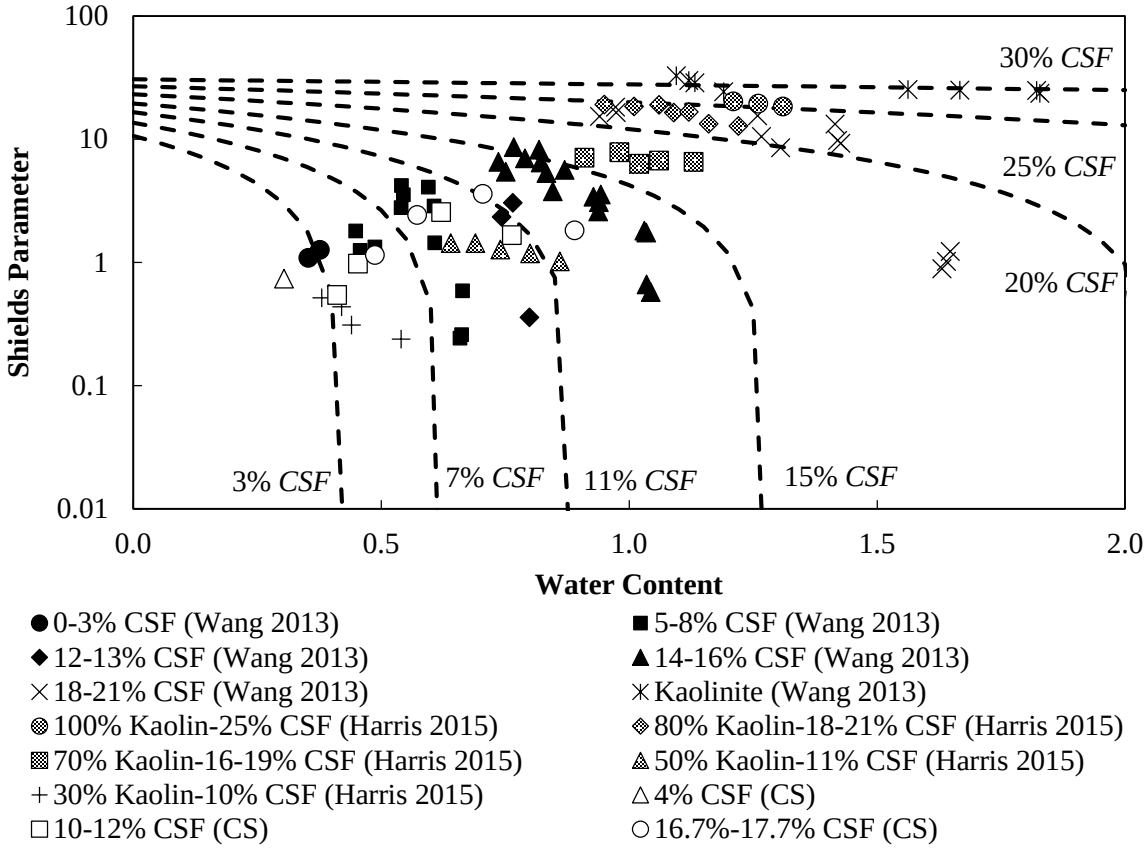

Figure 5.4: Shields Parameter vs. Water Content with Clay Size Fraction Estimates

Source: Wang et al. (2016)

As evidenced by the data from Wang and Harris, the use of Equation. 5.2 is effective at higher clay contents (*CSF* > 16%), but below this level the model is not as effective. When this equation was used to estimate Wang's measured τ_{*c} values it had goodness of fit statistics of R^2 = 0.88 and *SE* = 3.11. When similarly applied to a data set comprised of Wang and Harris the goodness of fit statistics drops only slightly and remains the best fit with R^2 = 0.82 and *SE* = 3.69.

Harris generated a new equation (Eqn. 5.3) based on the data from his study as well as Wang's study to see what could be improved from Equation. 5.2.

$$\tau_{*c} = 3.54 - 22.2w + 93.7CSF + 63.0(w\ x\ CSF) \qquad \text{(Eqn. 5.3)}$$

The equation was the best result from the linear regression analysis using the same variables as Equation 5.2, and improved the coefficients resulting in improved statistics for the combined Harris and Wang data set (R^2 = 0.83 and *SE* = 3.57). While the statistics of the new equation when applied to just the Wang data alone dropped slightly (R^2 = 0.87 and *SE* = 3.26.), the resultant decrease in goodness of fit is considered negligible.

Harris proceeded to further apply the comparison between Equation 5.2 and the Navarro and Hobson data as seen in Figure 5.5.

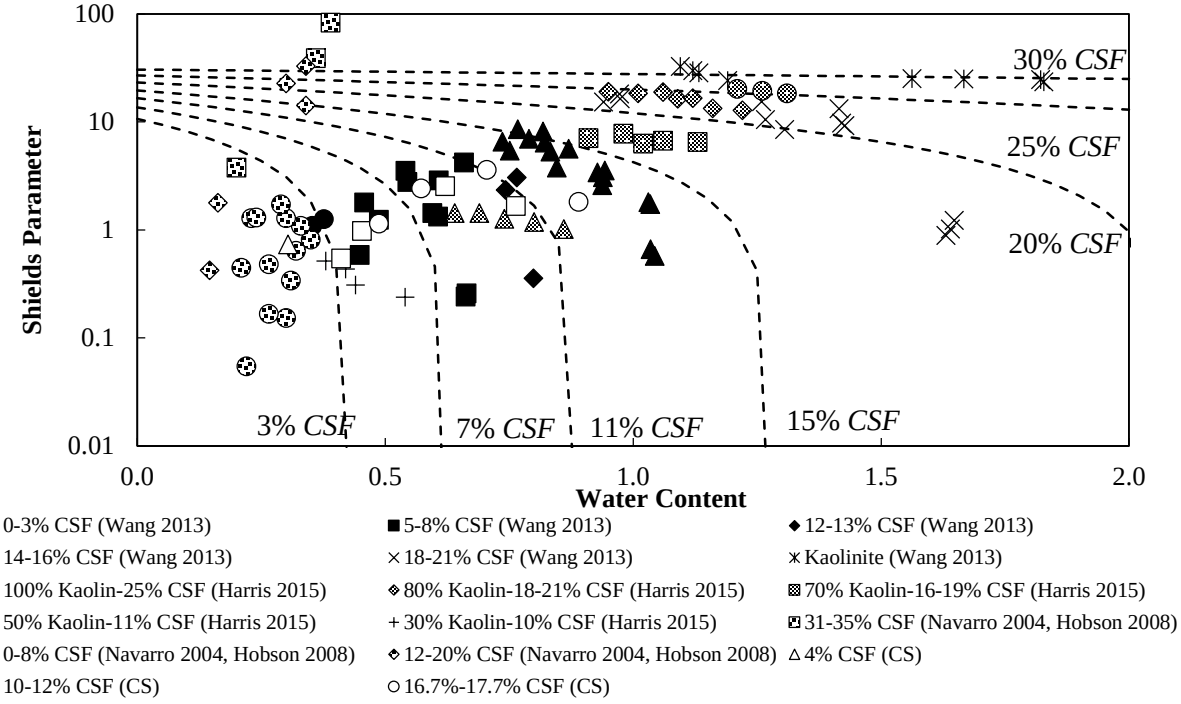

Figure 5.5: Shields Parameter vs. Water Content with Clay Size Fraction Estimates of "All Data" Source: Harris 2015 Figure 5.4

Figure 5.5 shows that the equation retained its ability to predict τ_{*c} for water content values exceeding 40% but the equation does not agree with the field data having high values of the Shields parameter. Between roughly 40% and 60% water content is a gap where only a few of the data points from Harris and the current study reside. It appears as if this gap might be a differentiating point between the field and lab data sets, and given the original reliance on *Fines* in Equation 5.1, Harris proposed *Fines* as an additional component of Equation 5.3. The resultant equation was very similar to Equation 5.3 and was given by

$$\tau_{*c} = 1.68 - 27.1w + 97.0CSF + 72.8(w\ x\ CSF) + 5.01Fines \qquad \text{(Eqn. 5.4)}$$

The use of *Fines* in Equation 5.4 instead of d_* was due to the co-dependence that d_* has with *CSF*. If *CSF* increases or decreases, then the d_* will certainly change, but *Fines* is not directly connected to *CSF*. Goodness of fit statistics for Equation 5.4 were found to be $R^2 = 0.66$ and $SE = 6.95$.

Harris also suggested another method for finding a unified equation that encompasses both coarse and fine sediments. The idea was to use a weighted equation combining the coarse sediment equation from Navarro and Hobson (Eqn. 5.1) with the fine sediment formula developed by combining Harris and Wang data (Eqn. 5.3) and relating the weighting factor to *Fines*:

$$\tau_{*c} = (Fines^{0.235})\ x\ (Eqn.\ 5.1) + (1 - Fines^{0.235})\ x\ (Eqn.\ 5.3) \qquad \text{(Eqn. 5.5)}$$

The equation (Eqn. 5.5) was found to have a high goodness of fit in predicting the Shields parameter for studies of the entire data set during his research ($R^2 = 0.71$ and $SE = 6.54$). However, when set to predict the Harris data alone it was not very suitable ($R^2 = 0.53$ and $SE = 5.40$), but Equation 5.5 was selected by Harris to be the preferred equation for the available data

set. The reason for this decision was because it fit both the coarse and fine sediment data better than the other equations proposed.

The data provided by the current study was meant to extend the work of Harris so that the data could transition between the coarse Navarro and Hobson field data and the very fine lab samples prepared by Wang. From past experience and from the literature (Grabowski et al. 2011), the use of water content and clay size fraction seem to be viable independent parameters on which to base an equation for τ_{*c}, especially if it is a fine sediment. The use of *Fines* in addition to water content and clay size fraction is also an interesting concept that will be explored in the next section with the analysis of previous work including the current study.

5.2 Regression Analysis of Expanded Data Sets with Current Study

This section will describe the procedure by which a series of equations were selected and analyzed for effectiveness in determining the Shields parameter based on data collected in this study and previous research.

As mentioned previously there are a number of sediment properties that can serve as variables for trying to evaluate an all-encompassing Shields parameter prediction equation. Deciding which independent variables to include in the equation can be difficult, especially when considering the differences between cohesive and non-cohesive sediments. A cohesive sediment is much more likely to rely on the use of water content and clay size fraction akin to what Wang found in her research. Other sources in the literature have also suggested using variables such as water content, clay size fraction, and percent fines (Rowell 1994, Ravisangar et al. 2001, 2005; Grabowski et al. 2011, Avinimelech et al. 2001, van Ledden et al. 2004, Thoman and Niezgoda 2008). The use of particle size as a discriminant between fine and coarse sediments is very

common, but its use in depicting erosion of the two types of sediment is not as clear. This is primarily due to the fact that fine sediments could have widely varying grain size distributions, making it difficult to define one erosion rate for a single sediment.

Non-cohesive sediments, much like those studied by Navarro and Hobson, tend to rely on particle size given that a non-cohesive sediment's particles resistance to erosion are more likely to be governed by gravitational forces. Many researchers have found that predominantly coarse sediments with small fines content, rely on a size distribution, a void space parameter, and a cohesive variable (Jacobs et al. 2011). In this study an additional variable of (*w x CSF*) was considered based on the previous research by Wang and Harris. This interaction term provides not only information based on the ratio of water to clay size fraction, it also serves as a statistical term to account for co-dependence in the equation. Water content interacts with clay and is a void size parameter since the samples in this study were assumed to be fully saturated. The size variable was chosen to be d_* since it functions as a dimensionless variable much like the other variables described previously. While d_{50} is included in the calculation for d_*, it also includes a sediment specific gravity variable which adds an effect of particle mineralogy although it varies among natural river sediments by a small amount. These five variables, water content (*w*), clay size fraction (*CSF*), percent fines (*Fines*), dimensionless particle size (d_*), and the interaction term (*w x CSF*) were placed into Minitab 16 software for data set analysis. The software calculates a series of best-fit equations using stepwise linear regression with coefficients related to the variables that are selected by the software as the best variables to fit the given data set. The best fit, or goodness of fit, is based on four statistical parameters: Standard Error (*SE*), R^2, R^2_{adj}, and the Mallows C_p. The Mallows C_p is a statistical representation for the proportion of the

sum of squares of errors (SSE_p) to the mean square error of the model (MSE_{total}). The equation is shown here

$$C_p = \frac{SSE_p}{MSE_{total}} - (Z - 2p) \qquad \text{(Eqn. 5.6)}$$

where p represents the total number of variables in the data set, and Z is the number of data points. The better fitting model is represented by a C_p value that is closer to the number of variables in the given model. If a C_p value is $(1+p)$ where p is the number of supplied variables, then the regression has most likely provided an equation using all parameters and is not necessarily a representative equation.

Shown below in Tables 5.2-5.4 are the results of the Minitab analysis with the variables selected for a given model and the resulting goodness of fit statistics. The three data sets are (A) all data sets selected (Navarro, Hobson, Wang, Harris, and Current Study), (B) all data for which $w < 40\%$ and $d_{50} > 0.04$mm, and (C) all other data not included in the second data set where $w > 40\%$. Highlighted rows are models that were selected by the computer independently of user input requiring specific parameters. The darkest highlighted rows are the equations that were selected for final consideration in this study.

5.2.1 Analysis of "All Data" data set

The darkest highlighted equations in Table 5.2 were selected based on their goodness of fit as well as if they agreed with previous work. In the data set given in Table 5.2 for which all data were considered, Models A3 and A4 best fit the data and the respective equations are shown below:

$$\tau_{*_c} = 1.163 - (20.8\ x\ w) + (102.0\ x\ CSF) + \big(59(w\ x\ CSF)\big) \qquad \text{(Eqn. 5.7)}$$

$$\tau_{*_c} = 1.242 - (27.8\ x\ w) + (89.7\ x\ CSF) + \big(79(w\ x\ CSF)\big) + (6\ x\ Fines) \quad \text{(Eqn. 5.8)}$$

The equations both exhibited the best combination of *SE* and Mallows *Cp*. Equation 5.7 is similar to previous equations as put forth by Wang (Eqn. 5.2) and Harris (Eqn. 5.3), further solidifying the use of the parameters *w*, *CSF*, and *w x CSF*. Equation 5.8 shows that the addition of *Fines* can improve the prediction capabilities of the equation slightly, much as Harris showed. *Fines* was chosen over d_* because of its capability to not be greatly influenced by *CSF*.

Table 5.2: Measures of Model Fit for "All Data" with Variation of Parameters

Model	R^2	R^2_{adj}	Mallows C_p	*SE*	*w*	*CSF*	*Fines*	*d**	*w x CSF*
A1	0.5527	0.5485	26.8	7.77		x			
A2	0.6068	0.5993	13	7.32	x	x			
A3	0.6338	0.6233	7.1	7.1	x	x			x
A4	0.6458	0.6320	5.6	7.01	x	x	x		x
A5	0.6512	0.6341	6	6.99	x	x	x	x	x
A6	0.6074	0.5960	14.8	7.35	x	x	x		
A7	0.2753	0.2543	111.9	9.98			x	x	x
A8	0.2691	0.2552	111.7	9.98				x	x
A9	0.6341	0.6199	9	7.13	x	x		x	x
A10	0.0659	0.0481	171.2	11.3			x	x	

The use of the three parameters, *w*, *CSF*, and (*w x CSF*), can be further proven as an acceptable choice by examining Figure 5.5 below in which the performance of Eqns. 5.2 and 5.7 is compared. The use of Equation 5.7 compared to Equation 5.2 shows a slight improvement in estimating the Shields parameter for sediments with low *CSF*. As the *CSF* increases, the predictions of Equation 5.7 increasingly agree with Equation 5.2. Data from Harris and the Current Study seem to be less sensitive to water content at low values of *CSF* suggesting non-cohesive behavior, but no definite conclusion can be drawn.

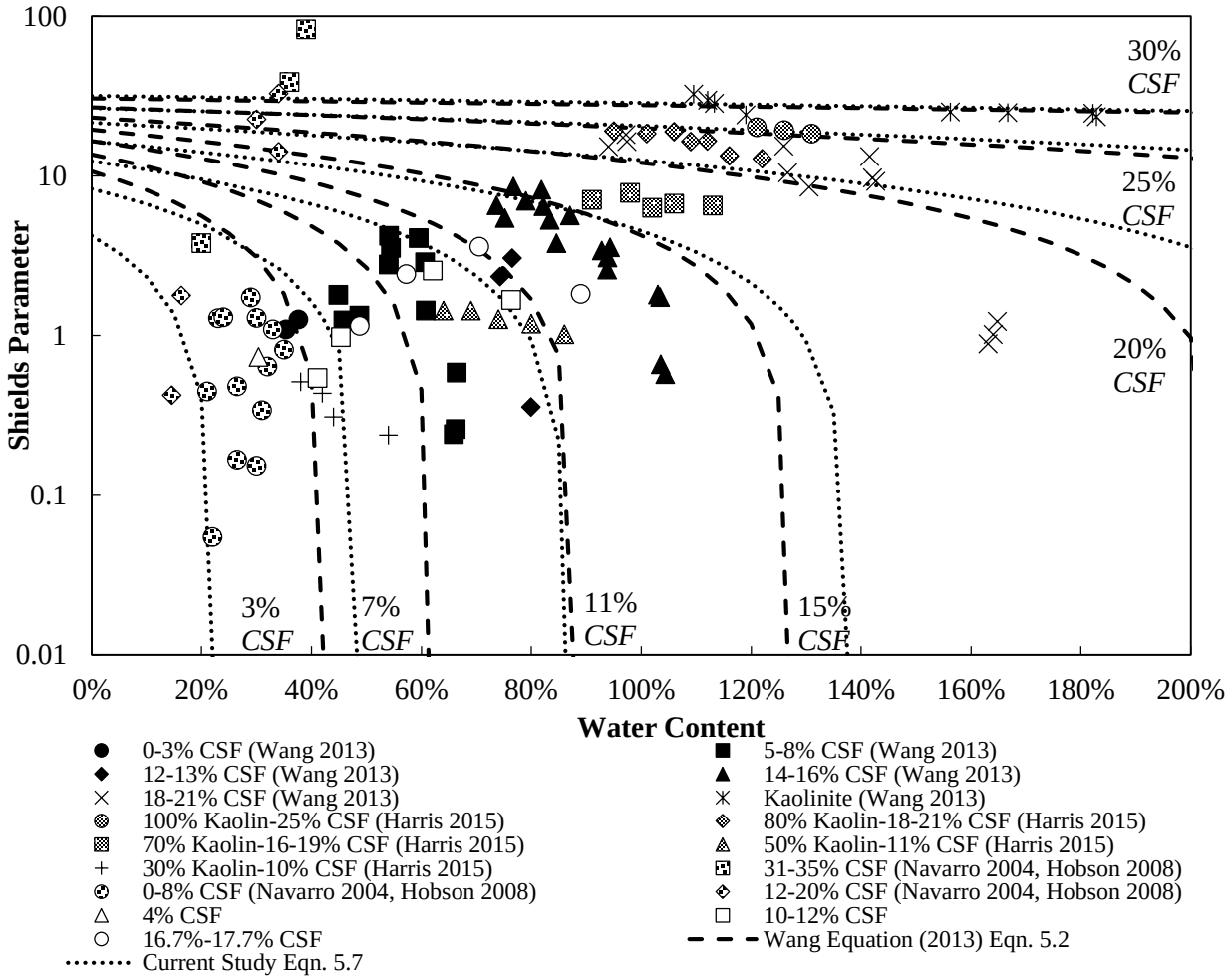

Figure 5.6: Shields Parameter vs. Water Content with Clay Size Fraction Estimates of "All Data" with Equation 5.7 from the Current Study

5.2.2 Analysis of "All Data" with $w < 40\%$ and $d_{50} > 0.04$ mm data set

The next proposed equation comes from revised data set B (Table 5.3) based on the water content and particle size of the data. In this case, all sediment erosion groups that had both $w > 40\%$ and $d_{50} < 0.04$ mm were removed from the data set and placed into a second data set in which all $w > 40\%$. The 40% water content dividing line originated from analyzing the combined data sets of previous researchers and the current study based on Figure 5.5. A gap is observed around the 40% water content mark where the majority of field data fall to the low end

of water content, while much of the lab data are on the high end of water content. This data set of $w < 40\%$ and $d_{50} > 0.04$ mm represents the coarser sediments, and while Navarro and Hobson make up the majority of the data, there are two points, one from Harris and one from the current study, that were included. The result of this analysis was the following equation:

$$\tau_{*c} = 8.3643 - (35\ x\ w) - (90\ x\ CSF) + \left(496\ x\ (w\ x\ CSF)\right) \qquad \text{(Eqn. 5.9)}$$

This equation has the same three independent variables as Wang's equation, and it has encouraging goodness of fit statistics with a Mallows C_p of 2.1 and a *SE* of 1.95. However, the equation has a negative sign in front of the *CSF* term which results in an increase in τ_{*c} with increases in both *w* and *CSF* contrary to the trends noted previously. Water content and clay size fraction are related, but they have opposite effects on τ_{*c} when increasing in magnitude for cohesive sediments. This data subset has coarser sediment sizes with relatively low water content but *CSF* values as high as 30%. So the physical meaning of this model is contrary to past experience.

Table 5.3: Measures of Model Fit for "All Data" of $w < 40\%$ and $d_{50} > 0.04$ mm with Variation of Parameters

Model	R^2	R^2_{adj}	Mallows C_p	*SE*	*w*	*CSF*	*Fines*	*d**	*w x CSF*
B1	0.4718	0.4407	6.8	2.36					x
B2	0.5693	0.6198	2.1	2.2		x			x
B3	0.6832	0.6198	2.1	1.95	x	x			x
B4	0.6854	0.5955	4	2.01	x	x		x	x
B5	0.3515	0.2705	13.8	2.7	x	x			
B6	0.5700	0.4840	6.8	2.27		x		x	x
B7	0.3530	0.2236	15.7	2.78	x	x		x	
B8	0.6837	0.5933	4.1	2.01	x	x	x		x
B9	0.6854	0.5644	6	2.08	x	x	x	x	x

5.2.3 Analysis of "All Data" with w > 40% data set

In this data set analyzed in Table 5.4 all the data points that were not part of the previous data set (B), but were part of the overall data set, were considered. Members of the data set included mostly the lab data that were primarily fine and cohesive, but there were a few field data points that were also included in this analysis. The regression equation selected for this data set is shown below:

$$\tau_{*c} = -2.353 - (21\ x\ w) + (162\ x\ CSF) + \left(27.9\ x\ (w\ x\ CSF)\right) \qquad \text{(Eqn. 5.10)}$$

This equation follows the format set forth in Equations. 5.2, 5.3, and 5.7, but its initial coefficient is a negative term which permits some negative estimates of τ_{*c}. The goodness of fit for this equation is also not the best for the data set with a SE = 6.16 and a C_p = 9.3 as compared to the statistically better equation defined by Minitab which includes d_* as a parameter with SE = 5.97 and C_p = 4.7. However, Equation 5.10 was retained for final analysis over the d_* based equation because of the similarity to the other three-parameter equations (Eqns. 5.2, 5.3, 5.7).

Table 5.4: Measures of Model Fit for "All Data" of w > 40% with Variation of Parameters

Model	R^2	R^2_{adj}	Mallows C_p	SE	w	CSF	$Fines$	d^*	w x CSF
C1	0.2137	0.2047	204.1	10.9					x
C2	0.7155	0.7059	21.6	6.59		x			x
C3	0.7545	0.7459	9.3	6.16	x	x			x
C4	0.7725	0.7616	4.7	5.97	x	x		x	x
C5	0.7709	0.7599	5.3	5.99	x	x	x		x
C6	0.7743	0.7607	6	5.98	x	x	x	x	x
C7	0.7508	0.7450	8.6	6.17	x	x			
C8	0.2107	0.1923	207.3	11.00			x	x	
C9	0.7679	0.7597	4.4	5.99	x	x	x		
C10	0.2211	0.2030	203.4	10.9				x	x

A summary of the best-fit regression equations and the data sets on which they are based is presented in Table 5.5.

Table 5.5: Selected Equations of Previous Research and from Current Study

Model	Eqn #	Data Set	Equation
N/A	5.2	W	8.46 - (27.76 x *w*) + (73.69 x *CSF*) + (83.22 x (*w x CSF*))
N/A	5.3	TH+W	3.54 - (22.2 x *w*) + (93.7 x *CSF*) + (63.0 x (*w x CSF*))
N/A	5.1	N+H	0.668 x (10^ (2.51 x *Fines*)) x (*d** ^(-0.423))
N/A	5.4	TH+W+N+H	1.68 - (27.1 x *w*) + (97.0 x *CSF*) + (72.8 x (*w x CSF*)) + (5.01 x *Fines*)
A4	5.8	CS+TH+W+N+H (ALL)	1.242 - (27.8 x *w*) + (89.7 x *CSF*) + 79(*w x CSF*) + (6 x *Fines*)
B3	5.9	ALL where *w* <40% + d50>0.004	8.3643 - (35 x *w*) - (90 x *CSF*) + (496 x (*w* x *CSF)*)
C3	5.10	ALL where *w* >40%	-2.353 - (21.5 x *w*) + (162 x *CSF*) + (27.9 x (*w x CSF)*)
A3	5.7	ALL	1.163 - (20.8 x *w*) + (102.0 x *CSF*) + (59 x (*w x CSF*))
N/A	5.5	TH+W+N+H	(*Fines* ^0.235) x (Eqn 5.3) + (1-*Fines* ^0.235) x (Eqn. 5.1)

Symbol Key: W = Wang, TH = Harris, N = Navarro, H = Hobson, CS = Current Study

5.2.4 Comparison of Equations

After compiling the best-fit regression equations, statistical analyses were performed by applying all nine equations to 10 distinct data sets. These data sets represent the original seven from which the equations were derived and three additional data sets that incorporate the current study with previous work. This can be seen in Table 5.6 below. The bolded values represent the coupling between an equation and the data set from which that equation was derived (e.g. Equation 5.8 was derived from the "All Data" data set). The data sets in Table 5.6 represent several combinations of data from different investigators in order to see how well a particular best-fit regression equation performs when applied to other data sets. A good example is that of Equation 5.8 derived from all data with SE = 6.88 compared with being applied to just the Wang and Harris data set (*SE* = 3.55), to Wang, Harris, and Current Study (*SE* = 3.48), and to Harris and Current Study (*SE* = 4.94).

Table 5.6: Statistical Results from Data Set Comparison between Proposed Equations

Data Set Applied	Equation Applied																	
	5.2		5.3		5.1		5.4		5.8		5.9		5.10		5.7		5.5	
Wang (Z = 54)	***SSE***	**503**	*SSE*	553	*SSE*	9862015	*SSE*	560	*SSE*	542	*SSE*	1298931	*SSE*	842	*SSE*	633	*SSE*	551
	SE	**3.11**	*SE*	3.26	*SE*	435.49	*SE*	3.28	*SE*	3.23	*SE*	158.05	*SE*	4.02	*SE*	3.49	*SE*	3.26
	$\mathbf{R^2}$	**0.88**	R^2	0.87	R^2	0.77	R^2	0.88	R^2	0.88	R^2	0.61	R^2	0.84	R^2	0.87	R^2	0.87
Wang + Harris (Z = 78)	*SSE*	1034	***SSE***	**968**	*SSE*	11092321	*SSE*	959	*SSE*	960	*SSE*	1615821	*SSE*	1192	*SSE*	1004	*SSE*	1181
	SE	3.69	***SE***	**3.57**	*SE*	382.04	*SE*	3.55	*SE*	3.55	*SE*	145.81	*SE*	3.96	*SE*	3.63	*SE*	3.94
	R^2	0.82	$\mathbf{R^2}$	**0.83**	R^2	0.36	R^2	0.83	R^2	0.83	R^2	0.62	R^2	0.81	R^2	0.83	R^2	0.81
Navarro + Hobson (Z = 21)	*SSE*	4181	*SSE*	3893	***SSE***	**965**	*SSE*	3732	*SSE*	3767	*SSE*	836	*SSE*	4319	*SSE*	3842	*SSE*	2967
	SE	14.83	*SE*	14.31	***SE***	**7.13**	*SE*	14.01	*SE*	14.08	*SE*	6.63	*SE*	15.08	*SE*	14.22	*SE*	12.50
	R^2	0.53	R^2	0.54	$\mathbf{R^2}$	**0.93**	R^2	0.55	R^2	0.55	R^2	0.90	R^2	0.52	R^2	0.54	R^2	0.68
Harris + Wang + Navarro + Hobson (Z = 99	*SSE*	5215	*SSE*	4861	*SSE*	11093286	***SSE***	**4690**	*SSE*	4728	*SSE*	1616657	*SSE*	5512	*SSE*	4846	***SSE***	**4148**
	SE	7.33	*SE*	7.08	*SE*	338.18	***SE***	**6.95**	*SE*	6.98	*SE*	129.10	*SE*	7.54	*SE*	7.07	***SE***	**6.54**
	R^2	0.63	R^2	0.65	R^2	0.10	$\mathbf{R^2}$	**0.66**	R^2	0.66	R^2	0.25	R^2	0.64	R^2	0.65	$\mathbf{R^2}$	**0.71**
All Data Sets (Z = 108)	*SSE*	5746	*SSE*	5322	*SSE*	11103460	*SSE*	5107	***SSE***	**5065**	*SSE*	1635666	*SSE*	6180	***SSE***	**5236**	*SSE*	4803
	SE	7.33	*SE*	7.05	*SE*	322.13	*SE*	6.91	***SE***	**6.88**	*SE*	123.64	*SE*	7.60	***SE***	**7.00**	*SE*	6.70
	R^2	0.61	R^2	0.63	R^2	0.12	R^2	0.64	$\mathbf{R^2}$	**0.65**	R^2	0.26	R^2	0.61	$\mathbf{R^2}$	**0.63**	R^2	0.68
All Data Sets (w<40%) (Z = 19)	*SSE*	1629	*SSE*	1435	*SSE*	90	*SSE*	1511	*SSE*	1342	***SSE***	**253**	*SSE*	2954	*SSE*	1398	*SSE*	899
	SE	9.79	*SE*	9.19	*SE*	2.30	*SE*	9.43	*SE*	8.88	***SE***	**3.86**	*SE*	13.18	*SE*	9.07	*SE*	7.27
	R^2	0.21	R^2	0.22	R^2	0.57	R^2	0.24	R^2	0.24	$\mathbf{R^2}$	**0.64**	R^2	0.22	R^2	0.22	R^2	0.28
All Data Sets (w>40%) (Z = 89)	*SSE*	4117	*SSE*	3887	*SSE*	11103370	*SSE*	3596	*SSE*	3724	*SSE*	1635412	***SSE***	**3226**	*SSE*	3838	*SSE*	3903
	SE	6.88	*SE*	6.68	*SE*	357.25	*SE*	6.43	*SE*	6.54	*SE*	137.11	***SE***	**6.09**	*SE*	6.64	*SE*	6.70
	R^2	0.72	R^2	0.73	R^2	0.07	R^2	0.74	R^2	0.73	R^2	0.21	$\mathbf{R^2}$	**0.75**	R^2	0.72	R^2	0.72
Harris + Current Study (Z = 33)	*SSE*	1063	*SSE*	877	*SSE*	1240480	*SSE*	816	*SSE*	756	*SSE*	335898	*SSE*	1019	*SSE*	761	*SSE*	1285
	SE	5.85	*SE*	5.32	*SE*	200.04	*SE*	5.13	*SE*	4.94	*SE*	104.09	*SE*	5.73	*SE*	4.96	*SE*	6.44
	R^2	0.45	R^2	0.55	R^2	0.53	R^2	0.55	R^2	0.56	R^2	0.79	R^2	0.50	R^2	0.59	R^2	0.71
Wang + Harris + Current Study (Z = 87)	*SSE*	1566	*SSE*	1430	*SSE*	11102495	*SSE*	1375	*SSE*	1298	*SSE*	1634829	*SSE*	1861	*SSE*	1394	*SSE*	1836
	SE	3.83	*SE*	3.66	*SE*	322.12	*SE*	3.59	*SE*	3.48	*SE*	123.61	*SE*	4.17	*SE*	3.61	*SE*	4.14
	R^2	0.75	R^2	0.77	R^2	0.39	R^2	0.79	R^2	0.79	R^2	0.64	R^2	0.73	R^2	0.78	R^2	0.75
Current Study + Harris + Navarro + Hobson (Z = 54)	*SSE*	5243	*SSE*	4769	*SSE*	1241445	*SSE*	4547	*SSE*	4523	*SSE*	336735	*SSE*	5339	*SSE*	4604	*SSE*	4252
	SE	10.04	*SE*	9.58	*SE*	154.51	*SE*	9.35	*SE*	9.33	*SE*	80.47	*SE*	10.13	*SE*	9.41	*SE*	9.04
	R^2	0.52	R^2	0.54	R^2	0.11	R^2	0.55	R^2	0.55	R^2	0.15	R^2	0.52	R^2	0.54	R^2	0.64

In order to best compare the equations in Table 5.6, the *SE* was considered to be the primary factor in determining the goodness of fit for the equation, with R^2 considered the next most important statistical parameter because it indicates what portion of the variance is explained by the regression equation. In the above case the equation that best fits across all the data sets is Equation 5.5 with a $SE = 6.70$ and $R^2 = 0.68$, which is the weighted equation set forward by Harris. This equation is followed closely by Equation 5.4 and Equation 5.8 which are the next best fitting across all data sets ($SE = 6.91$ and $R^2 = 0.64$; $SE = 6.88$ and $R^2 = 0.65$, respectively). However, when comparing the differences between Equations 5.5, 5.4, 5.8, and 5.7 the improvement in *SE* is very marginal, on the order of one to two percent (e.g. for Equation 5.7 with all data, $SE = 7.00$ and $R^2 = 0.63$ vs. Equation 5.8 for all data, $SE = 6.88$ and $R^2 = 0.65$). As a result, simpler equations with a strong connection to the physics of erosion should be selected as the preferred specification given the small differences between results.

The previous paragraph suggests that a single equation may be best for trying to estimate all data points, regardless of parameters involved. Harris also investigated this approach by creating Equation 5.5 with its weighted combination of Equation 5.2 and Equation 5.1 in which the weighting factor is a function of *Fines*. However, instead of choosing a single equation to model all data, a pair of equations each of which captures the specific factors affecting erodibility of coarse vs. fine sediments may be preferred. In the context of this study, the selected criterion for forming fine vs. coarse sediment subsets of the data was all data with $w < 40\%$ and $d_{50} > 0.04$ mm in the first data set, and then all data with $w > 40\%$ in the second data set. By making this differentiation, the goodness of fit in estimating the Shields parameter may increase by forming a closer relationship to the uniqueness of fine vs. coarse sediments. In choosing the low water content group equation, Equation 5.9 appears to be the best, but as mentioned

previously it produces some physically counterintuitive results. The next best equation is Equation 5.1 created by Navarro and Hobson (SE = 2.3 and R^2 = 0.57 for w<40% and d_{50}>0.04mm). Equation 5.10 is chosen for the high water content group as it is simple and is the best fit for this group (SE = 6.09 and R^2 = 0.75 for w>40%).

When comparing the data sets, the statistical values provide excellent insight, but graphical comparisons are also extremely valuable. In Figure 5.7 the comparisons data set for different combinations of equations and data sets are presented in terms of measured vs. predicted values of the Shields parameter.

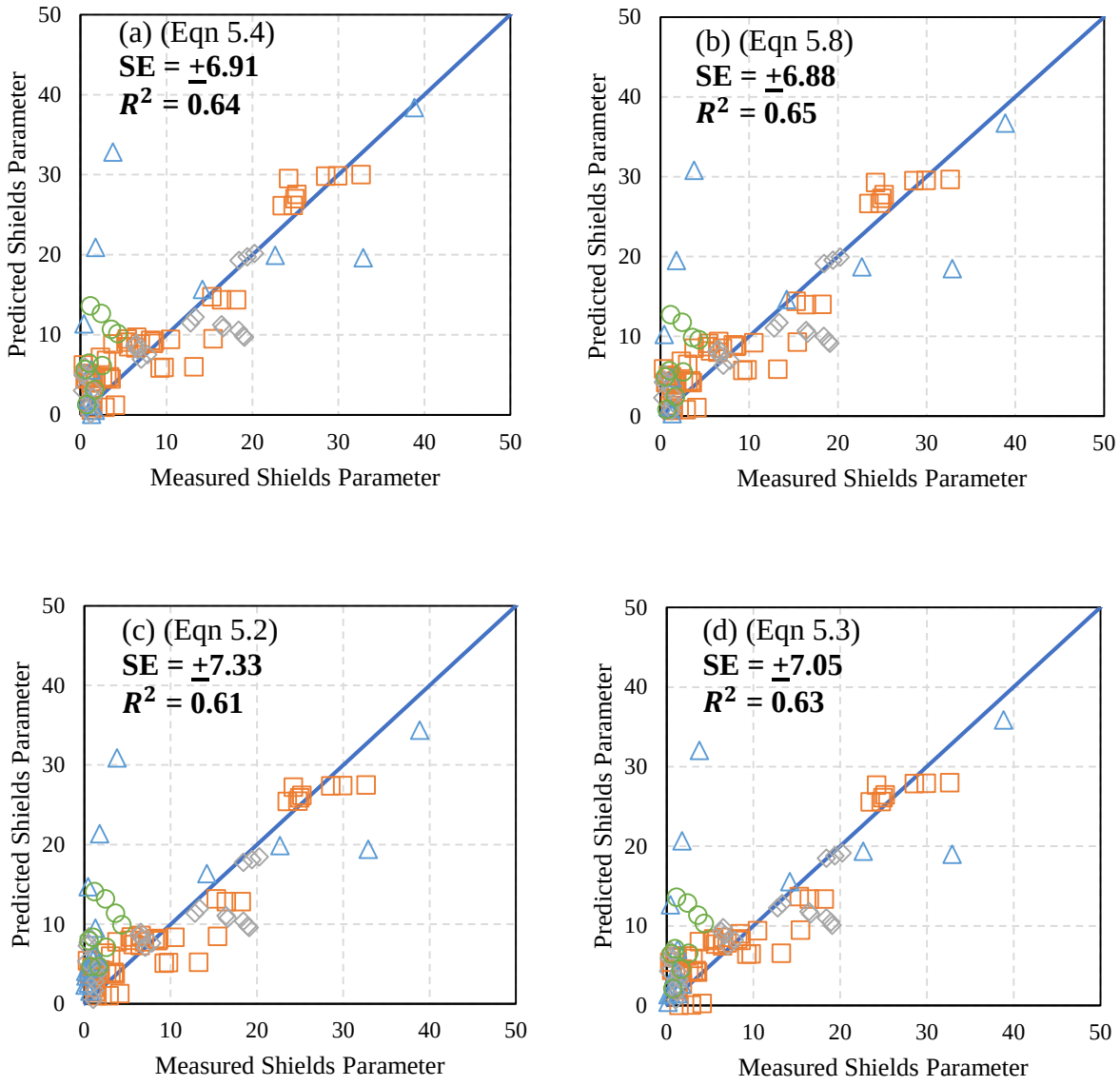
(a) (Eqn 5.4)
SE = ±6.91
R^2 = 0.64
(b) (Eqn 5.8)
SE = ±6.88
R^2 = 0.65
(c) (Eqn 5.2)
SE = ±7.33
R^2 = 0.61
(d) (Eqn 5.3)
SE = ±7.05
R^2 = 0.63
Predicted Shields Parameter
Measured Shields Parameter
0
10
20
30
40
50
Key
Navarro (2004) and Hobson (2008)
Wang (2013)
Harris (2015)
Current Study

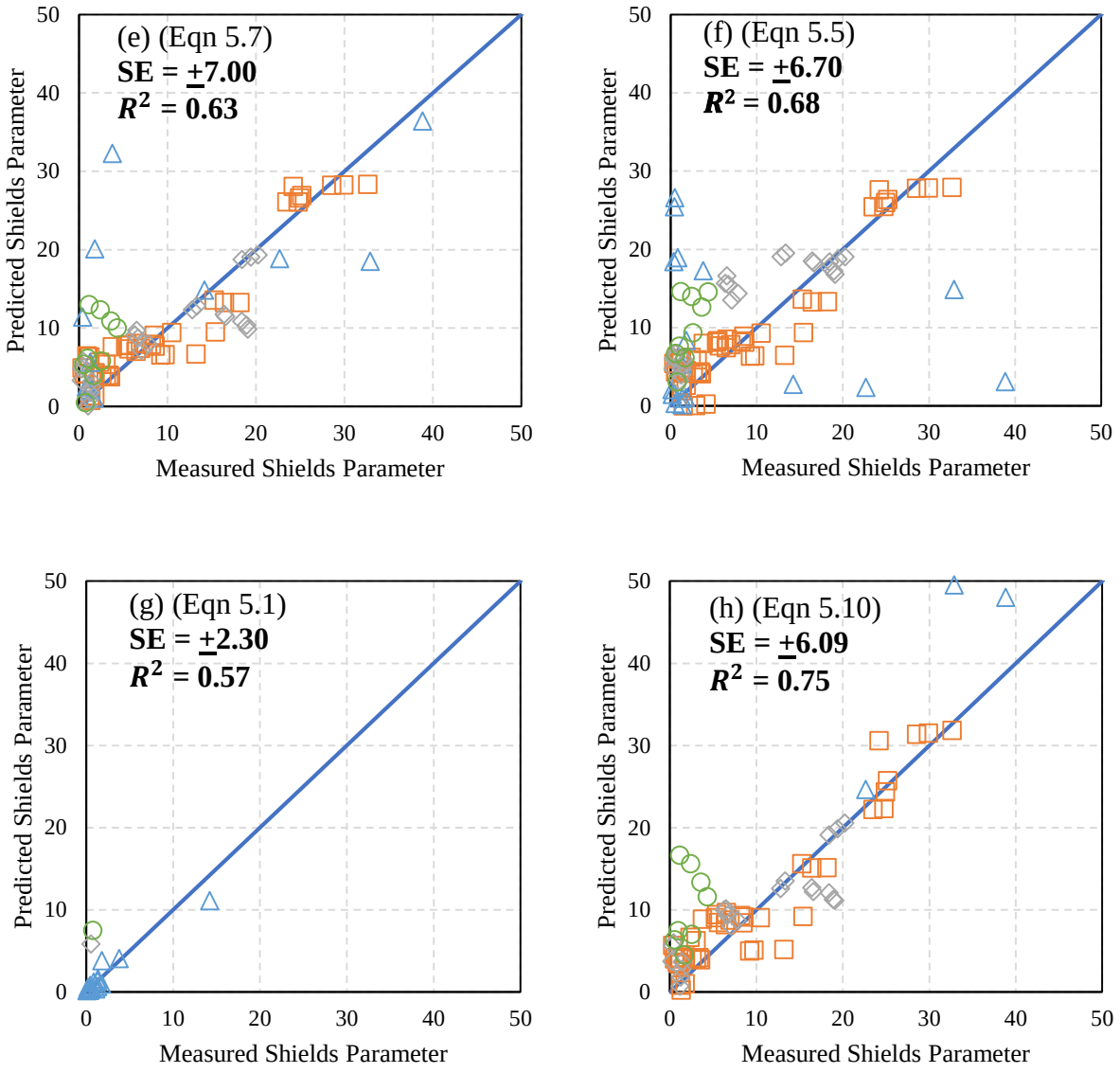

Figure 5.7: Measured vs. Predicted Shields Parameters for Equations 5.4 (a), 5.8 (b), 5.2 (c), 5.3 (d), 5.7 (e), 5.5 (f), 5.1 (g) and 5.10 (f) Where a, b, c, d, and e are from the "All Data" data set and f and g are Separated by Water Content at 40% and d_{50} > 0.04 mm

Figure 5.6 (a) and (b) show the improvement in predictions obtained by implementing the term *Fines* into the three-parameter equation established by Wang. Figure 5.6 (c)-(f) demonstrates the effect of including new data from previous research within the framework of the three-parameter equations. Figure 5.6 (f) shows the performance of the weighted equation

suggested by Harris, and while the statistical results show a slight improvement over the three-term equations, the occurrence of a few extreme outliers is observed. Lastly, Figure 5.7 (g) and (h) show the advantage of splitting the data into two distinct groups, which is similar to what Harris had discussed in his research by trying to make a weighted equation combining two different formulas. The linearity of the data in (g) shows that this approach works well for the coarser sediments of low water content as Navarro and Hobson first proposed for the field data. In addition, predictions for the remaining data subset for finer sediments with w>40% show a promising trend with data tending to cluster closer to the predicted vs. measured line compared to any of the other three-parameter equations (Eqns. 5.2, 5.3, 5.7).

To summarize, the best overall equation continues to be a combination of the three parameters *w*, *CSF*, and *w x CSF*. This is best expressed in the form of Equation 5.7 based on all of the data collected to date. A comprehensive overarching equation still shows promise in addressing the issue of calculating a Shields parameter using geotechnical variables. A better fitting equation could be formed with the addition of a *Fines* parameter like that of Equation 5.8, but the result is a negligible increase in the goodness of fit requiring additional data to be gathered. The use of a weighted equation seems to have promise, yet there are better equations to consider when trying to estimate the Shields parameter for the transitional data groups vs. the largely coarse or fine data sets. Also, the scattering of data as visualized in Figure 5.5 (f) shows the fault in only considering the statistics as the lone deciding factor. Lastly, the concept of splitting data into two groups based on water content and dimensionless diameter appears to be useful, but more lab data that aligns with the field data is necessary before this can be strongly proven.

The success of the three-parameter models first suggested by Wang, even across all data sets which include both fine and coarse sediments, is partly attributed to the inclusion of the interaction term of *w x CSF* to modulate the counteracting influences of *w* and *CSF* on τ_{*c}, particularly for the fine-grained sediments. Increases in w correspond to decreases in bulk density, or packing density, with a resultant decrease in τ_{*c}. However, as *CSF* increases, the effect of *w* or packing density becomes less important in comparison to cohesive forces which cause an increase in $\tau_{*c.}$ The disadvantage of the three-parameter model lies in the occurrence of more granular, or at least mildly cohesive sediments, with less dependence of τ_{*c} on water content. In this case, it is the granular size and the percent silt or *Fines* which begin to govern particle interactions and the strength of the resistance to erosion. The difficulty, as shown by this research, is in defining the transition point between cohesive and non-cohesive behavior.

Jacobs et al. (2011) studied experimentally the erosion threshold of sand-mud mixtures and used the concept of indirect plasticity index (*PI** = *Clay Activity* x *CSF*) as a separating parameter for modes of erosion in the mixtures. These modes were classified as granular (*PI**=0), low cohesive (*PI**<2), and cohesive (*PI**>2). Under this classification system granular mixtures are most closely associated with the original Shields criterion. Low cohesive mixtures begin to deviate from the Shields criterion as the amount of silt increases, which in turn increases the critical shear stress in agreement with the Navarro-Hobson approach. In the low cohesive mixtures, water content is not a reliable measure of critical shear stress. This is because the packing density of the mixture for this case has little variability despite an increase in critical shear stress. For cohesive mixtures, the plasticity index was found to be the most reliable indicator of erosion rather than packing density, but packing density also plays a role. This aligns with the idea that as water content increases in fine material with high *CSF*, the critical shear

stress increases modulated by the counteracting effect of water content as indicated by the three-parameter Wang equation. Since the plasticity index can be directly related to *CSF* (Skempton 1965) the idea that water content and particle size as suggested in this thesis can be used as separating parameters for cohesive vs. non-cohesive behavior seems valid.

The use of *PI** as a separating parameter was applied to the "All Data" data set and can be seen in Figure 5.8 below. The *PI** was calculated by multiplying Kaolinite activity (0.643 from Harris 2015) with *CSF* and the resultant values are in the Appendix.

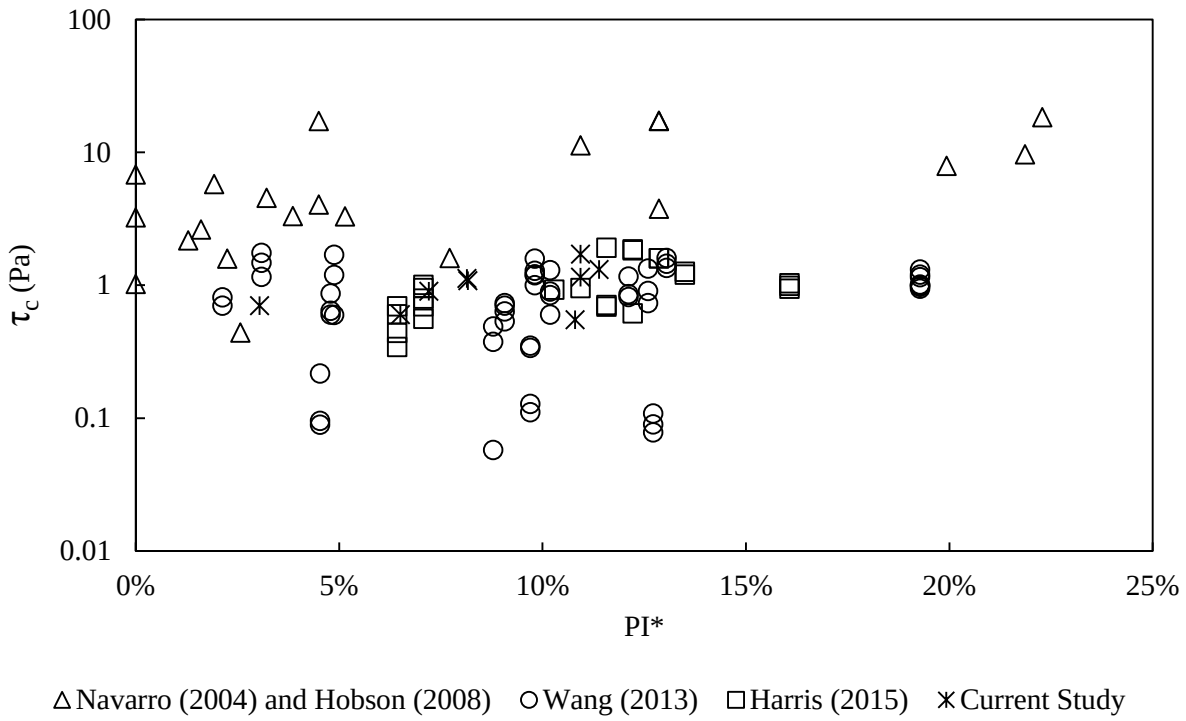

Figure 5.8: *PI** vs. Critical Shear Stress for the "All Data" Data Set

~~This~~ Figure 5.8 shows that *PI** < 2 may be too confining a definition for the line between low cohesive and cohesive sediments. While this is inconclusive, as more research should be conducted regarding this parameter, it does ~~show~~ confirm that the criterion for segmenting the

data sets deserves further study. ~~there could be a solution to defining the regions of variability for sediment erosion.~~

When performing the calculations for prediction of critical shear stress from these equations, it should be noted that sometimes negative values do occur. These negative values stem from the low *CSF* in some of the cohesive samples, which means that the negatively weighted *w* has much more control over the equation. Another limitation of this work comes from the inherent ranges of the sediment properties in both the field and lab-generated sediment mixtures as summarized in Table 5.1. While the "All Data" data set contains 108 data points (20 from Navarro (2004) and Hobson (2008), 54 from Wang (2013), 24 from Harris (2015), and 9 from the current study) there are relatively few points in the coarse sediment data set (19) which means that data set should be filled out before drawing major conclusions regarding the advantage of these separate equations. Other factors not accounted for include the effect of organic matter (it was small), differences in clay mineralogy (although Kaolinite is quite prevalent in Georgia) and a possible lack of full saturation of the few field samples that were high in *CSF* but low in *w* even though an effort was made to take all samples below the water table.

5.3 Summary of Data Analysis

Previous researchers have shown the ability to predict critical shear stress using geotechnical parameters from either coarse or fine sediments. Navarro (2004) and Hobson (2008) measured critical shear stress for largely coarse-grained field sediments and developed a prediction equation for the Shields parameter that depended on *Fines* and d_*. Wang (2013), who tested mixtures of Kaolinite and silt, found that the Shields parameter of fine sediments could be predicted by using a three-variable equation with *w*, *CSF*, and *w x CSF*. However, her equation

was not as good a fit in determining the erosion rate of coarse sediments like those of Navarro and Hobson. Similarly, the Navarro and Hobson equation could not properly calculate the Shields parameter of fine sediments due to its reliance on *Fines*. Harris (2015) had some success in formulating a weighted equation, with the weighting factor depending on Fines, which was applied to the Wang and Navarro-Hobson equations. This combined equation performed well for both coarse and fine sediments, but sediments that included a large proportion of both fine and coarse fractions could not be modeled as well.

In addition to testing the equations from previous researchers, the concept of using two separate equations for different data sets was tested in this research. By splitting the groups at 40% water content and a median particle size of 0.04 mm, two separate prediction equations for critical shear stress produced a standard error that was low for both the upper and lower water content groups. The weighted equation and the use of two equations split along a set of dividing parameters both show promise. However, these equations need additional work and more erosion data for coarse material. Based on the information collected and the methods implemented, the recommendation of this study is that the three-variable equation proposed by Wang and refined here (Eqn. 5.7) is the best way to calculate the Shields parameter.

Chapter 6

Conclusion and Recommendations

6.1 Summary of Findings

The objective of this study was to investigate the erodibility of sediments at bridge foundations which mimic the geotechnical characteristics of those found naturally in the state of Georgia in order to improve estimates of bridge scour depths during floods. Two separate experiments were conducted to measure sediment properties, (e.g. water content, particle size distribution, clay size fraction, pH, and conductivity) and to measure erosion rates and critical shear stress of these sediments in the erosion flume located in the Georgia Tech Hydraulics Laboratory. Artificially mixed sediments consisting of various proportions of Kaolinite, silt, and sand were tested. Sediment group properties were connected with erosion group properties using water contents to match them. This data set, in conjunction with data sets collected by other researchers, including field sediments in Georgia (Navarro 2004 and Hobson 2008) and lab-prepared sediments (Wang 2013 and Harris 2015), were analyzed using multiple linear regression to find the best representative equations for the estimation of the Shields parameter. An equation combining water content and clay size fraction variables as well as an interaction term, was shown to produce the best statistical fit of all the data. This equation aligns with equations found by Wang (2013) and Harris (2015). The addition of percent fines as an independent variable improved the fit of the data, but the increase was not substantial enough to warrant the use of a more complex equation. However, it is likely that a single equation or a pair

of equations delineated into coarse and fine segments by a specific criterion has promise as shown by Harris (2015) who proposed a weighting factor that was a function of percent fines applied to the best-fit equation of Wang (2013) for fine sediments and that of Navarro and Hobson for coarse sediments. This weighted equation by Harris showed statistical improvements, but it still did not perform well for sediments in the transitional region between coarse and fine sediments. In this study, a pair of equations was developed to apply separately to coarse and fine sediments separated by a water content of 40% and a size of 0.04 mm. The Navarro-Hobson equation was found to fit the coarse group of sediments well with independent variables of grain size and percent fines (clay and silt), while a three-variable equation depending on clay size fraction, water content, and an interaction term like that of Wang was determined to fit the fine size fraction well. These results showed that for fine sediments the effects of cohesion were best represented by clay size fraction and packing capacity as measured by water content (or bulk density) along with the interaction term of their product which modulates their opposite, interactive effects. For coarse sediments on the other hand, water content and clay size fraction did not have as much explanatory value but rather sediment size and percent fines were more representative of a granular structure and its effect on critical shear stress. These findings are consistent with the literature but the difficulty is in defining or classifying cohesive vs. noncohesive behavior. Clay size fraction alone as used by other researchers, or even water content and grain size as proposed herein, were not entirely satisfactory in differentiating between cohesive and noncohesive behavior. It is concluded that the criterion for separation into cohesive vs, noncohesive, or fine vs. coarse groups, and the applicable equations depends on finding a more fundamental property that depends on particle structure but yet is also easily measured.

These findings require additional lab data in order to broaden the range of properties of lab-generated sediment mixtures to more fully capture the field data properties measured in research by Navarro (2004) and Hobson (2008) and to find a satisfactory property for better classifying coarse vs. fine sediment erosion behavior. In the meantime, it is recommended that the simplicity and general goodness of fit of a three-parameter equation using water content, clay size fraction, and an interaction term found in this research from the entire data set is suitable for estimating the critical shear stress of sediments in Georgia.

6.2 Contributions to Existing Knowledge

Previous research demonstrated the feasibility of a few methodologies including separation of data based on median particle size for fine and coarse sediments or by percent clay for cohesive vs. noncohesive behavior. Separation based on particle size is effective, but its practical use for sediments that are not predominantly coarse is very limited. Percent clay alone also does not seem sufficient to separate different erosion behaviors. This research work focused on evaluating four equations from previous work and more from this study. A single formula that uses three independent variables of water content, clay size fraction, and an interaction term, had good results when applied to all data. However, this three variable equation did not perform as well for coarser sediment data. This same formula was further refined with the addition of a percent fines variable, but the improvement as a better fit was negligible. Adding a fourth term also increases the complexity of the equation, which is to be avoided. A weighted equation from previous work showed promise, but even with the addition of the current study, the equation did not predict the Shields parameter in the transition region well. Finally, instead of using a single equation, a pair of equations best suited for non-cohesive or cohesive sediments, were applied to two datasets that had been separated. The data sets in this study were separated by water content

and particle size resulting in a coarse and fine dataset. The evaluation of this method found that it holds promise, but more data is needed before a firm conclusion can be reached relative to the criterion for separation.

6.3 Recommendations for Future Research

Future research in this area should focus on replicating sediment mixtures that are much closer to the transition between cohesive and noncohesive erosion behavior and finding a new parameter to separate them that is dependent on particle structure. This may be best achieved by creating coarser sediments than in the present research while incorporating a range of small values of clay size fraction. A series of experiments in which the sediments contain 5-15% Kaolinite is recommended. This may provide the coarser lab samples that this study and previous studies have attempted to focus upon. While much of the previous fines data originated from lab -prepared samples, much of the coarse data were collected from field samples; therefore, it is important to make coarse lab samples in order to test the replicability of the erosion equations suggested both in previous research and in the current study. The weighted equation, simple three-parameter equation, and a pair of equations separated by water content should be the primary alternatives to be considered further. Another area of future work is to investigate the importance of organic matter, which was not included in this study.

The primary goal of future research is to establish either a single equation that accurately predicts the coarse-fine transition region or a pair of equations that are defined by a geotechnical parameter that best differentiates the type of erosion behavior expected. The importance of defining erosion characteristics of sediments will continue to be just as important as modeling the hydrodynamics of flood flows in predicting scour around bridges and other hydraulic structures.

Appendix A

All Data Collected and Implemented

Table A1: All Erosion Data Collected from Experiments

Percent of Kaolin by Weight	Average Water Content	Erosion Rate (kg/m2/s)	Applied Shear Stress (Pa)	Average Depth (mm)	Group
10%	135%	0.027	1.71	11.8	Group 1
10%	100%	0.063	2.15	9.9	
10%	99%	0.067	2.48	8.7	
10%	92%	0.025	1.71	10.3	
10%	90%	1.159	3.24	25.6	
10%	88%	0.032	2.83	9.0	
10%	85%	0.311	2.83	17.3	
10%	81%	0.912	3.24	25.0	
10%	81%	0.314	2.48	51.0	
10%	76%	0.122	2.15	24.8	
10%	69%	0.034	1.71	29.8	Group 2
10%	66%	0.204	3.24	38.3	
10%	64%	0.079	2.48	7.2	
10%	63%	0.080	2.48	17.8	
10%	59%	0.015	1.71	25.7	
10%	58%	0.042	2.15	25.6	
10%	58%	0.167	2.15	29.7	
10%	53%	0.116	2.48	33.6	
10%	52%	0.025	2.83	22.1	
10%	36%	0.082	1.71	43.6	Group 3
10%	36%	0.263	2.83	51.7	
10%	35%	0.167	2.48	30.3	
10%	34%	0.080	1.71	48.6	
10%	33%	0.094	2.15	45.6	
10%	32%	0.081	2.48	47.7	
10%	32%	0.166	2.83	49.3	
10%	30%	0.406	3.24	66.0	
10%	30%	0.068	2.15	69.0	
10%	30%	0.100	2.15	64.0	
10%	29%	0.060	1.71	69.9	

10%	29%	0.237	2.83	76.2	
10%	28%	0.070	1.71	66.6	
10%	28%	0.409	3.24	66.0	Group 3
10%	26%	0.087	2.15	70.9	
10%	25%	0.164	2.48	53.9	
20%	120%	0.024	1.71	9.1	
20%	91%	0.471	3.24	15.6	
20%	91%	0.036	2.15	10.5	
20%	88%	0.188	2.83	14.0	
20%	80%	0.021	1.71	5.9	Group 1
20%	79%	0.044	2.48	12.0	
20%	78%	0.031	2.48	8.9	
20%	72%	0.041	2.15	11.2	
20%	66%	0.180	3.24	40.7	
20%	62%	0.049	2.83	10.6	
20%	51%	0.024	1.71	22.3	
20%	49%	0.018	1.71	16.0	
20%	46%	0.023	2.83	26.5	
20%	46%	0.022	2.48	21.6	
20%	46%	0.017	1.71	23.2	Group 2
20%	45%	0.039	2.48	30.3	
20%	45%	0.067	2.83	35.5	
20%	45%	0.119	3.24	42.3	
20%	45%	0.009	1.71	28.5	
20%	44%	0.033	2.15	27.2	
20%	44%	0.020	2.83	35.2	
20%	43%	0.026	2.48	31.4	
20%	43%	0.027	2.48	42.0	
20%	42%	0.016	1.71	29.3	
20%	42%	0.053	3.24	62.6	
20%	41%	0.017	2.15	36.8	
20%	41%	0.015	1.71	34.5	Group 3
20%	41%	0.038	2.83	49.9	
20%	41%	0.013	2.15	43.1	
20%	41%	0.022	2.15	27.2	
20%	39%	0.022	2.83	60.8	
20%	39%	0.022	2.48	52.1	
20%	38%	0.023	2.15	37.2	
30%	116%	0.075	2.83	8.4	
30%	78%	0.002	1.71	10.0	Group 1
30%	76%	0.017	2.15	4.4	

30%	76%	0.181	3.24	10.3	Group 1
30%	72%	0.024	2.48	6.6	
30%	72%	0.014	1.71	4.9	
30%	69%	0.004	1.71	6.8	
30%	68%	0.028	2.83	7.8	
30%	68%	0.010	2.48	3.8	
30%	64%	0.047	2.83	27.5	
30%	60%	0.024	2.15	6.4	
30%	60%	0.027	3.24	5.3	Group 2
30%	58%	0.009	2.15	10.4	
30%	58%	0.038	3.24	29.5	
30%	58%	0.008	2.15	14.0	
30%	58%	0.007	2.48	9.8	
30%	57%	0.019	2.83	18.6	
30%	57%	0.010	1.71	12.9	
30%	56%	0.013	2.48	16.5	
30%	55%	0.004	2.15	16.7	
30%	55%	0.015	2.83	24.7	
30%	53%	0.014	2.48	22.9	Group 3
30%	53%	0.010	2.48	27.7	
30%	53%	0.017	1.71	20.4	
30%	53%	0.034	3.24	17.9	
30%	53%	0.026	3.24	43.5	
30%	53%	0.014	2.48	15.1	
30%	52%	0.012	1.71	2.5	
30%	52%	0.009	2.15	20.9	
30%	51%	0.011	2.15	15.5	
30%	49%	0.023	3.24	30.1	
30%	43%	0.040	2.83	45.0	
30%	39%	0.018	2.83	54.8	

Table A2: All Data from All Researchers

Navarro (2004) and Hobson (2008)					
τ^*_c	*d**	*CSF*	*w*%	*Fines*	*PI**
82.92	0.19	34.0%	39.0%	74.0%	21.9%
38.85	0.70	34.7%	36.0%	75.0%	22.3%
32.90	0.81	20.0%	34.0%	56.0%	12.9%
22.67	1.12	20.0%	30.0%	52.0%	12.9%
14.20	1.21	17.0%	34.0%	50.0%	10.9%
1.78	2.95	20.0%	16.3%	38.0%	12.9%
3.78	3.31	31.0%	20.0%	40.0%	19.9%
1.28	3.92	8.0%	23.0%	22.0%	5.1%
1.29	4.02	6.0%	30.0%	10.0%	3.9%
1.73	4.11	5.0%	29.0%	17.0%	3.2%
0.15	4.54	4.0%	30.0%	7.0%	2.6%
0.48	5.09	3.5%	26.5%	7.0%	2.3%
0.64	5.31	2.0%	32.0%	5.0%	1.3%
0.42	5.67	12.0%	14.6%	15.0%	7.7%
1.30	6.86	3.0%	24.0%	29.0%	1.9%
0.82	7.83	7.0%	35.0%	25.0%	4.5%
0.45	11.36	0.0%	21.0%	1.0%	0.0%
0.17	23.36	2.5%	26.5%	5.0%	1.6%
1.09	25.04	7.0%	33.0%	13.0%	4.5%
0.05	29.34	0.0%	22.0%	0.0%	0.0%
0.34	30.48	0.0%	31.0%	3.0%	0.0%
Wang (2013)					
τ^*_c	*d**	*CSF*	*w*%	*Fines*	*PI**
1.09	1.01	3.3%	35.3%	100%	2.1%
1.26	1.01	3.3%	37.6%	100%	2.1%
2.78	0.66	4.8%	54.0%	100%	3.1%
3.54	0.66	4.8%	54.5%	100%	3.1%
4.21	0.66	4.8%	54.1%	100%	3.1%
0.24	0.58	7.0%	65.9%	100%	4.5%
0.26	0.58	7.0%	66.2%	100%	4.5%
0.59	0.58	7.0%	66.4%	100%	4.5%
1.79	0.76	7.4%	44.9%	100%	4.8%
1.25	0.76	7.4%	45.8%	100%	4.8%
1.33	0.76	7.4%	48.7%	100%	4.8%
2.87	0.66	7.6%	60.7%	100%	4.9%
1.44	0.66	7.6%	60.8%	100%	4.9%

4.08	0.66	7.6%	59.5%	100%	4.9%
0.36	0.25	13.7%	79.9%	100%	8.8%
3.05	0.25	13.7%	76.5%	100%	8.8%
2.34	0.25	13.7%	74.3%	100%	8.8%
2.59	0.33	14.1%	93.8%	100%	9.1%
3.41	0.33	14.1%	92.8%	100%	9.1%
3.56	0.33	14.1%	94.3%	100%	9.1%
3.08	0.33	14.1%	93.9%	100%	9.1%
1.74	0.31	15.1%	103.4%	100%	9.7%
0.57	0.31	15.1%	104.3%	100%	9.7%
0.66	0.31	15.1%	103.5%	100%	9.7%
1.81	0.31	15.1%	103.0%	100%	9.7%
6.96	0.29	15.3%	79.0%	100%	9.8%
5.44	0.29	15.3%	75.1%	100%	9.8%
8.59	0.29	15.3%	76.7%	100%	9.8%
6.45	0.29	15.3%	82.2%	100%	9.8%
6.55	0.29	15.3%	73.7%	100%	9.8%
3.78	0.25	15.8%	84.6%	100%	10.2%
5.30	0.25	15.8%	83.3%	100%	10.2%
8.19	0.25	15.8%	81.9%	100%	10.2%
5.64	0.25	15.8%	87.0%	100%	10.2%
13.22	0.14	18.8%	141.5%	100%	12.1%
9.26	0.14	18.8%	142.6%	100%	12.1%
9.73	0.14	18.8%	142.1%	100%	12.1%
8.49	0.14	19.6%	130.5%	100%	12.6%
15.42	0.14	19.6%	125.9%	100%	12.6%
10.48	0.14	19.6%	126.7%	100%	12.6%
1.02	0.14	19.8%	164.0%	100%	12.7%
1.23	0.14	19.8%	164.8%	100%	12.7%
0.89	0.14	19.8%	163.1%	100%	12.7%
16.43	0.14	20.3%	97.4%	100%	13.0%
18.18	0.14	20.3%	97.2%	100%	13.0%
15.28	0.14	20.3%	94.0%	100%	13.0%
23.49	0.06	30.0%	182.8%	100%	19.3%
24.75	0.06	30.0%	182.2%	100%	19.3%
24.94	0.06	30.0%	166.7%	100%	19.3%
25.18	0.06	30.0%	156.3%	100%	19.3%
24.22	0.06	30.0%	119.1%	100%	19.3%
28.55	0.06	30.0%	113.3%	100%	19.3%
29.92	0.06	30.0%	112.1%	100%	19.3%
32.64	0.06	30.0%	109.5%	100%	19.3%

Harris (2013)					
τ^*_c	*d**	*CSF*	*w*%	*Fines*	*PI**
20.24	0.08	25.0%	121.0%	100%	16.1%
19.41	0.08	25.0%	126.0%	100%	16.1%
18.43	0.08	25.0%	131.0%	100%	16.1%
19.08	0.16	18.0%	95.0%	77%	11.6%
18.41	0.16	19.0%	101.0%	77%	12.2%
18.92	0.16	19.0%	106.0%	77%	12.2%
16.42	0.16	20.0%	109.0%	77%	12.9%
16.59	0.15	20.0%	112.0%	77%	12.9%
13.34	0.15	21.0%	116.0%	77%	13.5%
12.80	0.15	21.0%	122.0%	77%	13.5%
7.07	0.21	16.0%	91.0%	76%	10.3%
7.81	0.19	17.0%	98.0%	76%	10.9%
6.32	0.18	18.0%	102.0%	76%	11.6%
6.69	0.16	18.0%	106.0%	76%	11.6%
6.52	0.15	19.0%	113.0%	76%	12.2%
1.44	1.11	11.0%	64.0%	61%	7.1%
1.43	1.05	11.0%	69.0%	61%	7.1%
1.27	0.99	11.0%	74.0%	61%	7.1%
1.18	0.93	11.0%	80.0%	61%	7.1%
1.02	0.87	11.0%	86.0%	61%	7.1%
0.51	2.13	10.0%	38.0%	43%	6.4%
0.44	2.16	10.0%	42.0%	44%	6.4%
0.31	2.20	10.0%	44.0%	46%	6.4%
0.24	2.25	10.0%	54.0%	47%	6.4%
Current Study					
τ^*_c	*d**	*CSF*	*w*%	*Fines*	*PI**
4.34	0.44	17.7%	89.0%	79%	11.4%
2.55	0.64	12.7%	62.1%	66%	8.1%
0.74	1.39	4.7%	30.4%	44%	3.0%
1.67	0.94	12.7%	76.3%	56%	8.2%
0.98	1.34	11.2%	45.3%	50%	7.2%
0.54	1.61	10.1%	41.1%	46%	6.5%
3.59	0.70	17.0%	70.5%	58%	10.9%
2.42	0.70	17.0%	57.2%	58%	10.9%
1.15	0.70	16.8%	48.8%	58%	10.8%

Works Cited

Amos, C. L., Grant, J., Daborn, G. R., and Black, K. (1992). "Sea carousel--a benthic, annular flume." *Estuar. Coast. Shelf S.*, 34(6), 557-577.

ASTM International (American Society for Testing and Materials). (2001), "Standard test method for sieve analysis of fine and coarse aggregate." *C136-01*, West Conshohochen, Pa.

ASTM International (American Society for Testing and Materials). (2016), "Standard test method for Particle-Size Distribution (Gradation) of Fine-Grained Soils Using the Sedimentation (Hydrometer) Analysis." *D7928-16*, West Conshohochen, Pa.

ASTM International (American Society for Testing and Materials). (2010a), "Moisture content of soil." *D2216-10*, West Conshohochen, Pa.

Avnimelech, Y., Ritvo, G., Meijer, L. E., and Kochba, M. (2001). "Water content, organic carbon and dry bulk density in flooded sediments." *Aquacultural Engineering*, 25(1), 25-33.

Black, K. S., and Paterson, D. M. (1997). "Measurement of the erosion potential of cohesive marine sediments: A review of current in situ technology." *J. Mar. Environ. Eng.*, 4(1), 43–83.

Budhu, M., (2011). "Soil Mechanics and Foundations" 3 Ed. John Wiley & Sons, Inc., Hoboken, NJ.

Cornelisse, J. M., Mulder, H. P. J., Houwing, E. J., Williamson, H. J., and Witte, G. (1997). "On the development of instruments for in situ erosion measurements." N. Burt, R. Parker, and J. Watts, eds., Wiley, New York, 175–186.

Einstein, H. A. (1950) "The Bed Load Function for Sediment Transportation in Open Channels." *Technical Bulletin 1026*. Washington, DC: USDA, Soil Conservation Service.

Engelund, F. (1967). Closure to "Hydraulic Resistance of Alluvial Streams." *J. Hyd. Div.*, ASCE 93, no. HY7, pp.287-296.

Grabowski, R. C., Droppo, I. G., and Wharton, G. (2011). "Erodibility of cohesive sediment: The importance of sediment properties." *Earth-Sci. Rev.*, 105(3-4), 101-120.

Gerbersdorf, S. U., Jancke, T., and Westrich, B. (2005). "Physico-chemical and biological sediment properties determining erosion resistance of contaminated riverine sediments — temporal and vertical pattern at the Lauffen reservoir/river Neckar, Germany. ." *Limnologica*, 35(3), 132-144.

Gerbersdorf, S., Jancke, T., and Westrich, B. (2007). "Sediment properties for assessing the erosion risk of contaminated riverine sites. An approach to evaluate sediment properties and their covariance patterns over depth in relation to erosion resistance. First investigations in natural sediments (11 pp)." *J. Soil. Sediment.*, 7(1), 25-35.

Gust, G., and Morris, M. J. (1989). "Erosion thresholds and entrainment rates of undisturbed in situ sediments." *J. Coastal Res.*, 5, 87-99.

Harris, T. (2015) “Critical Shear Stress for Erosion of Fine and Coarse-Grained Sediments in Georgia,” Master Thesis, Georgia Institute of Technology, Atlanta, GA.

Hobson, P. M. (2008). "Rheologic and flume erosion characteristics of Georgia sediments from bridge foundations," Master Thesis, Georgia Institute of Technology, Atlanta, GA.

Jacobs, W., Le Hir, P., Van Kesteren, W., and Cann, P. (2011). “Erosion threshold of sand mud mixtures.” *Continental Shelf Research*, 31 (2011), S14-S25.

Julien, P. Y., and Lan, Y. (1991). "Rheology of hyperconcentrations." *J. Hydraul. Eng.*, 117(3), 346-353.

Mazurek, K. A., Rajaratnam, N., and Sego, D. C. (2001). "Scour of cohesive soil by submerged circular turbulent impinging jets." *J. Hydraul. Eng.*, 127(7), 598-606.

Mheta, A. Hayter, E., Parker W., Krone, R., and Teeter, A. (1989). “Cohesive Sediment Transport. I: Process Description.” *J. Hydraul. Eng.*, 10.1061/(ASCE)0733-9429(1989)115:8(1076), 1076-1093.

Meyer-Petyer, E., and R. Muller. (1948). “Formulas for Bed-Load transport.” *Paper at the Second Meeting of International Association for Hydraulic research*, Stockholm.

Navarro, H. R. (2004). "Flume measurements of erosion characteristics of soils at bridge foundations in Georgia," Master Thesis, Georgia Institute of Technology, Atlanta, GA.

Osman, A. M., and Thorne, C. R. (1988). "Riverbank stability analysis: I. Theory." *J. Hydraul. Eng.*, 114 (2), 134-150.

Pruett, R. J. (2000). “Georgia kaolinite: Development of a leading industrial mineral.” *Mining Engineering*, 52(10), 21.

Ravisangar, V. (2001). "The role of sediment chemistry in stability and resuspension characteristics of cohesive sediments," Ph.D. Thesis, Georgia Institute of Technology, Atlanta.

Ravisangar, V., Dennett, K. E., Sturm, T. W., and Amirtharajah, A. (2001). "Effect of sediment pH. on resuspension of kaolinite sediments." *J. Environ. Eng.*, 127(6), 531- 538.

Ravisangar, V., Sturm, T. W., and Amirtharajah, A. (2005). "Influence of sediment structure on erosional strength and density of kaolinite sediment beds.” *J. Hydraul. Eng.*, 131(5), 356-265.

Righetti, M., and Lucarelli, C. (2007). "May the shields theory be extended to cohesive and adhesive benthic sediments?" *J. Geophys. Res.*, 112(C5), C05039.

Roberts, J. D., Jepsen, R. A., and James, S. C. (2003). "Measurements of sediment erosion and transport with the adjustable shear stress erosion and transport flume." *J. Hydraul. Eng.*, 129(11), 862-871.

Rowell, D.L., (1994). “Soil Science: Methods and Applications,” Longman Scientific and Technical, Harlow, Essex.

Santamarina, J. C., Klein, K. A., and Fam, M. A. (2001). “Soils and Waves: Particulate Materials Behavior, Characterization and Process Monitoring”, John Wiley & Sons Ltd., New York.

Schofield, A. N., Wroth, C. D. (1968) “Critical State Soil Mechanics” McGraw-Hill, New York.

Shields, A. (1936). “Applications of similarity principles and turbulence research to bed load movement.” California Institute of Technology, Hydrodynamics Laboratory Publication 167, USDA, Soil Conservation Service Cooperative, Pasadena, CA.

Skempton, A. W. (1965) “The Colloidal activity of clay”. *Proceedings of the Third International Conference on Soil Mechanics and Foundation Engineering. Vol. I* 57-61.

Sturm, T. W. (2001). “Open channel hydraulics: Textbook Series in Water Resources and Environmental Engineering,” 2 Ed., McGraw Hill, New York.

Sturm, T. W. (2010). “Open Channel Hydraulics.” New York: McGraw Hill.

Ternat, F., Boyer, P., Anselmet, F., and Amielh, M. (2008). "Erosion threshold of saturated natural cohesive sediments: Modeling and experiments." *Water Resour. Res.*, 44(11), W11434.

Thoman, R.W., and Niezgoda, S.L. (2008). “Determining erodibility, critical shear stress, and allowable discharge estimates for cohesive channels: case study in the powder river basin of Wyoming.” *J. of Hydraul. Eng.*, 134 (12), 1677-1687.

Tolhurst, T. J., Black, K. S., Paterson, D. M., Mitchener, H. J., Termaat, G. R., and Shayler, S. A. (2000). "A comparison and measurement standardization of four in situ devices for determining the erosion shear stress of intertidal sediments." *Cont. Shelf Res.*, 20(10-11), 1397-1418.

Tolhurst, T. J., Black, K. S., Shayler, S. A., Mather, S., Black, I., Baker, K., and Paterson, D. M. (1999). "Measuring the in situ erosion shear stress of intertidal sediments with the cohesive strength meter (csm)." *Estuar. Coast. Shelf S.*, 49(2), 281-294.

Torfs, H., Mitchener, H., Huysentruyt, H., and Toorman, E. (1996). "Settling and consolidation of mud/sand mixtures." *Coast. Eng*., 29(1-2), 27-45.

Van Kessel, T., Winterwerp, J.C., Van Prooijen, B., Van Ledden, M., and Borst, W. (2011). “Modeling the seasonal dynamics of SPM with a simple algorithm for the buffering of fines in a sandy seabed.” *Cont. Shelf Res.*, 31(10), S124-S134.

Van Ledden M. (2003). “Sand-mud segregation in estuaries and tidal basins,” PhD Dissertation, Delft Univ. of Technol., Delft, Netherlands.

Van Ledden, M., van Kesteren, W. G. M., and Winterwerp, J. C. (2004). "A conceptual framework for the erosion behavior of sand-mud mixtures." *Cont. Shelf Res.*, 24(1), 1-11.

van Olphen, H. (1977). “An introduction to clay colloid chemistry,” 2nd Ed., John Wiley & Sons, New York.

Walder, J. (2015). “Dimensionless erosion laws for cohesive sediment.” *J. of Hydraul. Eng.*, 10.1061/(ASCE)HY.1943-7900.0001068, 04015047.

Wang, Y. (2013). “Effects of Physical Properties and Rheological Characteristics on Critical Shear Stress of Fine Sediments.” Ph.D. Thesis, Georgia Institute of Technology, Atlanta, GA, United States.

Wang, Y. and Sturm, T. (2016). “Effect of Physical Properties on Erosion and Yield Strengths of Fine-Grained Sediments.” *J. Hydraul. Eng.*, 10.1061/(ASCE)HY.1943-7900.0001193, 0401604

Williamson, H., and Ockenden, M. (1996). "Isis: An instrument for measuring erosion shear stress in situ." *Estuar. Coast. Shelf S.*, 42(1), 1-18.

Winterwerp, J. C., and van Kesteren, W. G. M. (2004). “Introduction to the Physics of Cohesive Sediment in the Marine Environment”, Elsevier, Amsterdam.

Winterwerp, J. C., van Kesteren, W. G. M., van Prooijen, B., and Jacobs, W. (2012). “A conceptual framework for shear flow-induced erosion of soft cohesive sediment beds.” *J. Geophys. Res. Oceans*, 117(C10), C10020.